NOTICE

The quality of this microform is heavily dependent upon the quality of the original thesis submitted for microfilming. Every effort has been made to ensure the highest quality of reproduction possible.

If pages are missing, contact the university which granted the degree.

Some pages may have indistinct print especially if the original pages were typed with a poor typewriter ribbon or if the university sent us an inferior photocopy.

Reproduction in full or in part of this microform is governed by the Canadian Copyright Act, R.S.C. 1970, c. C-30, and subsequent amendments.

AVIS

La qualité de cette microforme dépend grandement de la qualité de la thèse soumise au microfilmage. Nous avons tout fait pour assurer une qualité supérieure de reproduction.

S'il manque des pages, veuillez communiquer avec l'université qui a conféré le grade.

La qualité d'impression de certaines pages peut laisser à désirer, surtout si les pages originales ont été dactylographiées à l'aide d'un ruban usé ou si l'université nous a fait parvenir une photocopie de qualité inférieure.

La reproduction, même partielle, de cette microforme est soumise à la Loi canadienne sur le droit d'auteur, SRC 1970, c. C-30, et ses amendements subséquents.

Modelling of Ignition of Liquid Hydrocarbon Droplets at High Pressure

By

Renata Ruszalo

Ottawa, Ontario. November 1990

A THESIS

PRESENTED TO THE UNIVERSITY OF OTTAWA

IN PARTIAL FULFILLMENT OF THE

REQUIREMENTS FOR THE DEGREE OF

MASTER OF APPLIED SCIENCE

IN

CHEMICAL ENGINEERING

ISBN 0-315-68084-9

UNIVERSITÉ D'OTTAWA
UNIVERSITY OF OTTAWA

Abstract

This work presents a mathematical model for the auto-ignition process of a single droplet of pure liquid hydrocarbon at high pressure. The model solves the full transient equations of continuity, species diffusion and energy in the vapour phase surrounding the droplet using finite difference techniques. The Peng-Robinson equation of state is used to describe vapour-liquid equilibrium at the droplet surface. The effects on droplet evaporation and ignition of pressure, temperature, and liquid phase diffusion of dissolved air are discussed.

The model was tested with a droplet size of 1.5 mm and an ambient temperature of 973 K and pressure varying from 1 to 50 atm. For a pure (single component) fuels the ignition delay time was found to be a strong function of pressure, temperature and diameter. The ignition time decreases as pressure rises. At high pressure the reaction zone moves closer to the droplet surface. The air diffusion in the liquid phase and correction of transport properties for the effects of pressure have only small effects on ignition time. The model shows that the droplet cannot reach or pass the critical state but can only approach it asymptotically.

The ignition behaviour of a two-component mixture is strongly controlled by the more volatile component. A change in pressure does not have significant effects on the behaviour of ignition time with mixture composition. Liquid diffusion has no large effect on the ignition time , but may affect the subsequent combustion processes.

Acknowledgement

I would like to express my deep gratitude to Professor William Hallett for his motivating guidance and encouragement, for providing a comfortable working atmosphere and for being always available for discussions. His quick and careful editing of the text helped immensely in the compilation of this thesis.

A hearty thanks to Professor Benjamin C.-Y. Lu and Dr. Michael Margerum for their guidance and for providing computer software for calculation of vapour-liquid equilibrium.

The financial support provided by the Department of National Defence of Canada is greatly appreciated.

I wish to thank my colleagues and friends with whom I shared a warm academic experience.

Finally, I am indebted to my mother Eleonora, and my husband Saviz for their understanding and consistent moral support.

Nomenclature

a, b, c, a^0, S	coefficients of the discretization equations
a,b	reaction orders with respect to fuel, oxygen;
	constants in the Peng-Robinson equation
C_p	constant pressure specific heat, (kJ/kg K)
d	droplet diameter, (m)
D	diffusion coefficient, (m^2/s)
D_E,D_L	effective, and molecular diffusivity, (m^2/s)
E	energy of activation, (kcal/mol)
f	multiplication factor, fugacity
G	mass flux (kg/m^2)
h	heat of formation, (kJ/kg)
h_{fg}	heat of vaporization, (kJ/kg)
h_v	effective heat of vaporization, (kJ/kg)
$\overline{h}$	pure component enthalpy, (kJ/kmol)
$\overline{h}^\circ$	perfect gas enthalpy, (kJ/kmol)
H	partial enthalpy, (kJ/kg)
$\overline{H}$	partial molal enthalpy, ($kJ/kmol$)
j,J	diffusion flux in the vapour and liquid phase respectively, (kg/m^2s)

k	thermal conductivity, (W/m K)
k_{ij}	binary interaction parameter
K	pre-exponential factor
K_i	equilibrium constant
M	molecular weight, (kg/kmol)
N, NN	number of grid points in the vapour and liquid phase respectively
P	pressure, (kPa)
Q	total heat flux, (W/m^2)
r	radial position, (m)
R	droplet radius, (m)
$\mathcal{R}$	gas constant, (kJ/kmol K)
$\dot{R}$	$= dR/dt$
t	time, (sec)
T	temperature, (K)
v	radial velocity, (m/s)
V	volume, (m^3)
w	velocity relative to ξ coordinate
W	source term due to chemical reaction, (kg/m^3s)
y, x	mol fraction: vapour and liquid phase respectively
Y, X	mass fraction: vapour and liquid phase respectively
Z	compressibility factor

Greek Letters

α	relaxation factor
α_d	absorptivity of the droplet
$\Gamma=\rho D$	diffusion coefficient (kg/ms)

η	viscosity of the liquid
$\xi = r/R$	dimensionless coordinate
ρ	density (kg/m^3)
σ	Stefan-Boltzman constant ($W/m^2\ K^4$)
ϕ	fugacity coefficient
ω	acentric factor

Subscripts

A,F,O	air, fuel, oxygen
c	critical state
d	droplet
E,W	eastern and western grid point respectively
i,j	chemical species
l,L	liquid
m	mixture
P	grid point
r	reduced state
R	droplet surface
v	vapour
1,2	fuel components
∞	ambient

Superscripts

V,L	vapour and liquid phase
o	previous time step
t	trial value

Contents

List of Figures

List of Tables

Chapter 1

Introduction

1.1 Ignition Process

Droplet vaporization and ignition at near and super-critical conditions has long been a matter of serious practical concern in the development of high-pressure combustion systems. Examples include Diesel engines, gas turbines, liquid-propellant rockets, etc. The underlying physical mechanisms are different from those at low pressure, and contain many characteristics which the conventional low-pressure theories cannot deal with.

In high pressure combustion chambers, the influence of the droplet vaporization and ignition process on engine performance is of primary importance. Spray combustion systems are utilized in many fields of engineering, including Diesel engines, gas turbines and many industrial furnaces, where the fuel is atomized to fine droplets to enlarge the surface area for fast evaporation and easy control of combustion rate. In order to understand spray phenomena, it is a basic requirement to have a good knowledge of single droplet behaviour. The phenomena associated with the evaporation of a single droplet and methods of predicting its evaporation rate are also

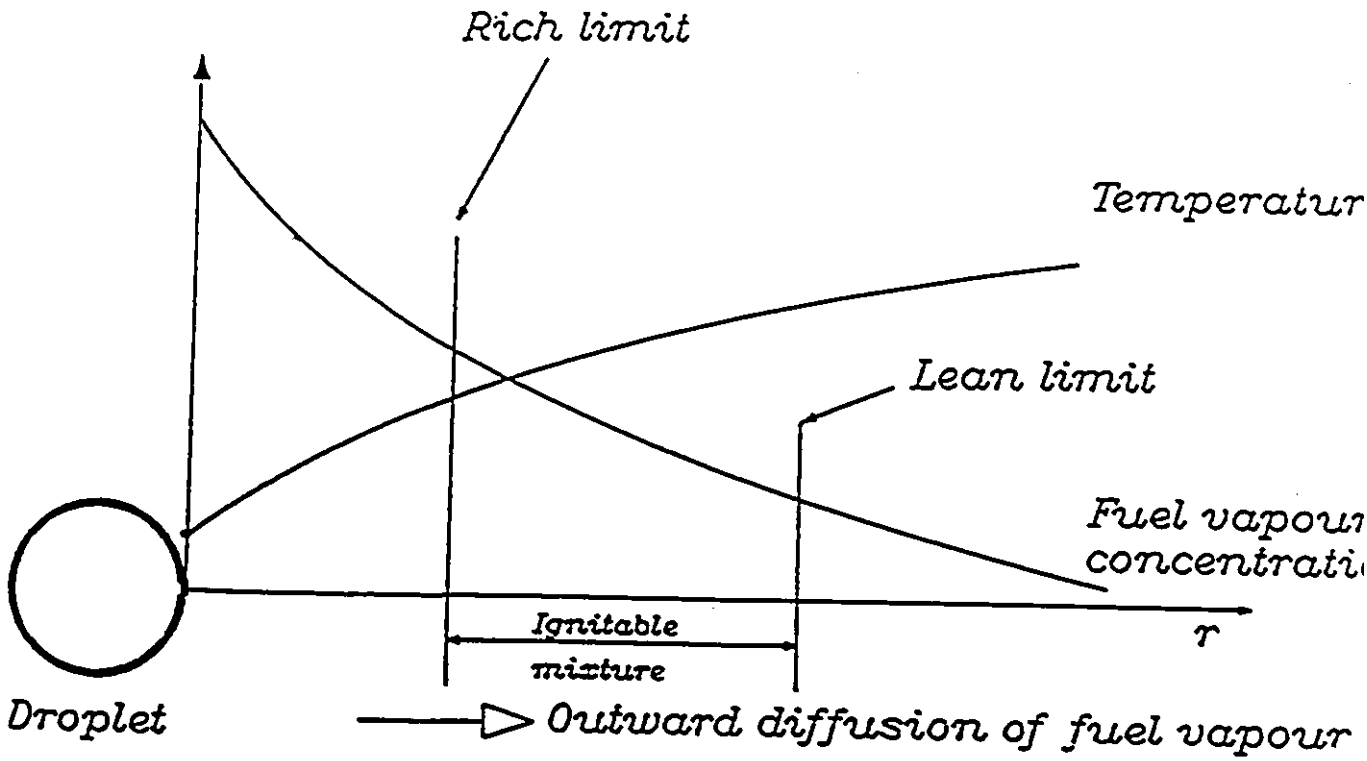

Figure 1: Temperature and fuel concentration profiles near a vaporizing fuel droplet.

important in the analysis of engineering operations involving the processes of spray cooling, and drying.

In a Diesel engine, ignition occurs shortly after fuel is injected into the hot, high-pressure environment existing in the cylinder at the end of the compression stroke. Fuel breaks up into a spray of fine droplets, which vaporize and mix with the surrounding air. Chemical reaction begins if enough ignitable mixture is produced. The temperature and pressure at injection in a modern Diesel range from 650 - 800°C and from 30 - 50 atm. This mode of ignition is called auto-ignition or spontaneous ignition, and is different from spark or flame ignition. The ignition delay time is the interval between fuel injection and ignition and is important in a Diesel because it affects the power output, efficiency and noise.

The present work is concerned with spontaneous (auto-) ignition of single droplets

at pressures well above atmospheric. It must be understood that a single droplet does not completely represent the process of spray evaporation and reaction in a Diesel, but is a necessary first step in studying the processes of liquid fuel ignition which occur in the engine.

When a cold droplet is injected into a combustion chamber, it is heated by heat conduction and convection from the surrounding air and by radiation from the hot walls of the chamber. The fuel evaporates at the droplet surface, and the vapour diffuses radially outward, mixing with air (see Fig. 1). The process of evaporation and diffusion must produce enough mixture to sustain chemical reaction. In other words, the total ignition delay consists of a "physical delay" which is the time that the droplet is exposed to hot air environment and heated up for initiation of gas phase reaction, and a "chemical delay", which accounts for the time for these reactions to accelerate to "runaway". The physical and chemical processes are coupled together.

The ignition process is affected by:

- the temperature of the surrounding air;
- the vapour pressure (volatility) of the fuel components;
- the reaction rate behaviour of the fuel components;
- the droplet diameter.

The vapour diffusion velocity is roughly inversely proportional to droplet radius, so vapour may leave a very small droplet at high velocity and make ignition impossible. Droplet ignition therefore involves the interaction of simultaneous physical and chemical processes.

1.2 Previous Work - Atmospheric Pressure Model

The purpose of the present work is to determine how pressure affects the ignition characteristics of fuels. It is part of an ongoing study of the relationship between ignition and boiling behaviour and chemical composition, with particular reference to the application of Canadian tar sand and other fuels in Diesels and gas turbines.

Previous work done by Bergeron and Hallett [5.4.3] described ignition of liquid fuel at atmospheric pressure. The work at atmospheric pressure was necessary to establish mathematical modelling and experimental techiques. The mathematical model of the autoignition process developed for a single droplet solved the energy, diffusion and continuity equations for the time-varying conditions in the vapour phase surrounding the droplet using the finite difference technique. A number of simplifying assumptions were made to reduce computational effort: spherical symmetry, negligible reactant consumption prior to ignition, constant transport properties (Bergeron and Hallett [3]), and a uniform (but time-dependent) droplet temperature. Chemical reaction rates were modelled with a one-step Arrhenius equation. For two-component fuels, the liquid diffusion equation was solved numerically, the combined effects of molecular diffusion and internal circulation being represented by an effective liquid diffusivity. In the experimental technique the single droplet was suspended on the end of a thin quartz fibre and an electric furnace rolled over the suspended droplet fast enough to approximate a step change in temperature. More details about the experiment and model development are found in Bergeron and Hallett [5]. Experiments were performed with the droplet size ranging from 1.0 - 1.6 mm and ambient temperature varying from 600 - 800°C. Reaction rate constants required for the model were fitted, using the experimental data for the pure fuel components. The following conclusions were drawn about the behaviour of liquid fuels:

1. **Single component fuel:**

   - the ignition delay time is nearly independent of droplet diameter, but decreases strongly as temperature rises;
   - the process of droplet ignition involves physical and chemical processes which are coupled together and occur simultaneously;
   - the ignition time is affected by the boiling point for fuels from the same chemical family: a higher boiling fuel will require a longer transient heating period before vapour is evolved and hence give a larger ignition time;
   - the most reactive fuel reacts only twice as rapidly as the least reactive fuels; hence, ignition times for fuels of similar volatility from different chemical families do not differ greatly;

2. **Two-component mixtures:**

   - the ignition behaviour of the mixture is strongly dependent on the behaviour of the more volatile component;
   - the mixture reaction rate may be modelled by taking a mole fraction weighted average of the rate constants of the components;
   - liquid phase diffusion has little effect on ignition time and a well-mixed model could be used for the liquid phase.

The model gave good predictions of experimental data for pure fuels and mixtures.

1.3 Research Proposal - High Pressure Model

The model developed in this thesis is an extension of the low pressure model just described to pressures high enough to properly simulate the Diesel environment.

Development of a model for high pressure vaporization and ignition is complicated by the fact that some of the assumptions used for low pressure are no longer valid and several modifications are necessary. It is therefore proposed to extend the low pressure work to pressures of 50 -60 bar. These pressures are well above the critical pressures for the fuels which we are concerned about (eg. n-heptane P_{cr} = 27.0 atm, n-hexadecane P_{cr} = 14.0 atm). Both experimental work and mathematical modelling are required, but the present work contains only the mathematical modelling. Work in the following areas is necessary to extend the model to high pressure:

1. Selection of a suitable description of vapour-liquid equilibrium at the droplet surface;
2. The effect of absorption and diffusion of air in the liquid phase;
3. Selection of correlations for transport properties at high pressure;
4. Pressure effects on reaction rate.

These considerations will be discussed in detail in the next several chapters. Chapter 2 presents a literature survey of experimental work, mathematical modelling, pressure effects on vapour-liquid equilibrium (VLE), and numerical methods for the study of single droplet ignition for one and two-component fuels. The mathematical model for a single component fuel is presented in Chapter 3. Results and discussion for single component fuels are presented in Chapter 4. Chapter 5 presents the mathematical model, results and discussion for two-component fuels, followed by conclusions and recommendations for future work (Chapter 6).

Chapter 2

Literature Survey

2.1 Introduction

Unfortunately there is not very much information in the literature about ignition at high pressure. Only one study (Kadota et al. [17]) of high pressure ignition is found in the literature; it presents a simple correlation, but does not shed much light on the phenomena involved in the process. However, several models are available for pure evaporation or steady combustion of a droplet which we will discuss later, including a number of theoretical and experimental studies using a single droplet at high pressure. This chapter will briefly review the available work, focusing on mathematical models and aspects of vapour-liquid equilibrium and transport properties which are different from those at atmospheric pressure.

2.2 Quasi Steady Theory

The simplest theory for the description of droplet evaporation and combustion is quasi-steady theory, which is the basis of the "classical" droplet vaporization theory. The main assumption in this theory is the omission of the transient terms from the diffusion, energy and continuity equations for the vapour phase. As a droplet begins to heat up the temperature increases, the vapour pressure at the surface also increases and the rate of vaporization rises. As the vapour pressure changes and chemical reaction occurs in the vapour, the gas phase undergoes transients to adjust itself. These transients are described by the $(\partial/\partial t)$ terms in the equations. The temperatures, concentrations, and velocities change faster in the vapour phase than at the droplet surface (because of the significant difference in liquid and vapour densities). The ratio of the gas-phase heat and mass diffusivities to the droplet regression rate is in order of 1000/1 (Law [19]), which is the same order as the ratio of the liquid to gas densities. The gas phase transient being much more rapid, its effects are assumed of low order and the liquid droplet heating becomes the controlling transient process. This allows the gas-phase transient terms to be eliminated. The whole solution depends only on surface droplet temperature and concentration (T_R, Y_R). This theory, for constant surface conditions (T_R, Y_R), predicts a constant droplet surface regression rate which is expressed in the "d^2-law" (Bergeron and Hallet [5]). This theory has its limitations at high pressure because as pressure rises the gas phase density increases and the transient terms become more significant. When the pressure approaches or exceeds the critical pressure of the fuel, the density ratio (ρ_l/ρ_g) approches unity and the liquid-gas interface is no longer recognizable, the enthalpy of vaporization approaches zero and the quasi-steady theory fails completely.

2.3 Experimental Work

The main issues dealt with in the literature on high pressure droplet evaporation and combustion are the extent to which behaviour at high pressure resembles the predictions of the classical quasi-steady theory, and the question of whether the droplet itself actually becomes supercritical under supercritical ambient conditions (critical state is used with reference to the critical state of the fuel, not the ambient gas).

The earliest known work on droplets at pressures above atmospheric is that of Hall and Diederichsen [11], who performed experiments on vaporizing and burning suspended droplets at pressures of up 20 atm. At high pressures, the droplet lifetime was found to decrease as $P^{0.25}$, while the flame moved closer to the droplet surface.

In experiments by Natarajan and Brzustowski [25] on burning pentane droplets a clearly defined droplet remained visible at total pressures up to 1.26 times the critical pressure, the highest value attempted, suggesting that the droplet remained subcritical. Measured droplet diameters showed that the linear relationship between the square of droplet diameter and time predicted by the quasi-steady theory (the "d^2 law") held approximately even at high pressure.

Faeth et al. [9] recorded the liquid temperature histories of burning n-decane droplets suspended on thermocouples, and concluded that the droplets became supercritical at pressures in excess of twice the critical. These experiments were conducted at zero gravity in a free-fall apparatus, thus excluding the effects of natural convection.

Similar experiments were performed for n-octane and n-decane by Lazar and Faeth [20]. Combustion experiments were performed on single droplets suspended from thermocouples by Kadota and Hiroyasu [17] for various paraffins; their results show that the droplet remains subcritical up to at least 1.5 times the critical

pressure.

2.4 Mathematical Models

The first model of high pressure droplet combustion devised was that of Spalding [33], which treats the droplet as a point source of fuel vapour of finite mass and solves the transient diffusion equation analytically to arrive at a simple expression for the flame radius and burning time. As no liquid phase is present in this model, it is strictly only valid for supercritical combustion (liquid pressure and temperature above the critical values).

A similar model is presented by Rosner [29] using a finite rather than a point source of vapour; its results agree closely with those of Spalding [33]. In both models constant density and transport properties were assumed.

Wieber [40] used results from the classical quasi-steady theory of droplet vaporization (see example Bergeron and Hallett [5]) to calculate liquid temperature histories at pressures up to the critical. Vapour pressures were taken from tabulated data. Although the quasi-steady theory is invalid at high pressures because of the increasing importance of gas phase transients, the calculations do give some qualitative idea of what is to be expected: they suggest that a stationary n-heptane droplet will not exceed the critical temperature unless the pressure is some 2.3 times the critical (1.8 times for a droplet with rapid external air flow).

2.5 Pressure Effects on VLE

Manrique and Borman [22] presented the earliest model to take into account the effects of high pressure on vapour-liquid equilibrium. Quasi-steady solutions to the

equations for the vapour phase were obtained numerically for a CO_2 droplet of constant diameter and temperature evaporating into N_2 (equivalent to a porous sphere experiment where fuel is supplied to the center of a porous sphere suspended in a combustion chamber. This experiment can be used to simulate steady state evaporation or combustion). Transport properties were allowed to vary in space, and the Redlich-Kwong equation of state was used both for vapour-liquid equilibrium and for gas-phase densities. The results show that a significant amount of ambient gas (N_2) dissolves in the surface of the droplet as the critical point is approached. Comparison with a low pressure model in which non-ideal effects were omitted and properties assumed constant showed that the low pressure model overpredicted droplet temperature and underpredicted vaporization rates somewhat at low pressures, and diverged wildly at pressures in excess of about 1.2 times the critical. It should be noted at this juncture that the critical point of significance here is not actually that of pure liquid, but rather is the critical mixing state for the mixture at the liquid surface, which varies with composition.

Savery and Borman [32] used the same vapour-liquid equilibrium model together with results from quasi-steady vaporization theory with constant properties to calculate the liquid temperature history for a droplet which heats up and vaporizes. Predictions were compared to data from experiments on suspended n-heptane and Freon-13 droplets, but the absence of the gas phase transient term from the equations makes the results inconclusive at high pressures because the difference in density of liquid and gas is smaller. Also, the model does not include liquid phase processes, but these processes are important. However, the results do show the importance of absorption of ambient gas in the liquid at high pressure.

Lazar and Faeth [20] presented an analytical quasi-steady theory with variable properties for combustion of a constant temperature, constant diameter sphere. The Redlich-Kwong equation of state was again used to describe VLE, but the gas phase density was evaluated using the perfect gas law. The droplet reached its critical

state at roughly 2.5 times the fuel critical pressure, at which point the mol fraction of dissolved nitrogen in the liquid was some 0.15 - 0.20.

This model was extended by Canada and Faeth [7] to include combustion products (H_2O and CO_2) in the vapour-liquid equilibrium calculation, giving four components in all; this did not significantly effect burning rates or droplet temperatures, but did change the calculated critical mixing states. High pressure and low pressure (i.e. with ideal mixture behaviour at the surface) theories were compared with each other and with results of porous sphere experiments on several n-paraffins and alcohols. Significant differences in droplet temperatures were observed between the two theories, although the predicted burning rates were very similar. Comparisons with experimental data were inconclusive, sometimes favouring one theory, sometimes the other.

Very similar results were obtained by Canada and Faeth [6] for combustion of a porous sphere in a gas flow.

Umemura [36] developed a mathematical model for supercritical liquid combustion for the binary systems of n-butane and nitrogen and of oxygen and nitrogen. The Redlich - Kwong equation of state was used to calculate vapour liquid equilibrium. In this model a critical state is achieved but model does not include liquid heating and absorption of ambient gas in the liquid.

It should be pointed out that solutions can be strongly affected by the choice of transport properties (thermal conductivity, specific heat, diffusivity); the models of Faeth and co-workers assume a linear variation of both specific heat and thermal conductivity in order to obtain an analytical solution to the equations in the gas phase, whereas conductivity actually varies roughly as the square root of temperature.

2.6 Numerical Solutions

Matlosz et al. [24] presented a numerical solution of the governing equations, including transient terms, the effects of droplet heating and surface regression, for evaporating n-hexane droplets in nitrogen. The Redlich-Kwong equation of state was used, but the solubility of ambient gas in the liquid was neglected on the grounds that it only becomes important towards the end of the droplet heating history. An important conclusion of the model was that the gas phase Lewis number, the ratio of thermal to mass diffusivity, had a strong effect on the predicted liquid temperature and diameter histories; this indicates that correct prediction of transport properties is important. The mass diffusivity required to fit the results to measured temperature and diameter histories for suspended droplets proved to be considerably higher than that predicted using an (unspecified) correlation; this could either be due to inadequacies in the correlation or to experimental error. This model also did not include the liquid phase heating process and they did not reach the critical point.

Gas phase transients were also included by Rosner and Chang [30] in a numerical solution with constant properties for a constant temperature droplet. Droplets of n-dodecane were predicted to become supercritical only at a pressure of 2.96 times the critical. The calculations showed that omitting the gas phase transient terms would result in a large underprediction of vaporization rate as pressure rose.

Lee and Fernandez-Pello [21] have presented a model for a droplet vaporizing at constant temperature, in which the energy equation is expanded in a series in time and then solved numerically. No vapour pressure relationship is used; instead, the energy equation is solved for the heat transfer to the droplet, thus fixing the evaporation rate, which in turn through conservation of fluxes at the surface is used to solve for the surface mass fraction. This results in the remarkable - and physically incorrect - conclusion that the surface vapour pressure varies while the liquid temperature remains fixed.

2.7 Two-Component Models

Two studies have been made of two-component droplets evaporating at high pressure. Jin and Borman [16] presented a model for the heating up and evaporation of a pentane/octane droplet, in which a simple quasi-steady solution for the gas phase was coupled with a detailed numerical solution of heat conduction and component diffusion in the droplet liquid. The Redlich-Kwong equation was used to describe the mixtures at the liquid surface, but the gas phase was assumed ideal.

Most recently, Hsieh and Shuen [13] have developed numerical solutions to the full transient governing equations for a two-component (n-pentane/n-octane) fuel droplet using the Redlich-Kwong equation of state. Again, the importance of including high pressure effects (transient effects, surface regression, solubility of ambient gas in the liquid phase) is demonstrated. A comparision of calculations made with a diffusivity which varied with temperature and pressure with those for constant diffusivity showed a substantial difference.

2.8 Ignition

Only one paper has appeard on droplet ignition at high pressure: this is the work of Kadota et al. [17], who performed suspended droplet experiments similar to those of Bergeron and Hallett [5,4,3]. A simple model of vaporization based on quasi-steady theory and correlation of the results with pressure and temperature were presented, but no complete model of the ignition process was developed. This paper presents experimental and theoretical studies on the ignition delay for normal paraffin hydrocarbon droplets at ambient gas temperatures of 220–700°C. In the theory, a model was developed for droplet ignition, which consisted of the evaporation of a droplet and ignition of a homogeneous gas mixture. From that the ignition time was

calculated. The results were that ignition delay decreases rapidly with an increase in temperature and increases with an increase in the number of carbon atoms in a molecule of fuel and is independent of droplet size. This model includes droplet heating but there is not specific mention of pressure effects in the model.

2.9 Summary

From the papers reviewed here, a number of conclusions for the present work can be drawn:

- an adequate model for high pressures must account for non ideal behaviour and absorption of air by the liquid;
- many models use quasi-steady solutions for the gas phase, but more detailed solutions show that the transient terms must be included at high pressures;
- the droplet will not become supercritical during its lifetime unless the ambient pressure is much greater than the critical pressure of fuel;
- most models include non-ideal effects at droplet surface eg. correct accounting for enthalpy changes in vaporization and absorption of ambient gas in the liquid by using the Redlich–Kwong EOS. Not including these leads to large errors in of droplet temperature;
- some models used vapour pressure correlations instead an equation of state at high pressure, which can lead to large errors in calculations of evaporation rates or droplet temperature;
- models did not include the pressure and temperature dependence on transport properties, but these can greatly influence the results;

- most models did not include liquid phase processes (except droplet heating). Their effect is unknown and must be investigated.

These conclusions will be investigated and discussed later.

Chapter 3

Mathematical Model

3.1 Introduction

The purpose of a mathematical model is to allow reliable extrapolation of experimental results and to yield information and conclusions about the fundamental processes at work which cannot be obtained from experiments.
The mathematical model is to predict the ignition delay of liquid fuel droplets which are suddenly exposed to a hot, high pressure environment. A mathematical model of the ignition process of liquid droplets requires solution of continuity, energy and species diffusion equations in the vapour phase surrounding the droplet. These must be coupled with a description of the heating of the liquid phase, and, in the case of a multicomponent fuel, of diffusion of fuel components in the droplet.

The model uses finite difference techniques to solve the governing equations as in the earlier model of Bergeron & Hallett [5]. In order to extend the earlier model to high pressure, several modifications are necessary:

- The Antoine equation for vapour pressure and the perfect gas law used by Bergeron and Hallett [5] lose their validity at high pressure, and must be replaced by a suitable equation of state.
- Transport property correlations suitable for high pressure are required.
- The effects of pressure on reaction rate must be accounted for by proper selection of concentration exponents for fuel and air.

3.2 Assumptions

The following assumptions were made to produce a simplified model and reduce computational effort:

- the droplet temperature is uniform (but may vary in time);
- the reactant consumption prior to ignition is neglected. This allows diffusion equations for oxygen and products to be omitted and the ratio of oxygen to nitrogen to be set constant and equal to the ambient value;
- transport properties are uniform in space, but may vary in time. These are evaluated at a suitable average temperature and composition;
- spherical symmetry of the droplet and surroundings , so that only radial transport is possible. Thus the analysis is reduced to one dimension.

These same assumptions were used for the earlier model; they are discussed and justified in Bergeron & Hallett [5].

3.3 Basic Equations

3.3.1 Vapour Phase

The governing differential equations for the vapour phase are:

Energy Equation:

$$\rho C_p \frac{\partial T}{\partial t} + \rho v C_p \frac{\partial T}{\partial r} = \frac{1}{r^2}\frac{\partial}{\partial r}(r^2 k \frac{\partial T}{\partial r}) - \sum C_{pi} j_i \frac{\partial T}{\partial r} - \sum h_i \dot{W}_i \qquad (3.1)$$

Diffusion Equation:

$$\rho \frac{\partial Y_i}{\partial t} + \rho v \frac{\partial Y_i}{\partial r} = \frac{1}{r^2}\frac{\partial}{\partial r}(r^2 \Gamma_i \frac{\partial Y_i}{\partial r}) + \dot{W}_i \qquad (3.2)$$

Continuity Equation:

$$\frac{\partial \rho}{\partial t} + \frac{1}{r^2}\frac{\partial}{\partial r}(r^2 \rho v) = 0 \qquad (3.3)$$

In one earlier version of the model of Bergeron & Hallett [5] the transient ($\frac{\partial}{\partial t}$) terms were dropped from the diffusion and continuity equations, so that vapour-phase concentrations and flow velocities could be represented by the "classical" quasi-steady theory of droplet vaporization. The basis for this assumption is the observation that vapour-phase densities are much less than that of the liquid phase. At high pressure, this is no longer true, and the quasi-steady assumption is no longer valid. A full transient solution of the governing equations is then necessary, as described in Bergeron & Hallett [3,4].

3.3.2 Liquid Phase

With the assumption of uniform liquid temperature, the transient heating of the droplet is described by a simple heat balance:
Energy absorbed in droplet + Energy for evaporation = Heat flux to droplet

$$\frac{4}{3}\pi R^3 \rho_l C_{Pl} \frac{dT_l}{dt} + 4\pi R^2 G h_v = 4\pi R^2 Q \tag{3.4}$$

where heat flux Q to the droplet surface is calculated from the temperature gradient at the surface (conduction) and the thermal radiation transfer to the droplet

$$Q = k \frac{\partial T}{\partial r} \mid_R + \alpha_d \sigma (T_\infty^4 - T_R^4) \tag{3.5}$$

The shrinking of the droplet as evaporation proceeds is described by

$$\frac{dR}{dt} = \dot{R} = -\frac{G}{\rho_l} \tag{3.6}$$

The flux expression required to calculate G will be discussed later.

At high pressure some air can be dissolved in the liquid phase. The species transport in the liquid phase is modelled by a single radial diffusion equation with an equivalent diffusivity equal to some multiple f of the molecular diffusivity D_L:

$$\frac{\partial Y_i}{\partial t} = \frac{1}{r^2} f D_L \frac{\partial}{\partial r}(r^2 \frac{\partial Y_i}{\partial r}) \tag{3.7}$$

The factor f accounts for the fact that some internal circulation is nearly always present in a droplet, so that the effective rate of diffusion is higher than given by D_L alone (Talley and Yao [34]).

3.3.3 Boundary and Initial Conditions

The boundary and initial conditions applied to the system are:

1. Boundary conditions:

   - at the droplet surface (r = R): $T = T_R$, $X = X_{FR}$, $Y_F = Y_{FR}$
   - at infinity ($r \rightarrow \infty$): $T = T_\infty$, $Y_F = 0$
   - at the centre of the droplet $\partial X_F / \partial r = 0$ (symmetry)

2. Initial conditions:

   - t = 0: $T = T_\infty$ for $r > R$
   - t = 0: $Y_F = 0$ for $r > R$
   - t = 0: X_F, X_A uniform for all $r < R$

3.3.4 Chemical Reaction Modelling

The mathematical model is completed by calculating the reaction rate of hydrocarbon mixture.

The actual reactions of hydrocarbon fuels with oxygen are complex chain processes, involving dozens of reaction steps and intermediate species. Recent kinetic work presents detailed kinetic models of the oxidation of paraffins, but these are too complex for inclusion in the present model. For the present work a one-step irreversible reaction model was adopted as in the earlier model (Bergeron & Hallett [4]):

$$C_n H_m + (n + \frac{m}{4}) O_2 \rightarrow nCO_2 + \frac{m}{2} H_2 O$$

with the rate given by the Arrhenius equation:

$$W_F = -M_F K \rho^{a+b} \frac{Y_F^a Y_O^b}{M_F^a M_O^b} exp(-\frac{E}{\mathcal{R}T}) \tag{3.8}$$

The present model uses the same a, b, K and E parameters as the previous model of Bergeron & Hallett [3]. The exponents a and b were taken from work by Westbrook

and Dryer [39], but values of K and E were fitted to experimental droplet ignition data using the model. The constants a and b dictate the pressure dependence of the rate; they are not based on much data, and may have to be modified when experimental data become available.

Table 1. presents these values for the substances of interest.

3.4 Finite Volume Solution

Equations (3.1-3.7) together with the boundary and initial conditions were cast into finite difference form as described in the previous work (Bergeron & Hallett [5]). Although development of the finite difference equations and the algorithm required to solve them was not part of the work undertaken for this thesis, the methods used are briefly summarized here for the sake of convenience.

- Coordinate transformation

$$\xi = \frac{r}{R} \tag{3.9}$$

  It was necessary to introduce a new transformed coordinate to keep the surface of the droplet on the first grid point, otherwise the droplet surface would recede with respect to the first grid point as the droplet vaporized.

- New velocity

  The mixture velocity relative to the new coordinate system is:

$$w = v - \xi \dot{R} \tag{3.10}$$

- Transformed equations:

  Energy Equation:

$$\xi^2\frac{\partial}{\partial t}(\rho T) + \frac{1}{R}\frac{\partial}{\partial \xi}(\xi^2 \rho w T) + \rho T\frac{\dot{R}}{R}\frac{\partial}{\partial \xi}(\xi^3) - \frac{\xi^2}{R^2}\left[\sum_{i=1}^{N}\frac{C_{pi}}{C_p}\Gamma\frac{\partial Y_i}{\partial \xi}\right]\frac{\partial T}{\partial \xi}$$
$$= \frac{1}{R^2}\frac{k}{C_p}\frac{\partial}{\partial \xi}\left(\xi^2\frac{\partial T}{\partial \xi}\right) - \frac{\xi^2}{C_p}W_F H_F \qquad (3.11)$$

Diffusion Equation:

$$\xi^2\frac{\partial}{\partial t}(\rho Y_F) + \frac{1}{R}\frac{\partial}{\partial \xi}(\xi^2 \rho w Y_F) + \rho Y_F\frac{\dot{R}}{R}\frac{\partial}{\partial \xi}(\xi^3) = \frac{1}{R^2}\Gamma\frac{\partial}{\partial \xi}\left(\xi^2\frac{\partial Y_F}{\partial \xi}\right) \qquad (3.12)$$

Continuity Equation:

$$\xi^2\frac{\partial \rho}{\partial t} + \frac{1}{R}\frac{\partial}{\partial \xi}(\xi^2 \rho w) + \rho\frac{\dot{R}}{R}\frac{\partial}{\partial \xi}(\xi^3) = 0 \qquad (3.13)$$

Liquid Equation:

$$\xi^2\frac{\partial N_i}{\partial t} - \frac{\dot{R}}{R}\xi^3\frac{\partial N_i}{\partial \xi} = \frac{f D_L}{R^2}\frac{\partial}{\partial \xi}\left(\xi^2\frac{\partial N_i}{\partial \xi}\right) \qquad (3.14)$$

The finite volume techniques described by Patankar [26] were used to integrate these equations over a radial control volume (see Fig. 2 and Fig. 3) to obtain algebraic difference equations of the following form:

- temperature:

$$\mathbf{a}T_P = \mathbf{b}T_E + \mathbf{c}T_W + a^\circ T_P^\circ + S \qquad (3.15)$$

- concentration:

$$\mathbf{a}Y_{iP} = \mathbf{b}Y_{iE} + \mathbf{c}Y_{iW} + a^\circ Y_{iP}^\circ \qquad (3.16)$$

where P is the point being solved for and W and E are its west and east neighbours. The coefficients **a**, **b**, **c**, and a° are obtained by integrating each term of the differential equation over the control volume and over the time interval t to $t + \Delta t$.

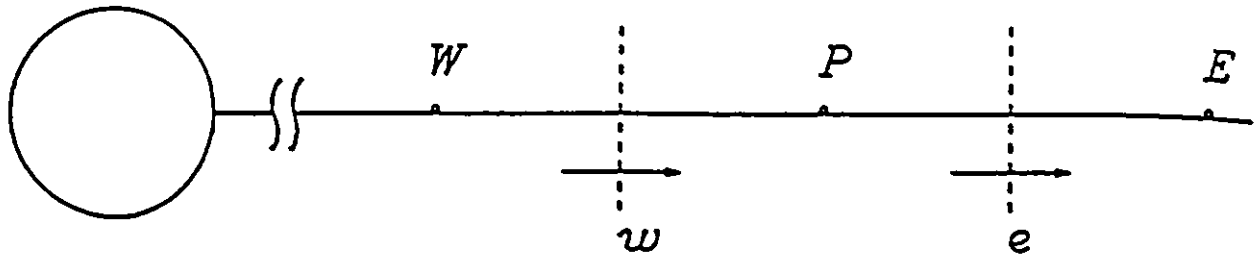

Figure 2: Diagram of cell around droplet

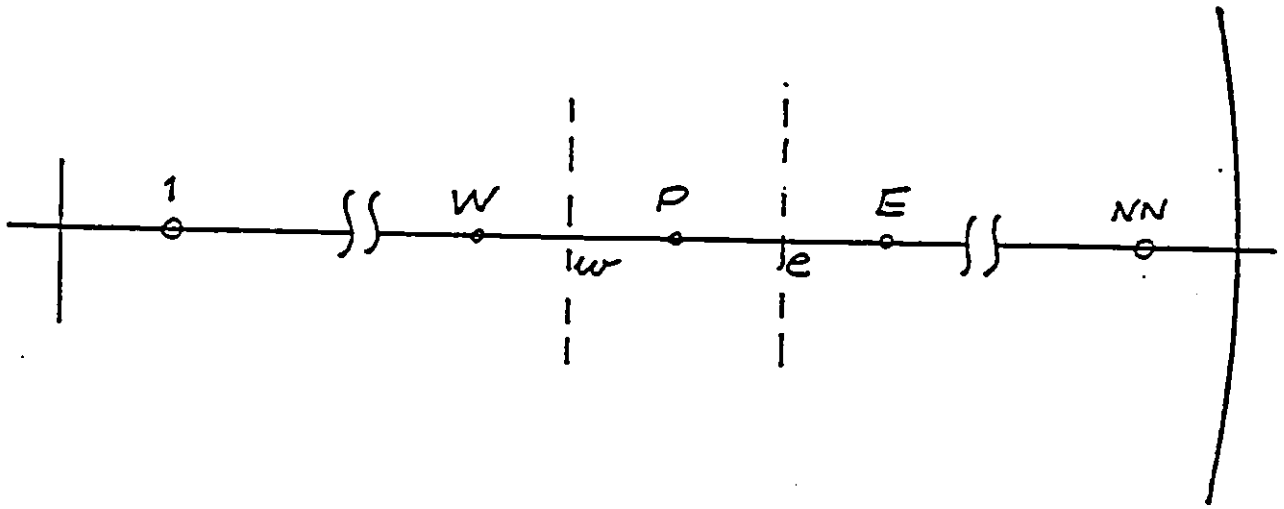

Figure 3: Diagram of cell inside droplet

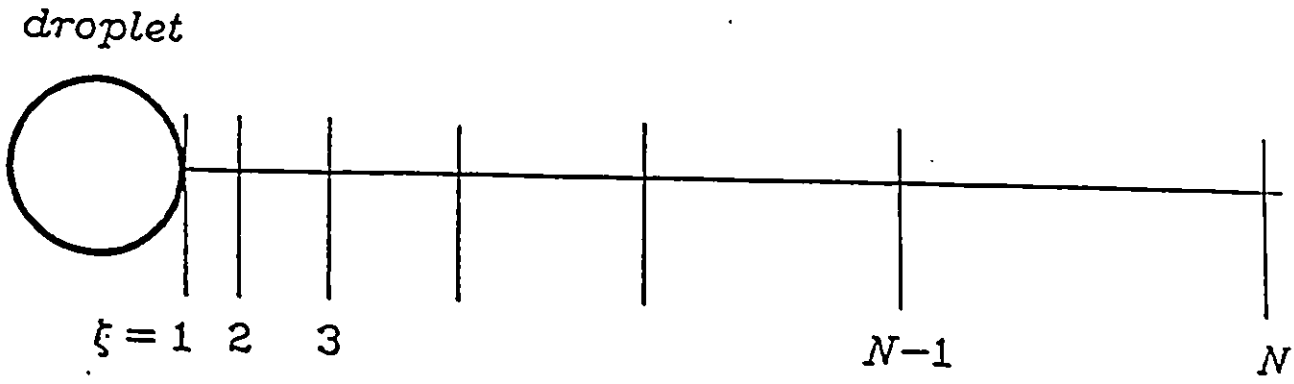

Figure 4: Exponentially spaced grid

To deal with the transient behaviour of the system an implicit solution was used: T and Y represent values at the current time step ($t + \Delta t$), while T^o and Y^o are those from the previous time t. For more details see Patankar [26] or Bergeron and Hallett [4]. The difference equations are presented in Appendix A.

The resulting sets of simultaneous algebraic equations are then solved iteratively at each time step, and the solution proceeds step by step through time.

An iterative process is required to establish values of temperature, liquid and vapour phase mass fractions, and mass fractions at the droplet surface. The interdependence of density, concentration, temperature and velocity in the governing equations also requires that these be solved iteratively for given set of surface conditions.

3.4.1 Grid spacing

Because of the nature of the temperature and concentration profiles it is necessary to have more points near the droplet surface and fewer points far from the surface. To obtain this, a suitable choice of grid points is necessary and is shown on Fig. 4.

In the vapour phase an exponentially spaced grid is used:

$$\xi(i) = exp\left[\frac{\ln \xi(N)}{N-1}(i-1)\right] \tag{3.17}$$

In the liquid phase most of the droplet mass lies near the surface; hence a cubic equation is used for the grid, which carves the droplet up into layers of roughly equal mass:

$$\xi(i) = \left[\frac{i-1}{NN-1}\right]^{\frac{1}{3}} \tag{3.18}$$

where N and NN are the number of grid points outside and inside the droplet respectively.

It should be noted that an increase in pressure requires changes in the grid calculation. For pressures of 1, 5 and even 10 atm the outer boundary is situated at $\xi = 500$ droplet radii, which allows sufficient room for concentration profiles to develop as though the vapour phase were of infinite extent, and the temperature profile near the boundary is nearly flat. For higher pressure it was necessary to situate the outer boundary at 50 droplet radii in order to give enough points close to the droplet surface to make calculations sufficiently accurate.

3.5 Vapour-Liquid Equilibrium Model (VLE)

As the literature on droplet evaporation and combustion at high pressure shows, the correct treatment of VLE must consider departures from ideal solution and perfect gas behaviour at the liquid surface, accounting for enthalpy changes in vaporization, and the absorption of ambient gas in the liquid. A number of authors have confirmed this by making calculations for quasi-steady vaporization, for which these effects are

the only high-pressure phenomena to be modelled (Lazar and Faeth [20], Manrique and Borman [22], Canada et al. [7,6]). Omission of these does not affect the evaporation rate very strongly, except at pressures well in excess of the critical (Manrique and Borman [22]), but does result in significant overprediction of droplet liquid temperatures. However, calculations which include gas-phase transients show a much larger influence of non-ideal effects on evaporation rates (Matlosz et al.[24], Hsieh and Shuen [13]). Neglect of ambient gas absorption alone can lead to large errors in both quantities (Manrique and Borman [22], Savery and Borman [32]).

The approach favoured for calculating VLE in the literature cited is to use an equation of state rather than a vapour pressure correlation. This is the approach usually recommended for high pressure (Reid et al.[27]). The same equation of state can be used to evaluate vapour-phase densities, although some authors have used the perfect gas law here (Lazar and Faeth [20], Canada and Faeth [7], Jin and Borman [16]).

The VLE calculations reviewed have treated air as pure nitrogen and have neglected combustion products, thus reducing the problem to a two-component mixture - fuel and nitrogen (for a single component fuel) and a three-component mixture in the case of two-fuel component mixture (two fuels and nitrogen). This appears to be justified by the calculations of Canada and Faeth [7] for a more complex mixture with products included.

3.5.1 Choice of Equation of State (EOS)

Having concluded that an equation of state is to be used for modelling VLE at the droplet surface, a suitable equation must be selected. All of the works cited with detailed models of VLE have employed the Redlich-Kwong equation. This is one of a family of equations of state referred to as cubic equations, because they are cubic in specific volume. The general form of these equations is:

$$P = \frac{RT}{V - b} - \frac{a}{V^2 + ubV + wb^2} \tag{3.19}$$

The simplest of these is the classical van der Waals equation, which is not sufficiently accurate for practical use. Parameters a and b are functions of critical temperature and pressure, but for mixtures are also functions of composition. For mixtures of two or more components these parameters are calculated with well-established mixing rules which are valid for all forms of cubic equation (Reid et al. [27]):

$$a_m = \sum_i \sum_j y_i y_j (a_i a_j)^{1/2} (1 - k_{ij}) \tag{3.20}$$

$$b_m = \sum_i y_i b_i \tag{3.21}$$

The binary interaction coefficients k_{ij} must be known from experimental data for each pair of components involved. Since in the present work VLE calculations must always be made for a mixture with at least two components so as to allow for absorption of gas into the liquid surface, the choice of equation of state will be partly constrained by the availability of k_{ij} values for the compounds of interest.

The Redlich-Kwong equation is no longer considered to be the best one and has been superseded by newer versions, the most popular of which are the Soave-Redlich-Kwong and the Peng-Robinson EOS. Extensive tabulations of binary interaction coefficients are available for both of these (Knapp et al. [18]). A recent survey of the accuracy of 10 different cubic EOS for 75 pure components (Trebble and Bishnoi [35]) showed that the Peng-Robinson EOS is one of the best for the prediction of vapour volumes at and near saturation. For the 75 compounds tested, the Peng-Robinson equation predicted the vapour pressure to within an absolute average deviation of 1.39% (best equation 1.27%) and the saturated vapour volume to within 5.34% (best equation 5.08%); deviations for hydrocarbons were even

lower than these. The Peng-Robinson equation is not the best for predicting liquid volumes (8.58% average deviation), but this is a little concern in the present work, as the liquid volume affects only the droplet diameter, a parameter which is known to be of little importance (Bergeron and Hallett [5]).

The work of Adachi et al.[2] also shows the superiority of the Peng-Robinson equation for predicting the saturated vapour volume of paraffin hydrocarbons. Adachi and Lu [1] have recently developed another cubic EOS which for pure components is slightly more accurate than the Peng-Robinson (Trebble and Bishnoi [35], Adachi and Lu [1]), and shows some improvement for two-component mixtures (Adachi and Lu [1]). However, only a limited number of binary interaction coefficients k_{ij} are tabulated for this equation.

More complex EOS are available, the most popular of which is probably the Lee-Kesler (Reid et al. [27]). It is claimed to give better results far from the saturation state than the cubic equations; however, since the prediction of VLE is the main concern here, this advantage is of little consequence. A prime advantage of a cubic equation is its computational simplicity, as it can be solved explicitly (without iteration) for volume.

3.5.2 Peng-Robinson EOS

From the above discussion, it will be clear that the choice falls upon the Peng-Robinson EOS. It is defined by:

u = 2, w = -1, and

$$b = \frac{0.07780\mathcal{R}T_c}{P_c} \tag{3.22}$$

$$a = \frac{0.45724\mathcal{R}^2T_c^2}{P_c}[1 + f(1 - T_r^{1/2})]^2 \tag{3.23}$$

where

$$f = 0.37464 + 1.54226\omega - 0.26992\omega^2 \tag{3.24}$$

To solve this equation it is more convenient to write it in terms of compressibility factor Z :

$$Z^3-(1+B+C+D)Z^2+(A+C+D+BC+BD+CD)Z-AB-CD-BCD = 0 \tag{3.25}$$

where A, B, C, D are dimensionless constants, which are :

$$A = \frac{aP}{\mathcal{R}^2T^2}$$

$$B = \frac{bP}{\mathcal{R}T}$$

$$C = -(1+\sqrt{2})B$$

$$D = -(1-\sqrt{2})B$$

For a mixture, a and b are calculated from the pure component a and b using Eq. 3.20 and 3.21.

The acentric factor ω is a constant which is tabulated for most compounds of interest in Reid et al. [27]. The literature cited has shown that this equation works very well, particulary for hydrocarbons near the saturation state. As a caveat, it should be noted that the Peng-Robinson equation, together with many other EOS, is not generally recommended for polar molecules: for alcohols, for example, it gives errors that are 2-3 times as great as the averages quoted earlier (Trebble and Bishnoi [35]). This is of little concern at the moment, as the present work is only concerned with hydrocarbons.

An iterative solution is necessary for solving the equation of state for the equilibrium compositions of two or three component mixtures (fuel and air or two fuel components and air) in both liquid and vapour phases.

The computer software for most of the VLE calculation steps was kindly provided by Prof. B.C.-Y. Lu and Dr. M. Margerum of the Department of Chemical

Engineering at the University of Ottawa. The calculations and numerical methods are general procedures, applicable to most cubic equations of state with most mixing rules. The following procedure explains briefly the calculation of VLE :

- For a given P, T and initial trial values of x_F and y_F (note that x_A=1-x_F, y_A=1-y_F) the root secant method (subroutine RTSEC) is used to solve iteratively for the correct value of x_F, subject to

$$\sum y_i = \sum K_i x_i = 1$$

- At each iteration step the equilibrium constant $K_i = y_i/x_i$ for each component is calculated (subroutine KCALC) as

$$K_i = \phi_i^L/\phi_i^V$$

- From the Peng-Robinson equation the fugacity coefficients ϕ are

$$\begin{aligned}\ln\phi_i &= \frac{\hat{B}_i}{Z-B} - \ln(Z-B) + \left(\frac{\hat{C}_i - \hat{D}_i}{C-D} - 1 - \frac{\hat{A}_i}{A}\right)\frac{A}{C-D}\ln\frac{Z-D}{Z-C} \\ &- \frac{A}{C-D}\left(\frac{\hat{C}_i}{Z-C} - \frac{\hat{D}_i}{Z-D}\right)\end{aligned}$$

  where $\hat{A}_i$, $\hat{B}_i$, $\hat{C}_i$ are the derivatives of A_i, B_i, C_i (subroutines MIXGEO, MIXAR).

- The compressibility factors Z for vapour (V) and liquid (L) are found by solution of Eq. 3.25 using subroutine RTCUB.

- In calculating the K_i at each step new values of the y_i are calculated (FBUBP) as

$$y_i' = \frac{K_i x_i}{\sum K_i x_i}$$

The calculations are controlled by routine BUBX. Further details about the method and modelling techniques can be found in the Ph.D. thesis of Michael R. Margerum [23].

3.5.3 Enthalpy Change on Evaporation

At high pressure, as air is absorbed in to the liquid, the enthalpy change due to evaporation is no longer the pure fuel enthalpy of vaporization (h_{fg}). Instead, the enthalpy change for each component must be accounted for separately, so that an effective heat of vaporization (h_v) can be defined as:

$$h_v = \frac{1}{G}\left[G_F\left(H_F^V - H_F^L\right) + G_A\left(H_A^V - H_A^L\right)\right] \tag{3.26}$$

where $H_i = \overline{H}_i/M_i$.

This equation weights the component enthalpy changes in passing from the liquid to the vapour phase by the mass fluxes of the individual components from the surface. The partial molal enthalpy $\overline{H}_i$ is a function not only of temperature and pressure but also of mixture composition and is not equal to the pure component enthalpy $\overline{h}_i$ unless the mixture is ideal.

The $\overline{H}_i$ include the effects of enthalpy changes on mixing. The $\overline{H}_i$ are best evaluated as (Van Wylen and Sonntag [37]) :

$$\overline{H}_i = \overline{h}_i^\circ - \overline{\mathcal{R}}T^2\frac{\partial}{\partial T}(\ln\phi_i)_{P,y} \tag{3.27}$$

where $\phi_i = \frac{f_i}{y_i P}$ is the fugacity coefficient. The perfect gas enthalpies $\overline{h}_i^\circ$ are given by polynomial expressions derived by integration of the ideal gas specific heat equation given by Reid et al [28]

$$\overline{h}_i^\circ = A_i T + \frac{B_i}{2}T^2 + \frac{C_i}{3}T^3 + \frac{D_i}{4}T^4 \tag{3.28}$$

where $A_i, \ldots, D_i$ - are constants, given by Reid et al. [28].

The expression $\frac{\partial}{\partial T}(\ln\phi_i)$ was evaluated numerically, as recommended by Walas [38] :

$$\frac{\partial(\ln\phi_i)}{\partial T} = \frac{(\ln\phi_i)_T - (\ln\phi_i)_{T-\Delta T}}{\Delta T} \tag{3.29}$$

where ΔT is a small increment in temperature, in our case selected as 0.2 K, and the values of ϕ_i were calculated from the solution of the Peng-Robinson equation.

3.6 Diffusion in the Liquid Phase - Single Component Fuel

3.6.1 Flux Expressions at the Liquid Surface

Although at low pressure air does not penetrate the surface, at high pressure air can either be absorbed by the liquid ($G_A < 0$, $G_F > G$) or desorbed from the liquid ($G_A > 0$).

The liquid and vapour phases are coupled by the fluxes at the liquid surface. The fluxes in the vapour phase are given by:

$$FUEL: \quad G_F = GY_{FR} - \Gamma \frac{\partial Y_F}{\partial r} |_R \tag{3.30}$$

$$AIR: \quad G_A = G(1 - Y_{FR}) + \Gamma \frac{\partial Y_F}{\partial r} |_R = G - G_F \tag{3.31}$$

where the total flux $G = G_F + G_A$;

and in the liquid phase by :

$$FUEL: \quad G_F = X_{FR}G - \Gamma_L \frac{\partial X_F}{\partial r} |_R \tag{3.32}$$

$$AIR: \quad G_A = X_{AR}G - \Gamma_L \frac{\partial X_A}{\partial r} |_R = G(1 - X_{FR}) + \Gamma_L \frac{\partial X_F}{\partial r} |_R \tag{3.33}$$

where the first term represents the recession of the droplet surface due to evaporation.

For a given temperature and total pressure the state (X_{FR}, Y_{FR}) at the surface is determined by VLE.

Equating the expressions for G_F in the liquid and vapour phases :

$$G = \frac{\Gamma_L \frac{\partial X_F}{\partial r}|_R - \Gamma \frac{\partial Y_F}{\partial r}|_R}{X_{FR} - Y_{FR}} \tag{3.34}$$

The earlier model of Bergeron and Hallett [4,5] essentially sets $X_{FR} = 1$ and does not require the liquid diffusion term since air is not absorbed .

Work with the earlier model showed that a linear approximation to the concentration gradient in the vapour phase at the liquid surface was not sufficiently accurate; instead $(\frac{\partial Y_F}{\partial r})_R$ was evaluated by fitting a concentration profile of the form of the solution for quasi-steady droplet evaporation to the space between the surface and the first finite difference node in the vapour phase (Bergeron and Hallett [5]) :

$$\frac{1 - Y_F}{1 - Y_{FR}} = (A - Y_{FR})^{\frac{R-r}{r}} \tag{3.35}$$

The parameter A is solved for by substituting r and Y_F at this first node. This leads to the following equation for G:

$$G = \frac{\Gamma_L \frac{\partial X_F}{\partial r}|_R - \frac{\Gamma}{R}(1 - Y_{FR}) \ln(A - Y_{FR})}{X_{FR} - Y_{FR}} \tag{3.36}$$

This expression shows that the mass fluxes in the vapour phase are affected by events in the liquid. In order to assess the importance of this, transport of dissolved air in the liquid phase was modelled by solving the diffusion equation in the droplet (eq. 3.7), with the value of diffusivity being varied to assess the effects of the degree of internal mixing.

An important topic in the literature on droplet ignition has been the question of whether the liquid phase ever becomes supercritical. Since Y_{FR} and X_{FR} approach each other at the critical point, the above equation suggests that attaining the critical point would require an infinite mass flux, and hence be impossible.

3.6.2 Flux Expression for a Well-Mixed Liquid Phase

If the liquid phase is well-mixed the concentration gradient becomes zero , and the expression for liquid diffusion in Eq. 3.33 becomes undefined. In this case a new approach in writing mass flux equations is necessary.
Defining $\mathcal{G}_i = G_i/G$ and using the form of concentration profile near the surface defined by eq. 3.35, the component mass fluxes in the gas phase become :

$$G_i = \frac{\mathcal{A}_i}{1 - \frac{Y_{iR}}{\mathcal{G}_i}} = \mathcal{G}_i G \tag{3.37}$$

where $\mathcal{A}_i$ = - $\frac{\rho}{R}(1 - Y_{iR})\ln(A - Y_{iR})$ is the diffusion flux.

Solving for G

$$G = \frac{\mathcal{A}_i}{\mathcal{G}_i - Y_{iR}} \tag{3.38}$$

Writing this for i=fuel and i=air and equating

$$\frac{\mathcal{A}_F}{\mathcal{G}_F - Y_{FR}} = \frac{\mathcal{A}_A}{\mathcal{G}_A - Y_{AR}} \tag{3.39}$$

Now $\mathcal{G}_A$ = 1 - $\mathcal{G}_F$, so that

$$\mathcal{G}_F(1 + \frac{\mathcal{A}_F}{\mathcal{A}_A}) = \frac{\mathcal{A}_F}{\mathcal{A}_A}(1 - Y_{AR}) + Y_{FR} \tag{3.40}$$

This allows $\mathcal{G}_F$ to be found explicitly, from which G and G_A can be found.

3.7 Gas Phase Equation of State

The next, very important step in the modeling of ignition at high pressure was to test the behaviour of the vapour phase to see if it could be treated as a perfect gas.

Sample values of compressibility factor were obtained using typical vapour fuel mass fractions from the results of the present model for P = 50 atm and T_{amb} = 973 K for n-heptane and n-hexadecane. Data at points next to the liquid surface were used for tests, as these will show the largest deviations from ideal gas behaviour (low T, large fuel fraction). The air was treated as a mixture of nitrogen and oxygen. The Prausnitz - Gunn correlations for the pseudocritical parameters of the fuel/air mixture were used (Reid et al. [27]) :

$$T_{cm} = \sum_j y_j T_{cj} \tag{3.41}$$

$$P_{cm} = \mathcal{R} T_{cm} (\sum_j y_j Z_{cj}) / \sum_j y_j V_{cj} \tag{3.42}$$

The compressibility factor was obtained from the compressibility chart in Van Wylen and Sonntag [37] :

$$Z = Z(P_r, T_r) \quad \text{with} \quad P_r = P/P_{cm} \quad \text{and} \quad T_r = T/T_{cm}$$

and for all the cases Z was within 2.4% of 1. This shows that the use of the perfect gas law for the vapour phase is justified. The same test was performed for P = 50 atm and T_{amb} = 773 K for the same mixtures. In that case also the vapour phase is an ideal gas ($Z \approx 1$). Since the enthalpy of a perfect gas is a function only of temperature, the ideal gas specific heat can continue to be used for enthalpy calculations at high pressure. By definition the enthalpy of mixing of an ideal gas mixture is zero. Hence, the ideal gas assumption allows the low pressure model for the energy equation to be used without modification at high pressure .

The density of the local gas mixture is estimated using the ideal gas law.

$$\rho = \frac{MP}{\mathcal{R}T} \tag{3.43}$$

where M is the local mixture molecular weight:

$$M = \frac{1}{\sum \frac{Y_i}{M_i}} \tag{3.44}$$

with the temperature calculated from the previous time step.

3.8 Transport Properties

An important stage in development of the high pressure model is to account for the effects of pressure on the transport properties, especially the thermal conductivity and the diffusion coefficient.

3.8.1 Reference State for Vapour Phase Properties

The transport properties are generally a function of temperature and mixture composition in the gas phase and they can vary with time and location owing to change in the temperature and concentration gradients. However, Hubbard et al [14] concluded that the vaporization rate could be calculated with good accuracy using constant properties if these are evaluated at an average temperature and composition using Sparrow's 1/3 rule to estimate a reference temperature and composition:

$$T = \frac{2}{3}T_R + \frac{1}{3}T_\infty \tag{3.45}$$

$$Y_i = \frac{2}{3}Y_{iR} + \frac{1}{3}Y_{i\infty} \tag{3.46}$$

where subscripts R and ∞ represent the droplet surface and ambient conditions respectively.

3.8.2 Thermal Conductivity in the Gas Phase

The thermal conductivity varies significantly with small changes in pressure and temperature near the critical point and shows anomalous behaviour near the critical point. The explanation of this phenomenon is still not clear (Reid et al. [27]). However, the results of calculations so far suggest that the droplet itself cannot reach the critical state, so that the vapour phase away from the surface will always be superheated. Available correlations for properties at high pressure neglect the anomalies occurring at the critical point in any case.
Many investigators have correlated excess thermal conductivity as a function of PVT properties of the system (Reid et al. [27]) :

$$(k - k^{\circ}) = f(\rho)$$

with k° as low-pressure thermal conductivity at the same temperature.

The effects of T and P are included in k° and ρ respectively. Recent theoretical papers have not, as yet, led to accurate predictive techniques to estimate thermal conductivity at high pressure.

There are three estimation methods which give a good estimate of the excess thermal conductivity with errors averaging about 5 - 7% (Reid et al. [27]). All are about equally accurate:

1. Stiel and Thodos
2. Chung et al.
3. Ely and Hanley

None of these methods are applicable for polar substances, hydrogen or helium. For the present model the method of Stiel and Thodos was chosen for calculation

of thermal conductivity at high pressure, because of its simplicity and because the properties for this method were already in the model.
Stiel and Thodos assumed that $f(\rho)$ depends only on the critical parameters T_c, P_c, V_c, and on M and ρ. Based on data for many nonpolar substances including hydrocarbons a correlation was established (Reid [27]):

$$(k-k^\circ)\Gamma Z_c^5 = 1.22\cdot 10^{-2}[exp(0.535\rho)-1] \qquad \rho_r < 0.5 \qquad (3.47)$$

$$(k-k^\circ)\Gamma Z_c^5 = 1.14\cdot 10^{-2}[exp(0.670\rho)-1] \qquad 0.5 < \rho_r < 2. \quad (3.48)$$

$$(k-k^\circ)\Gamma Z_c^5 = 2.60\cdot 10^{-3}[exp(1.155\rho)+2.016] \qquad 2.0 < \rho_r < 2.8 (3.49)$$

with:

$$\Gamma = 210(T_c M/P_c^4)^{1/6}$$

$$\rho_r = V_c/V$$

$$V = ZRT/P$$

This procedure can be adapted for mixtures, since mixing and combining rules are available for determination of the pseudocritical parameters for mixtures. Of the several mixing rules available, that of Prausnitz and Gunn was used to determined pseudocritical parameters for the mixtures (Eq. 3.41 and 3.42) (Reid et al. [27]).

The low-pressure thermal conductivity k° is calculated as in the earlier atmospheric pressure model using the Eucken equation (Reid et al. [28]).

3.8.3 Diffusion Coefficient - Vapour Phase

For multicomponent mixtures an exact description of diffusion is given by the Stefan - Maxwell equations rather than Fick's law. Most workers, however, prefer to approximate multicomponent diffusion as binary diffusion of a component in the

mixture, using an effective binary diffusivity. In general this effective diffusivity is a function of concentration, but at low concentrations it becomes constant. In our case, the gas mixture behaviour is approximately ideal and the fuel concentration is quite low. Under these conditions the effective diffusivity becomes constant and can be taken equal to the binary diffusivity of fuel in air. This is the approach taken in this work.

At high pressure, the product DP or Dρ is no longer constant but decreases with an increase in P or ρ (Reid et al.[27]) . The gas phase may deviate significantly from an ideal gas, and some effects of composition have been noted (Reid et al.[27]). Therefore, equations for calculation of the diffusion coefficient agree with experiment at low or moderate pressures, but they are much less successful at high pressure. There are few experimental studies of binary diffusion coefficients at high pressure. Up to about half the critical pressure D_{AB}P is essentially constant. Above that pressure D_{AB}P decreases and at a P_r of about $2D_{AB}$ becomes proportional to $P_r^{1/2}$ (Reid et al. [27]). The value of D_{AB} is much less than that at low pressure. A few estimation methods have been proposed (Reid et al. [27]):

1. Takamashi has suggested a simple corresponding states method:
   $D_{AB}/(D_{AB})^\circ = f(T_r, P_r)$

2. Martur and Thodos suggested that D$\rho \approx$ (Dρ)°. This can be a good guideline, but near the critical point, it should be used with caution.

Here o refers to low-pressure values.

From the previous arguments (section 3.6.1) we know that the droplet cannot reach the critical condition during its life time, so that it is safe to assume D$\rho \approx$ constant. The method used to estimate the diffusion coefficient is the Chapman - Enskog theory with the Leonard - Jones 12-6 potential as in the earlier model of

Bergeron and Hallett [5] :

$$D_{AB} = 1.858 \cdot 10^{-3} T^{3/2} \frac{[(M_A + M_B)/M_A M_B]^{1/2}}{P \sigma_{AB}^2 \Omega_D} (1 \cdot 10^{-4}) \qquad (3.50)$$

with Ω_D and σ_{AB} calculated as in the previous model of Bergeron and Hallett [5].

3.8.4 Specific Heat - Vapour Phase

Heat capacity is calculated using the ideal gas polynomial equations given in Reid et al. [28] for fuels, oxygen and nitrogen. Component heat capacities are combined by their mass fraction, and since gas behaviour is ideal no heat of mixing is needed.

3.8.5 Diffusion Coefficient - Liquid Phase

The molecular diffusivity D_L was predicted using the Vignes corelation as in the earlier model of Bergeron and Hallett [5]:

$$D_L = (D^\circ_{AF})^{X_F} (D^\circ_{FA})^{X_A} \qquad (3.51)$$

where A is for air and F for fuel. Since X_A is very small and $X_F \approx 1$,

$$D_L \approx D^\circ_{AF} \qquad (3.52)$$

The correlation used for estimating D°_{AF} is the Wilke-Chang method (Reid et al. [28])

$$D^\circ_{AF} = 7.4 * 10^{-8} \frac{(\phi M_F)^{1/2} T}{\eta_F V_A^{0.6}} \qquad (3.53)$$

where ϕ is an association factor of solvent B which for unassociated solvents is equal to one. The liquid molal volume at the normal boiling point is estimated using the

Tyn and Calus method (Bergeron and Hallett [5]) :

$$V_b = 0.285 V_c^{1.048} \tag{3.54}$$

The liquid viscosity is estimated using a correlation given by Reid et al. [28]:

$$log\eta = (VISB)((1/T) - (1/VISTO)) \tag{3.55}$$

where *VISTO*, *VISB* are constants listed in Reid et al. [28].

3.8.6 Specific Heat - Liquid Phase

Heat capacity is calculated using the Luria and Benson liquid-heat capacity equation (Reid et al. [28]) :

$$C_{Pl} = A + BT + CT^2 + DT^3 \tag{3.56}$$

where $A.....D$ are coefficients obtained from Reid at al. [28].
For the liquid mixtures it is assumed that the mixture heat capacity is a mass-fraction average of the pure component values:

$$C_{Plm} = \sum_i X_i C_{Pli} \tag{3.57}$$

3.8.7 Radiant Absorptivity of Droplet

The absorptivity of the droplet to thermal radiation is treated in the same way as in the earlier model where the curve obtained for absorption with both refraction and internal reflection by Hottel et al [12] was fitted to give approximations to the absorptivity of the droplet in the model. The equation is:

$$\alpha_d = 0.89(1 - e^{-5.4R}) \tag{3.58}$$

where α_d is the absorptivity of droplet.

The absorptivity of large droplets is about 0.8, so that radiation makes a significant contribution to droplet heating (Faeth and Olson [10]).

3.9 Solution of the System of Equations

The equations developed in the previous sections must be solved at each time step. The sequence of calculation used is shown in Fig. 5.

An implicit scheme was chosen for the solution of the temperature and diffusion equations as in the earlier model of Bergeron and Hallett [5].

For trial values of temperature, concentration and mass fluxes the energy equation and the EOS are solved, which gives a surface vapour pressure, and a new gas phase temperature field. By solving the diffusion equation and liquid diffusion equation new fields of concentration in the vapour and liquid phases are obtained. After this the density and continuity equations are solved. Next the mass fluxes are obtained and checked for convergence, the criterion being

$$abs(\frac{G'_F - G_F}{G_F}) < 0.00001 \tag{3.59}$$

By calculation of heat flux to the liquid, the surface temperature is calculated and checked for convergence:

$$abs(\frac{T'_R - T_R}{T_R}) < 0.0001 \tag{3.60}$$

and a new value of T_R is calculated for the next iteration

$$T_{RNew} = \alpha T_R + (1 - \alpha) T'_R \tag{3.61}$$

where α is a relaxation factor equal to 0.3 which gives quick and reliable convergence.

As an ignition criterion it is said that ignition occurs if the temperature anywhere

in the gas phase exceeds 2000 K. which is approximately the adiabatic flame temperature for hydrocarbons. An iteration is performed at each time step to solve the differential equations and properties are updated at every time step.

Table 1: Chemical reaction constants of the fuels

Fuel	K x 10^{-4}	E	a	b
n-Heptane C_7H_{16}	0.36	14.2	0.25	1.50
n-Dodecane $C_{12}H_{26}$	0.95	17.7	0.25	1.50
n-Hexadecane $C_{16}H_{34}$	0.76	17.8	0.25	1.50

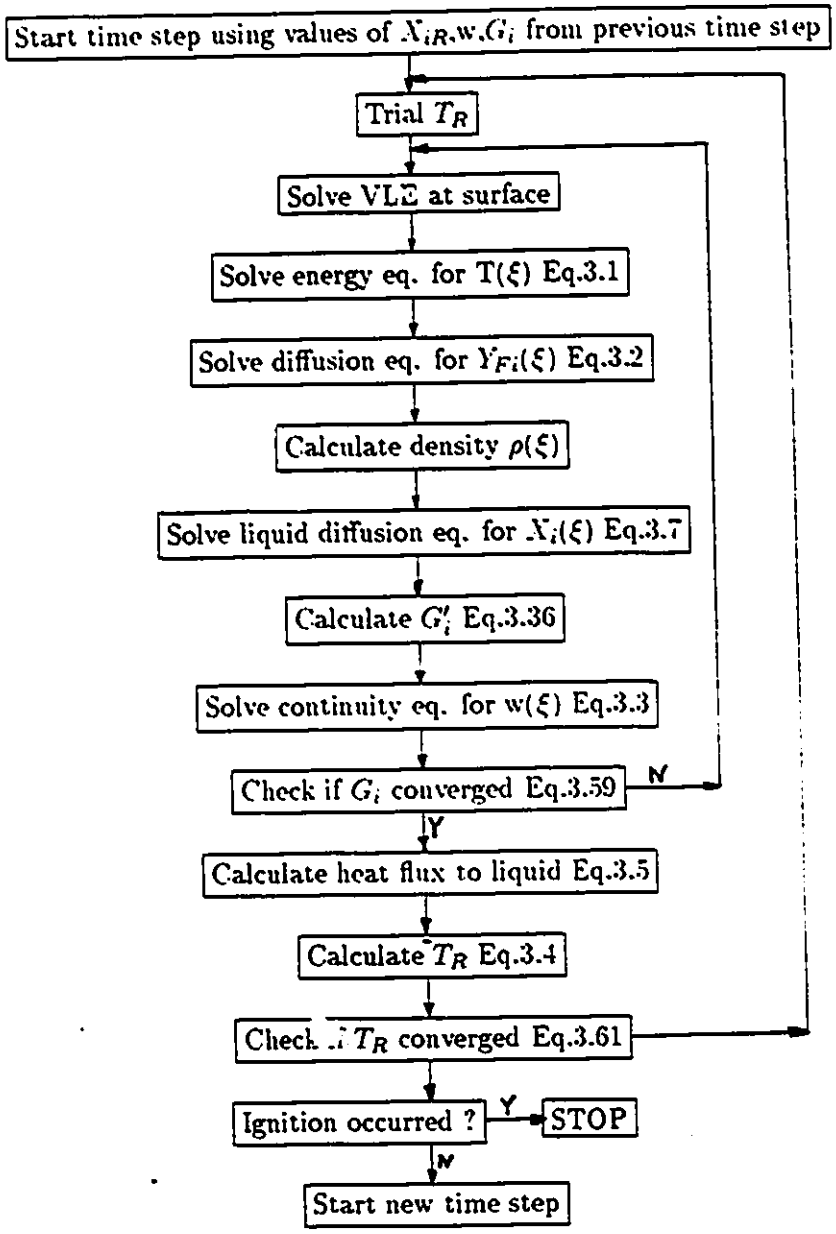

Figure 5: Flowchart of model

Chapter 4

Results and Discussion - Single Component Fuel

4.1 Effect of Pressure on VLE

As was mentioned in a previous section, at high pressure there is a possibility of air dissolving in the liquid surface and a simple vapour-pressure correlation is no longer applicable.

Some trial calculations for the system nitrogen/n-heptane, representing the surface of a heptane droplet evaporating in air, are shown in Fig. 6 as a pressure-composition phase diagram for the pressure range of interest. For each phase envelope the upper branch represents saturated liquid (ie the bubble point) and the lower saturated vapour (ie the dew point), while the regions above and below the envelope represent compressed liquid and superheated vapour respectively. The critical points shown were not calculated explicitly, but determined by examining solutions at successively higher pressure for equality of liquid and vapour compres-

sibility factors. Points close to the critical states are approximate, as the calculations do not converge to a high degree of accuracy here. The critical pressures of the mixture are substantially higher than those of either component (nitrogen P_c = *33.5 atm*, heptane P_c = *27.0 atm*); this is characteristic of mixtures of components with widely differing boiling and critical temperatures. In the present work, since the ignition time becomes shorter as the pressure rises, ignition always occurs when the droplet is far short of the critical state. At 50 atm pressure, the air concentration in the liquid phase at ignition was of the order of 2% by mass. For pure evaporation or steady combustion, involving much longer droplet lifetimes, the droplet temperature can of course rise much higher, and phase envelopes of Fig. 6 show that larger dissolved air concentrations can be reached. Some experimental data points from Knapp et al [18] are also shown, and it can be seen that the results agree very well with them. The calculations show that significant amounts of air will dissolve in the liquid surface at pressures in excess of about 20 atm; the effects of this on the ignition process will be discussed later.

4.2 Effect of VLE Model

At the beginning of the development of the present model attention was concentrated on conditions at the liquid surface. These results outline the effects of adding, step by step, the elements to the model which describe processes at the liquid surface at high pressure. The sample calculations are made for pure evaporation (no chemical reactio) of typical droplets.

The first step was to replace the Antoine vapour pressure corelation in the earlier model with the VLE calculation based on the Peng-Robinson equation discussed in Section 3.5. Some sample calculations were made for n-heptane and n-hexadecane droplets evaporating in air for the pressure range of interest. The deviation of the

vapour phase fuel mass fraction at the droplet surface and the change in vaporization history for pure evaporation from that predicted by the Antoine equation are shown in Figures 7 -12. For these calculations no account was taken of liquid phase diffusion of air and the enthalpy of vaporization was still that of pure fuel.

From Figures 7-12 it can be seen that there is no significant change in the behaviour of the new model at low pressures (1 atm, 5 atm), but there is a greater change at high pressures, because the Antoine equation is not satisfactory at high pressure. Fig. 9 and Fig. 10 also show that an increase in pressure causes a reduction in fuel mass fraction at the surface. As droplet radius decreases the mass flux from the droplet surface increases (Figs 11, 12), which can cause a slight cooling of the droplet so that the surface mass fraction decreases slightly (Figs 7, 8).

The difference between the models is not large; however, it should be noted that the comparison can only be carried out at pressures below the critical pressure (P_{cr} = 33.9 atm for n-heptane, 14.0 atm for n-hexadecane) as the Antoine equation cannot be used at all at supercritical pressures. The very good agreement between models at 1 atm shows that the model is working properly. From the physical point of view, an increase in pressure reduces the fuel fraction at the surface and the evaporation rate, which in turn allows the droplet liquid to heat up more quickly.

4.3 Effect of Enthalpy Change on Evaporation

At high pressure as air is absorbed in the liquid, the enthalpy change on evaporation is no longer that of the pure fuel. Following the discussion in the Section 3.5.3 some tests were done with n-heptane for different ranges of temperature and pressure. Fig. 13 shows that the enthalpy of evaporation decreases with increasing pressure

and temperature and approaches zero at the mixture critical point. The calculated values of h_v at the boiling point agree well with the heat of vaporization of the pure substance, but are lower at temperatures above the boiling point. Similar behaviour is shown in Hsieh and Shuen [13] and Kadota and Hiroyasu [17]. In the calculations of enthalpy in Fig. 13 the vapour mass fraction of fuel has been used instead of the mass fluxes as the weighting factor, since mass fluxes were not available in this calculation.

Figures 7–12 record the effects of adding the new calculation of h_v to the model. At 1 atm the effects are insignificant, again indicating that the model works properly at low pressure. At high pressure, the lower enthalpy of vaporization causes the droplet to heat up more rapidly, increasing the surface fuel vapour concentration and mass flux, and causing the droplet to evaporate more rapidly. The effect on the mass flux is large, since this is sensitive to any increase in Y_{FR}. This is especially true for n-heptane (Fig. 11). An increase in pressure causes a reduction in fuel mass fraction at the surface, and consequently the rate of vaporization becomes much slower.

Fig. 14 shows that ignition times decrease sharply as ambient pressure rises. Surprisingly, in view of the effects on fuel vapour concentration and mass fluxes, Fig. 14 shows that ignition times predicted by the new model are similar to those of the low pressure model. This suggests that the process is to a large degree chemically controlled and not strongly dependent on physical processes. At pressures above the critical, the low pressure model fails completely as $h_{fg} \rightarrow 0$. This figure agrees qualitatively with the measurements of Kadota et al [17].

4.4 Effect of Liquid Phase Diffusion

The expressions for mass flux include terms which represent liquid phase diffusion; these terms have been set to 0 up till now. To include them requires solving equation 3.7 for the diffusion of air (nitrogen) in the liquid phase.

The parameter f which multiplies the diffusivity in this equation represents the state of mixing in the droplet, depending on its value:

- f = 0 droplet completely unmixed - no diffusion, air does not penetrate from surface into droplet.
- f = 1 laminar diffusion.
- f - large - droplet well-mixed, uniform concentration of air.

Talley and Yao [34] estimate that the internal circulation in a droplet with an external flow Reynolds number of 100 is equivalent to $f = 4$.

In a well-mixed model the mass flux is controlled by diffusion in the vapour phase. The fluxes of the components are then determined by fuel concentration, which is fixed as long as the droplet temperature remains constant. Any increase in temperature leading to a change in vapour-liquid equilibrium will result in the concentration of the whole droplet changing at once. In the diffusion limited model (smaller f) a change in the liquid composition which occurs at the surface will spread through the droplet by diffusion and the mass fluxes of the components will change to reflect this. In the unmixed model the droplet surface has an equilibrium concentration of air corresponding to a given T and P, but air does not penetrate into the droplet. In that model the air is removed by evaporation of the liquid layer as fast as it is absorbed. Any change in fuel diffusion will be balanced by an equal

change in air diffusion, so that the liquid and vapour phase gradients will adjust to keep the difference constant.

Some calculations for n-heptane and n-hexadecane droplets were made. The events occuring during droplet evaporation and ignition are affected not only by diffusion in the liquid phase (ie the value of f) but also by the initial conditions. Two different initial conditions for the air concentration in the liquid were tested:

a - zero initial concentration of air in fuel liquid

b - uniform initial concentration of air in fuel liquid.

In a Diesel engine the fuel spray is suddenly exposed to high pressure, and for this case the condition (a) is valid, but in experiments of the suspended droplet type the fuel droplets are in contact with air at high pressure for some time prior to the start of ignition and condition (b) is more realistic. Tests were therefore made of the effects both of initial condition and of the state of mixing, choosing values of f = 0, 1, and 100.

The results show in general that both the value of f and the initial condition have remarkably little effect on ignition time (see Table 2), although they can significantly influence events at the liquid surface. An initial concentration of 0 combined with a diffusion-limited liquid phase at sufficiently high pressure can cause the air mass flux absorbed to exceed the fuel mass evaporated ($G_A < 0. \mid G_A \mid > G_F$) so that the net flux G becomes negative and the droplet actually grows! This is a transient condition, however, and after a sufficiently long time G becomes positive again. These effects become smaller as f increases. For a well-mixed droplet, the net flux was always positive, regardless of pressure. Calculations for a droplet evaporating at room temperature with $f = 1$ showed that the liquid concentration field was essentially uniform after about 30 sec. This indicates that the uniform initial

concentration model is the most realistic for comparison with the experiments to be performed. Fig. 15 shows the change in air mass fraction with droplet radius for these conditions; as expected, air concentration decreases from the surface to the droplet centre. Figure 16 shows how the air concentrations at the surface behave under ignition conditions. As tests for n heptane and n hexadecane showed that air diffusion in the liquid phase has no significant influence on ignition times, it will be neglected in future modelling, and the droplet assumed well mixed. This conclusion is at least partly the result of the low air concentrations in the liquid phase.

4.5 General Results and Discussion

At this point the model is completed by adding the pressure corrections to the transport properties. Some final results from the model are shown in Figures 17-25. Fig. 17 shows that ignition delay times decrease sharply as ambient pressure rises, owing largely to the pressure dependence of the reaction rate. The correction of the transport properties for the effects of pressure is seen to have a relatively small effect on predicted ignition times. Examination of predicted temperatures and fuel concentration profiles showed that as pressure rises the fuel mass fraction near the droplet surface decreases (Fig. 18); this is to be expected, since the air partial pressure is rising while the fuel partial pressure remains largely unchanged. This leads to lower evaporation rates for droplets at high pressure, which in turn means that more of the heat transferred to the droplet is used to heat the liquid. Hence, droplet heating is more rapid at high pressure. The results are presented in Fig. 18. Figures 19 and Fig 20 show that the concentration changes cause the reaction zone and the subsequent location of ignition to move closer to the droplet surface at high pressure. Reaction was found to take place under progressively leaner conditions as pressure rises.

It should be noted that the behaviour of ignition delay with pressure depends strongly on the reaction orders in Eq. 3.8 (exponents of fuel and oxygen concentration in the reaction rate expression in the model). At present the values used are those from the work of Westbrook and Dryer [39]: an exponent of a = 0.25 for fuel and b = 1.50 for oxygen. To find effect of pressure on exponents a and b it was decided to change reaction constants to a = 1 for fuel and b = 1 for oxygen and a = 0.25 and b = 1.75 . For these calculation the pre-exponential constant K had to be changed so as to give the same ignition time at 1 atm. The fitted values of K are presented in Table 3. The significance of a = b = 1 is that it was used by most ignition models in past; this was proven to be incorrect by Westbrook and Dryer [39]. Figures 21 and Fig. 22 show the effect of changing these exponents. These changes have a significant effect on the reaction zone, which moves towards the droplet surface as a or b increases. Another result is a large change in delay time, evidence of a strong degree of control by chemical kinetics. It should be noted that overall pressure dependence of rate is given by (a + b) (see Eq. 3.8). Therefore a = 0.25, b = 1.75 (a + b = 2) gives a steeper drop of ignition time with pressure than a = 0.25, b = 1.5 (a + b = 1.75). However, a = b = 1 (a + b = 2) gives a less steep dependence. The reason for this is that a = 1 gives a much stronger effect of fuel concentration but a lower effect of oxygen, hence requires more fuel to ignite. It can be seen from the Fig. 22 that ignition for case 2 (a = b = 1) occurs in a much richer mixture. It will be necessary to vary only b to fit pressure dependence to experimental data. Experimental results will be required to see if these values are correct.

The temperature dependence of the ignition time (Fig. 23 and Fig. 24) is almost a straight line on an Arrhenius plot (ln ignition time vs 1/T) whose slope changes little with pressure. The slope of this plot gives an effective activation energy of about 37 kJ/gmol for n heptane, which when compared to the activation energy of

60 kJ/gmol used for the chemical reaction itself suggests a large degree of control of the process by chemical kinetics.

A plot of ignition time versus droplet diameter (Fig. 26 and Fig. 25) shows the familiar phenomenon of a minimum droplet diameter below which ignition cannot occur: this limiting diameter decreases as pressure rises. The effect of droplet diameter on ignition time is small for the example of n-heptane, but becomes somewhat larger for fuels of higher boiling point. Both the temperature and the diameter dependence of ignition delay time are similar to those at low pressure. It can therefore be concluded that high pressure does not introduce any fundamental changes in ignition behaviour beyond a reduction in ignition delay time.

An important topic in the literature on droplet behaviour at high pressure has been the question of whether the liquid phase ever becomes supercritical. In the present work, since the ignition time becomes shorter as the pressure rises, ignition always occurs when the droplet is far short of the critical state: Fig. 18, for example, shows that n-heptane droplets ignite at a liquid temperature below 370 K regardless of pressure, while the critical temperature for pure n-heptane is 540 K. At 50 atm pressure, the air concentration in the liquid phase at ignition was of the order of 2% by mass. For pure evaporation or steady combustion, involving much longer droplet lifetimes, the droplet temperature can of course rise much higher, and the sample phase envelopes calculated in an earlier section show that larger dissolved air concentrations can be reached.

Further insight into the question of whether the critical point is reached is given by the expression for the total evaporated mass flux G developed previously:

$$G = \frac{\Gamma_L \frac{\partial X_F}{\partial r} |_R - \Gamma \frac{\partial Y_F}{\partial r} |_R}{X_{FR} - Y_{FR}} \tag{4.1}$$

Since vapour and liquid phase fuel mass fractions at the surface Y_{FR} and X_{FR}

approach each other at the critical point (by definition, liquid and vapour phases have identical compositions and densities at the critical state), this equation suggests that attaining the critical point would require an infinite mass flux, and hence be impossible. It is therefore postulated that it is possible for a droplet to approach the critical state asymptotically, but not to reach it or pass through it, regardless of pressure.

Table 2: Effect of f on ignition time for a 1.5 mm n-heptane and n-hexadecane droplets at 973 K and 50 atm.

ignition time (sec)	$f = 1$ initial $Y_A = 0$	$f = 100$ initial $Y_A = 0$	$f = 1$ initial $Y_A = 1 - Y_F$	$f = 100$ initial $Y_A = 1 - Y_F$
n-heptane	0.116	0.122	0.115	0.116
n-hexadecane	0.532	0.528	0.532	0.532

Table 3: Fitted values of chemical reaction constants for a 1.5 mm n-heptane droplet at 973 K with different values of exponent a and b.

	a = 0.25 b = 1.50	a = 1.0 b = 1.0	a = 0.25 b = 1.75
K x 10^{-4}	0.82	29.5	3.8

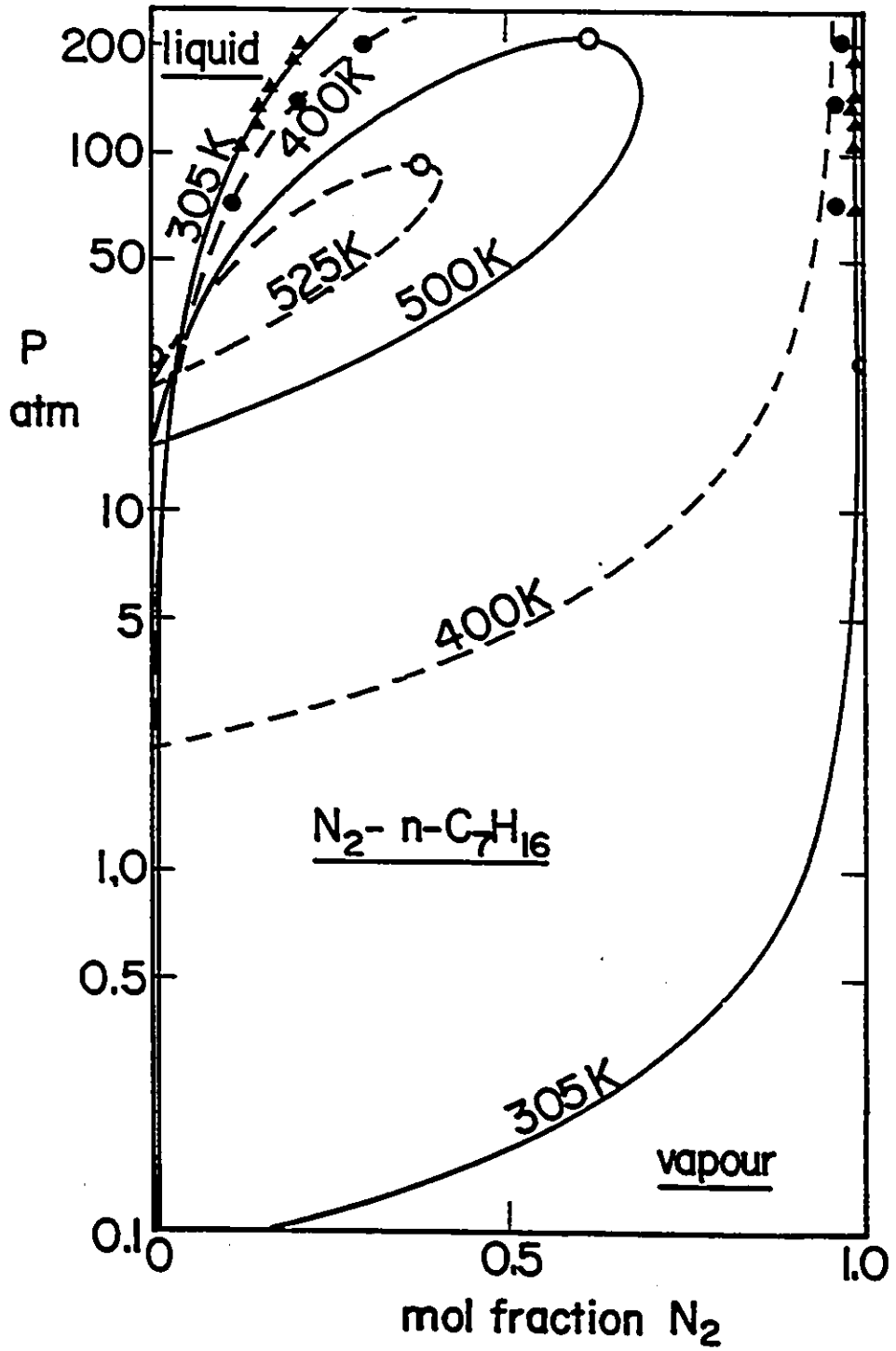

Figure 6: Pressure-mol fraction diagram for nitrogen-n-heptane mixtures, showing sample calculated isoterms. The points are experimental data from [18]: ▲ 305 K; • 400 K.

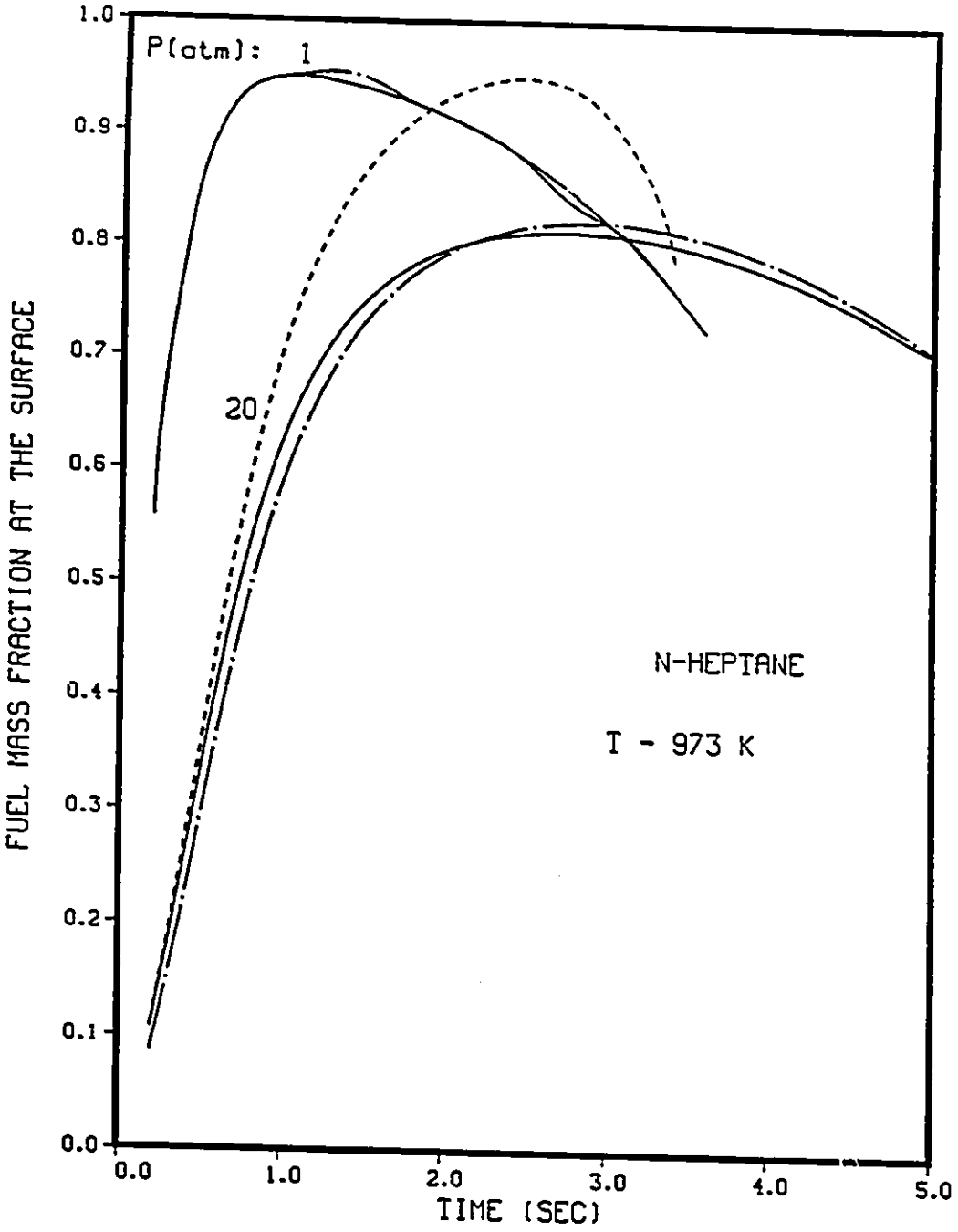

Figure 7: History of fuel vapour mass fraction at the surface Y_{FR} for a 1.5 mm n-heptane droplet at 973 K. Key: - • - low pressure model, —— low pressure model with P-R equation to calculate VLE, - - - model with P-R equation, new expression for enthalpy of vaporization and mass fluxes, but no liquid phase diffusion.

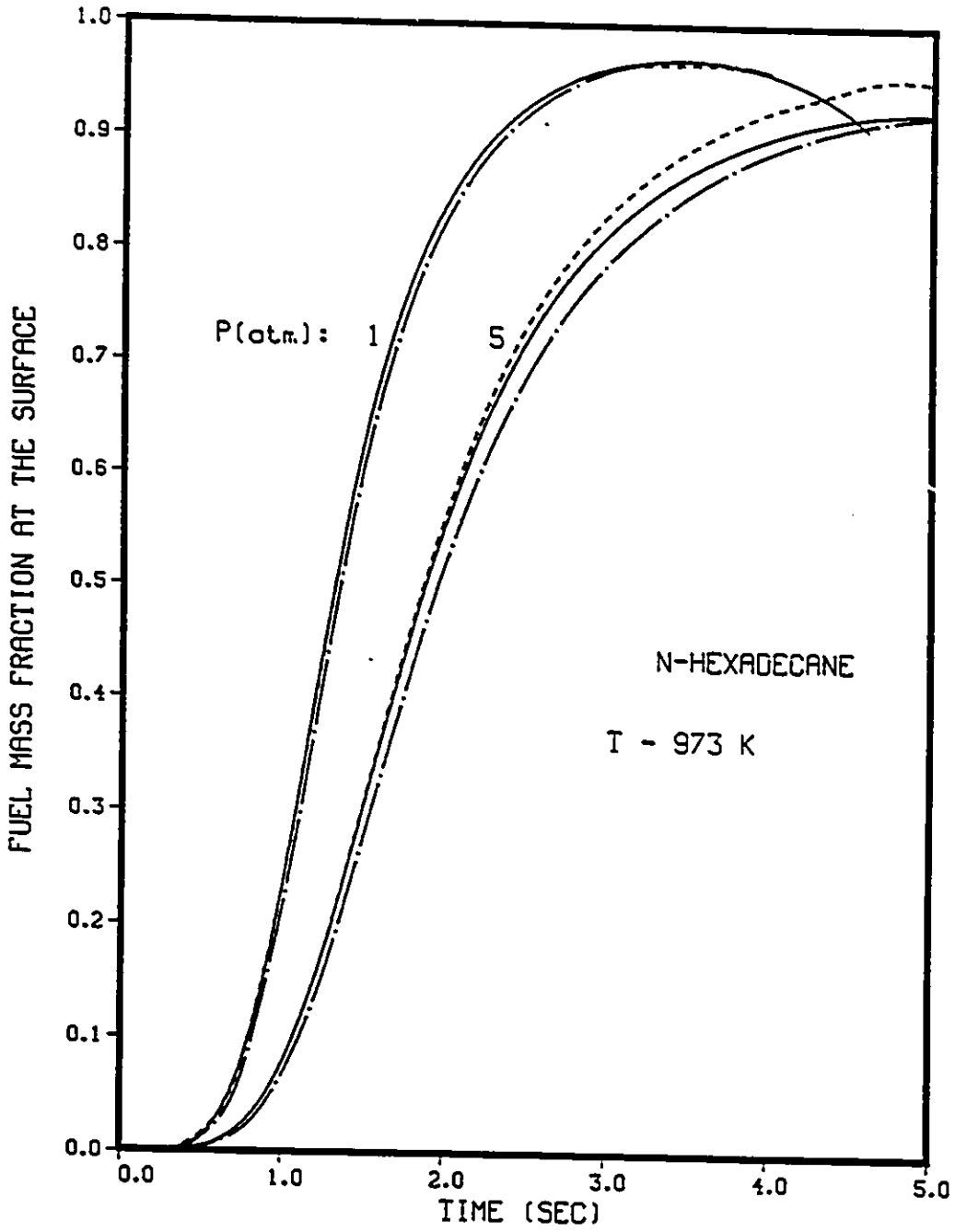

Figure 8: History of fuel vapour mass fraction at the surface Y_{FR} for a 1.5 mm n-hexadecane droplet at 973 K. Key: -•- low pressure model, —— low pressure model with P-R equation to calculate VLE, - - - model with P-R equation, new expression for enthalpy of vaporization and mass fluxes, but no liquid phase diffusion.

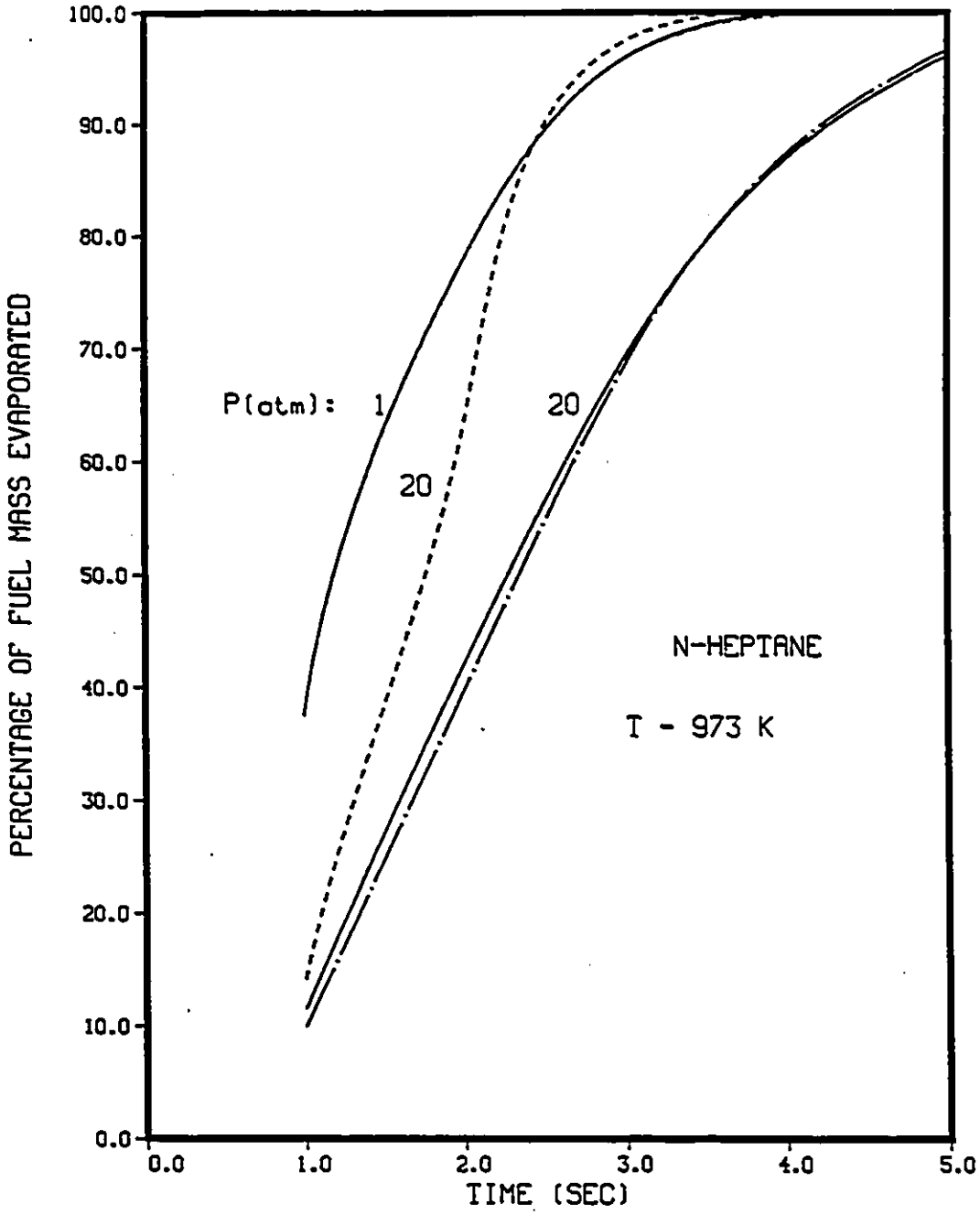

Figure 9: History of liquid mass fraction evaporated for a 1.5 mm n-heptane droplet at 973 K. Key: - - - low pressure model, —— low pressure model with P-R equation to calculate VLE, - - - model with P-R equation, new expression for enthalpy of vaporization and mass fluxes, but no liquid phase diffusion.

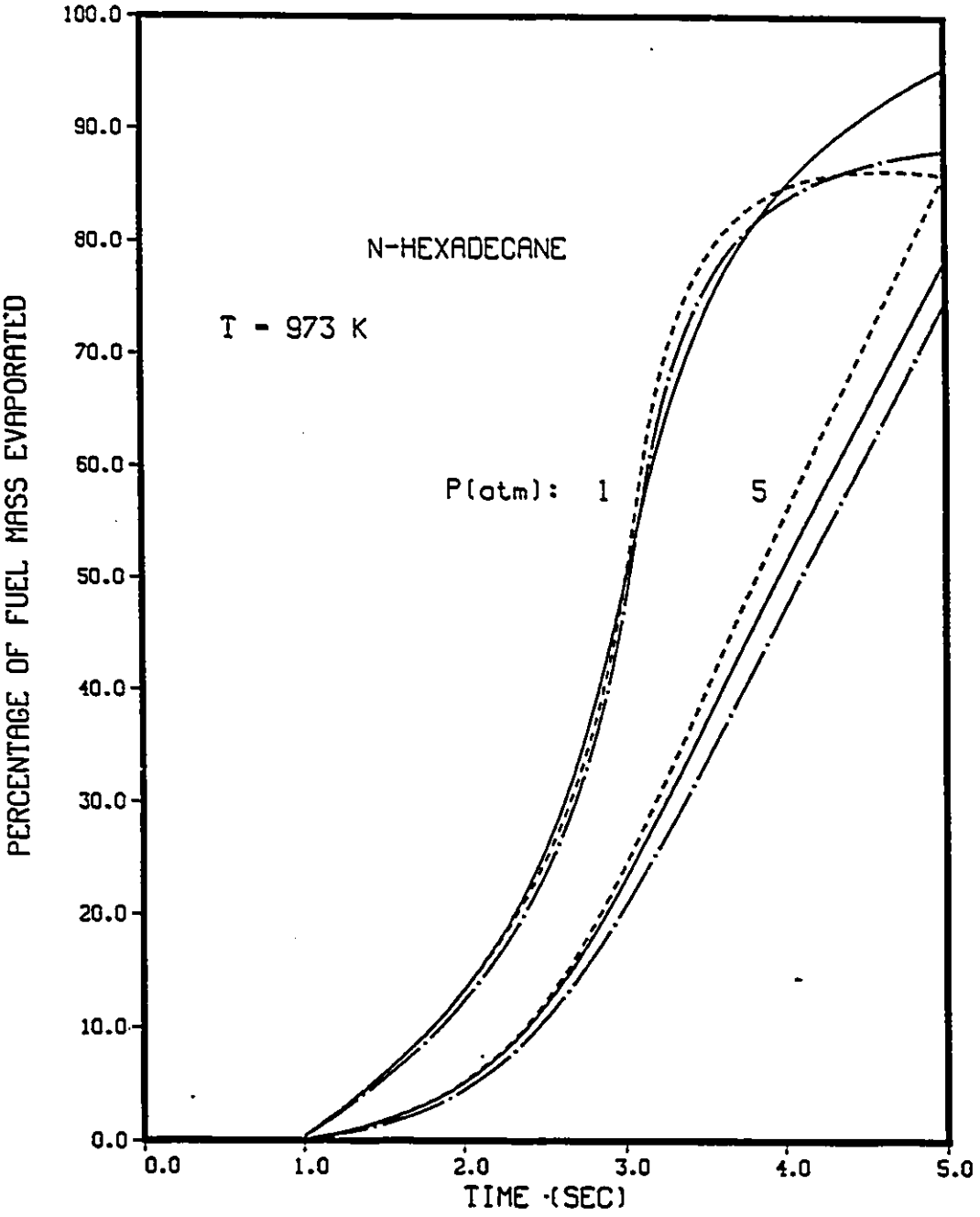

Figure 10: History of liquid mass fraction evaporated for a 1.5 mm n-hexadecane droplet at 973 K. Key: -- - low pressure model, —— low pressure model with P-R equation to calculate VLE, - - - model with P-R equation, new expression for enthalpy of vaporization and mass fluxes, but no liquid phase diffusion.

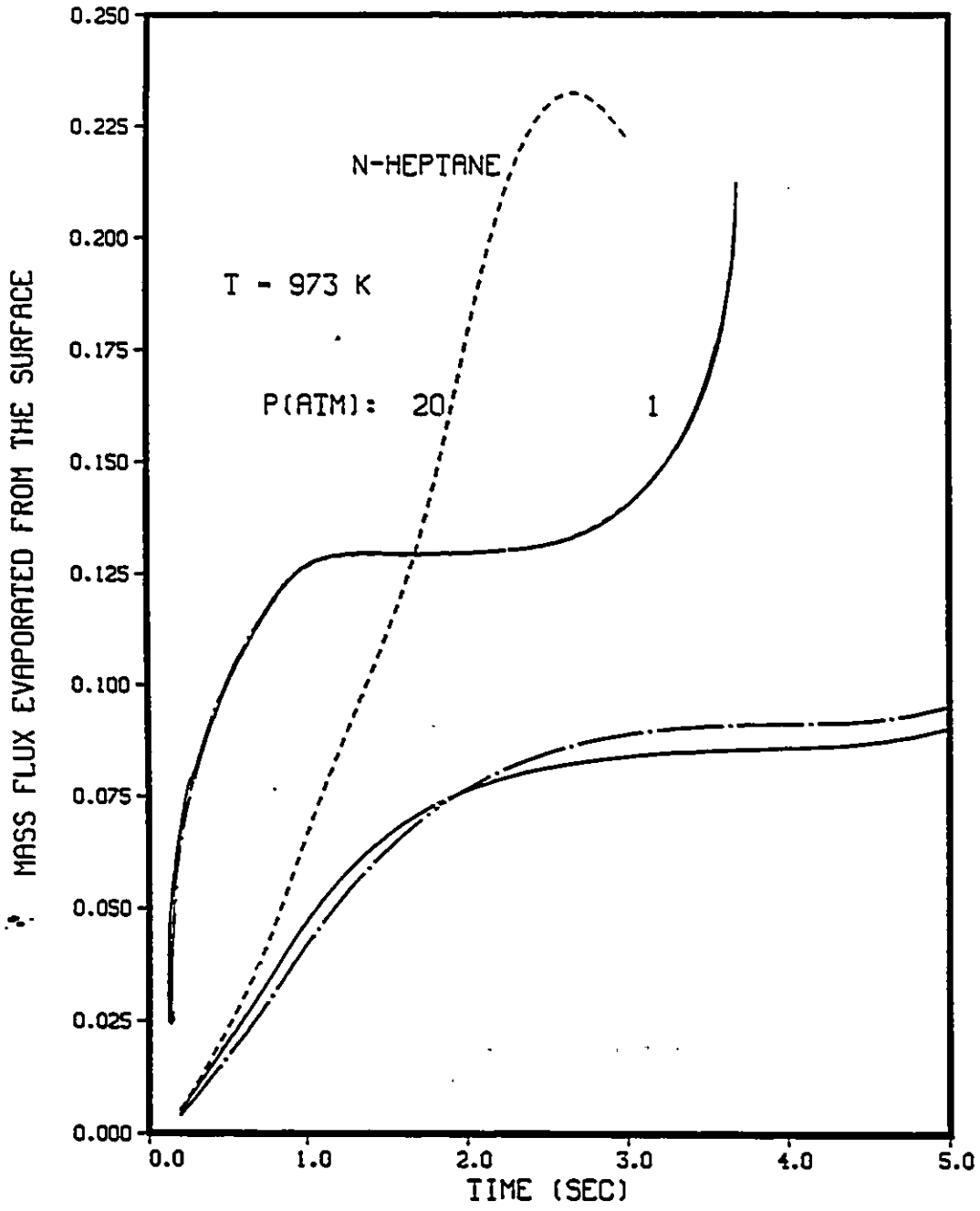

Figure 11: Comparision of total mass flux evaporated from the surface for a 1.5 mm n-heptane droplet at 973 K. Key: - - - low pressure model, —— low pressure model with P-R equation to calculate VLE, - - - model with P-R equation, new expression for enthalpy of vaporization and mass fluxes, but no liquid phase diffusion.

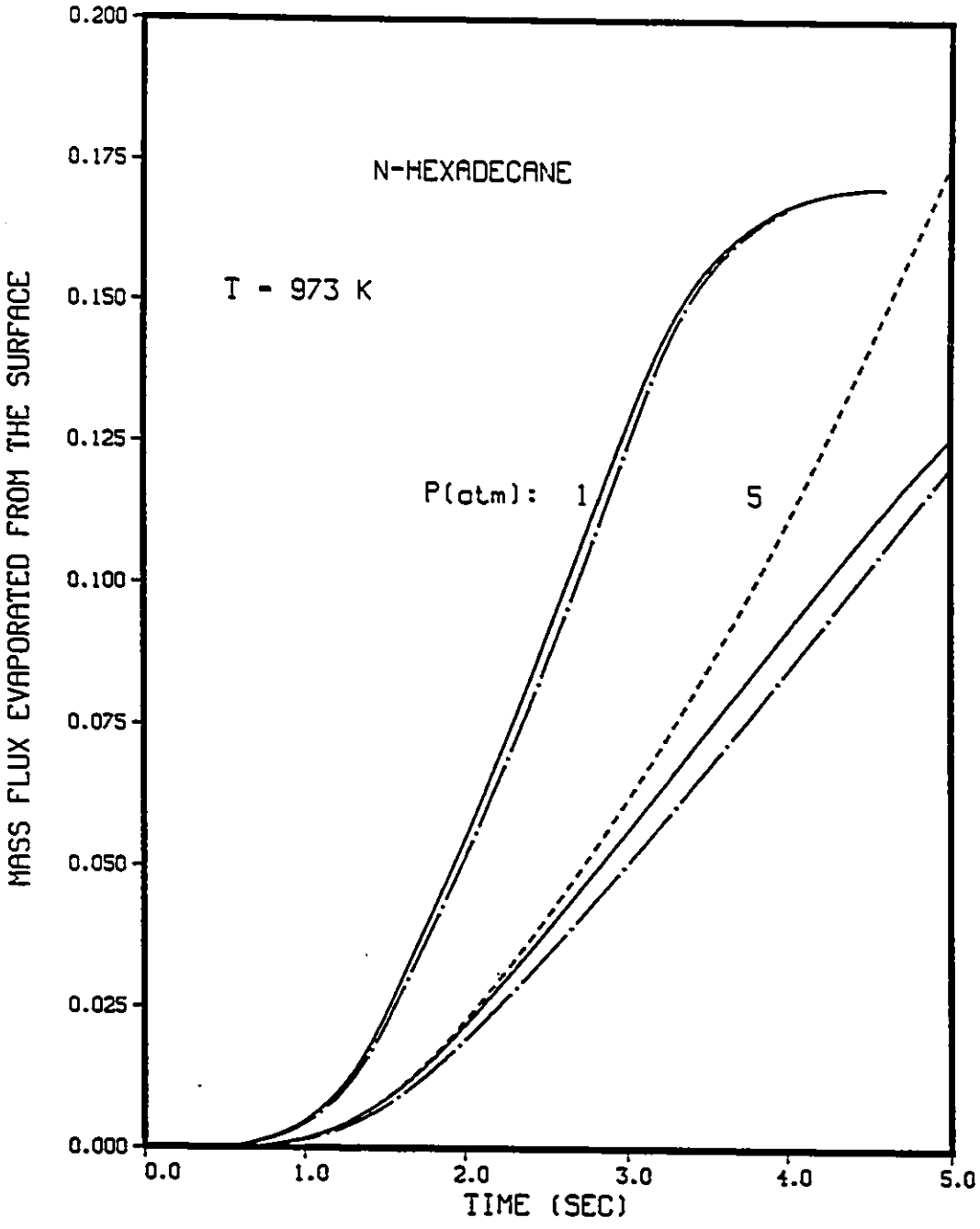

Figure 12: Comparision of total mass flux evaporated from the surface for a 1.5 mm n-hexadecane droplet at 973 K. Key: - . - low pressure model, —— low pressure model with P-R equation to calculate VLE, - - - model with P-R equation, new expression for enthalpy of vaporization and mass fluxes, but no liquid phase diffusion.

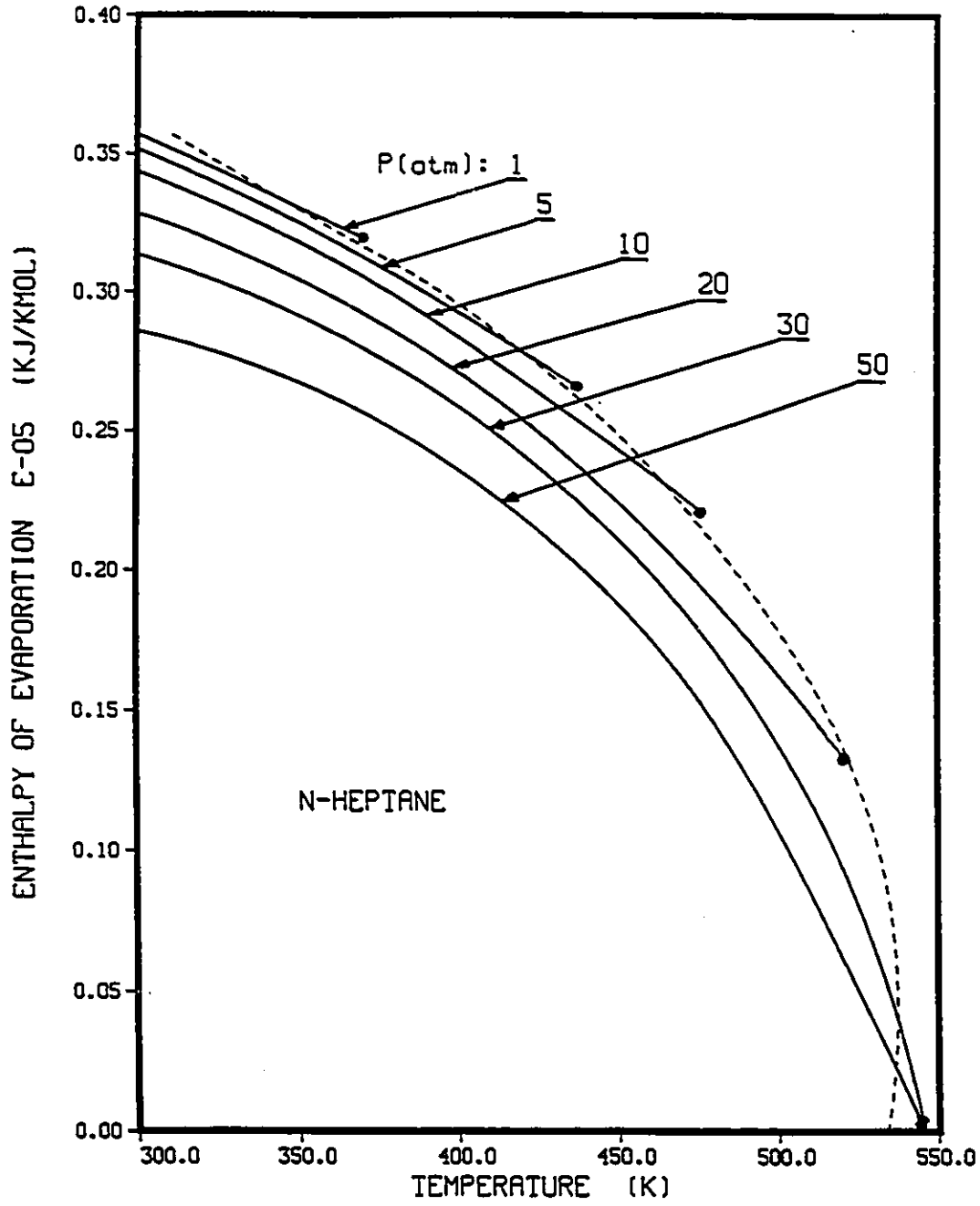

Figure 13: Enthalpy of evaporation for a 1.5 mm n-heptane droplet at 973 K. - - - Enthalpy at normal boiling point from [15], • - Boiling point.

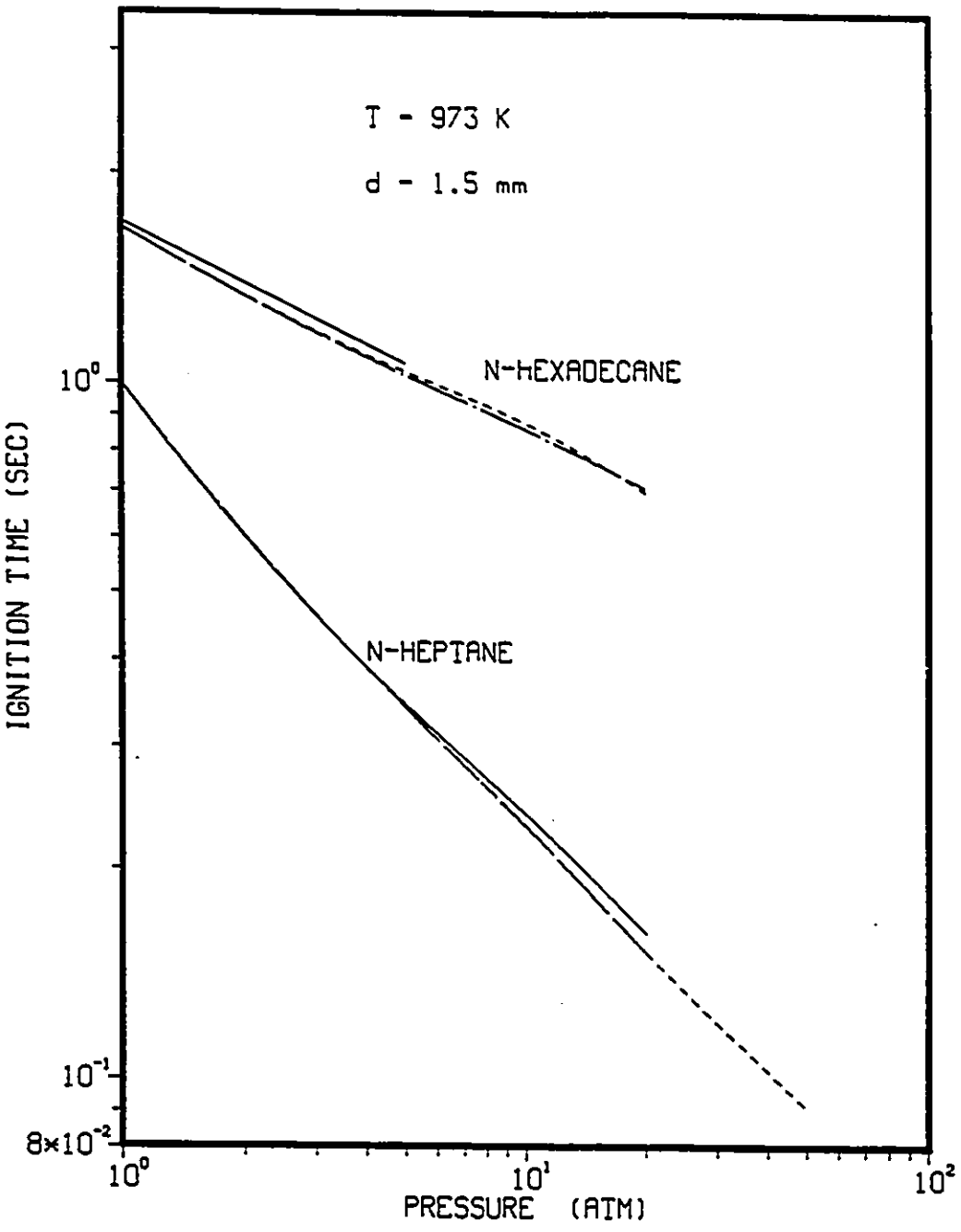

Figure 14: Comparision of ignition delays time for n-heptane and n-hexadecane mixtures at 973 K . Key: - · - low pressure model, —— low pressure model with P-R equation to calculate VLE, - - - model with P-R equation, new expression for enthalpy of vaporization and mass fluxes, but no liquid phase diffusion.

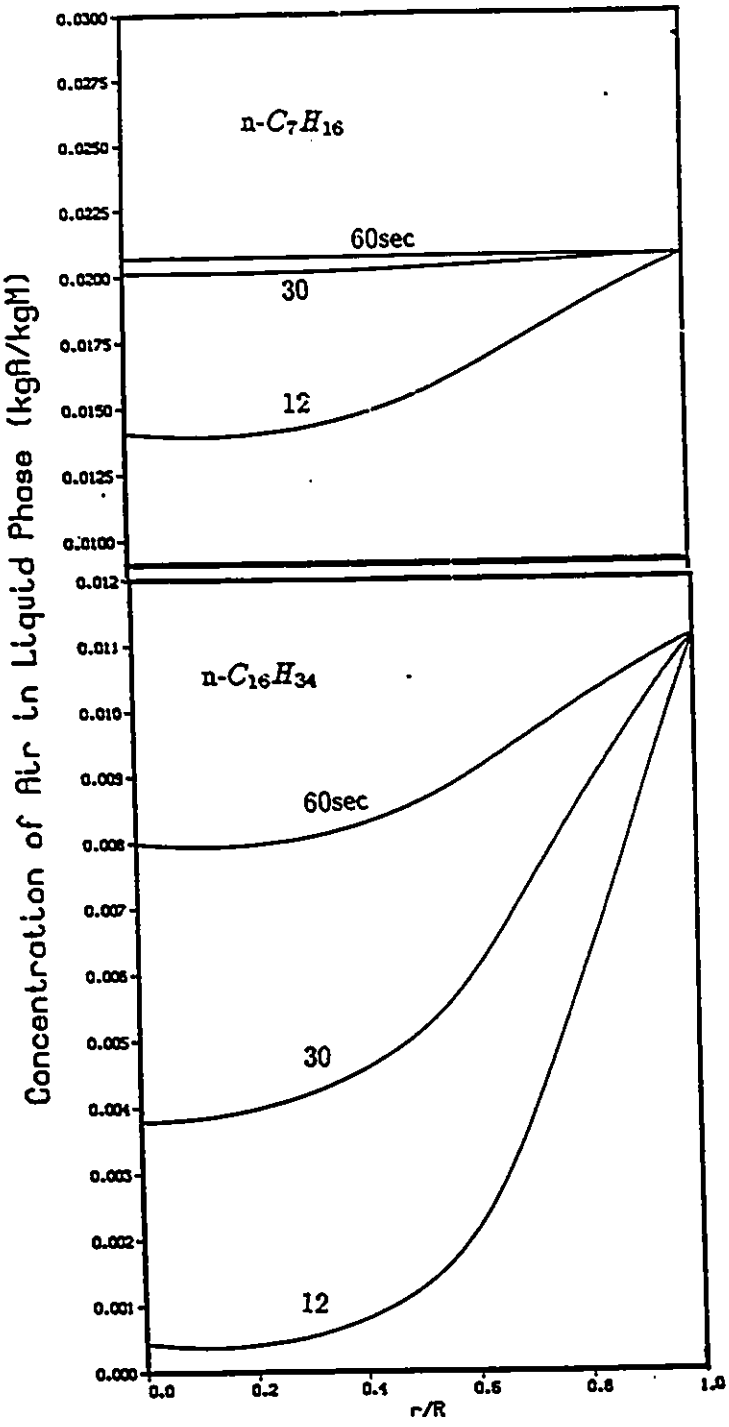

Figure 15: History of air concentration in liquid phase for 1.5 mm n-heptane and n-hexadecane droplets at 300 K and 50 atm.

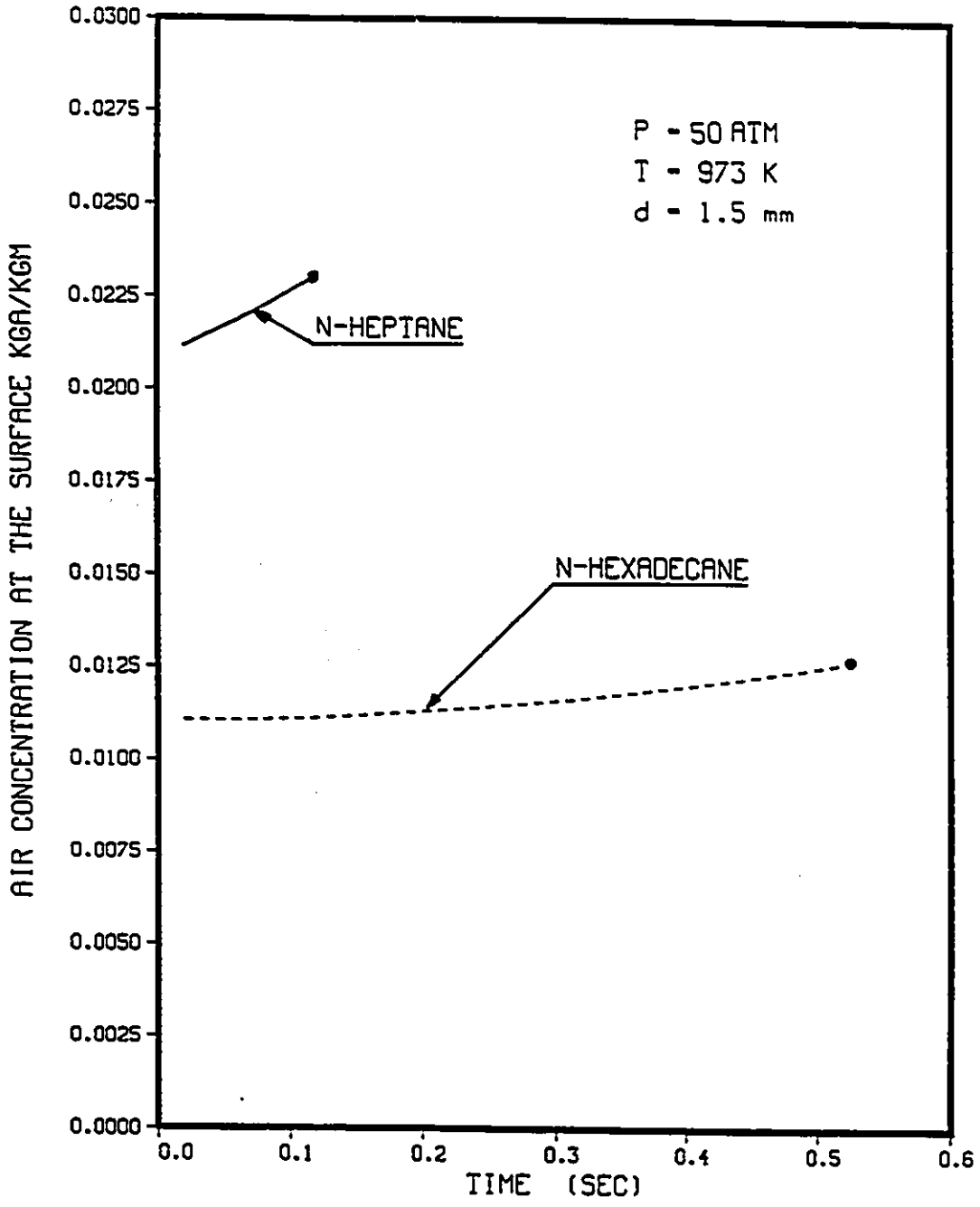

Figure 16: History of air concentration at the liquid surface under ignition conditions for 1.5 mm n-heptane and n-hexadecane droplets at 973 K and 50 atm. Curves end at ignition time : —— n-heptane t = 0.115 sec, - - - n-hexadecane t = 0.532 sec.

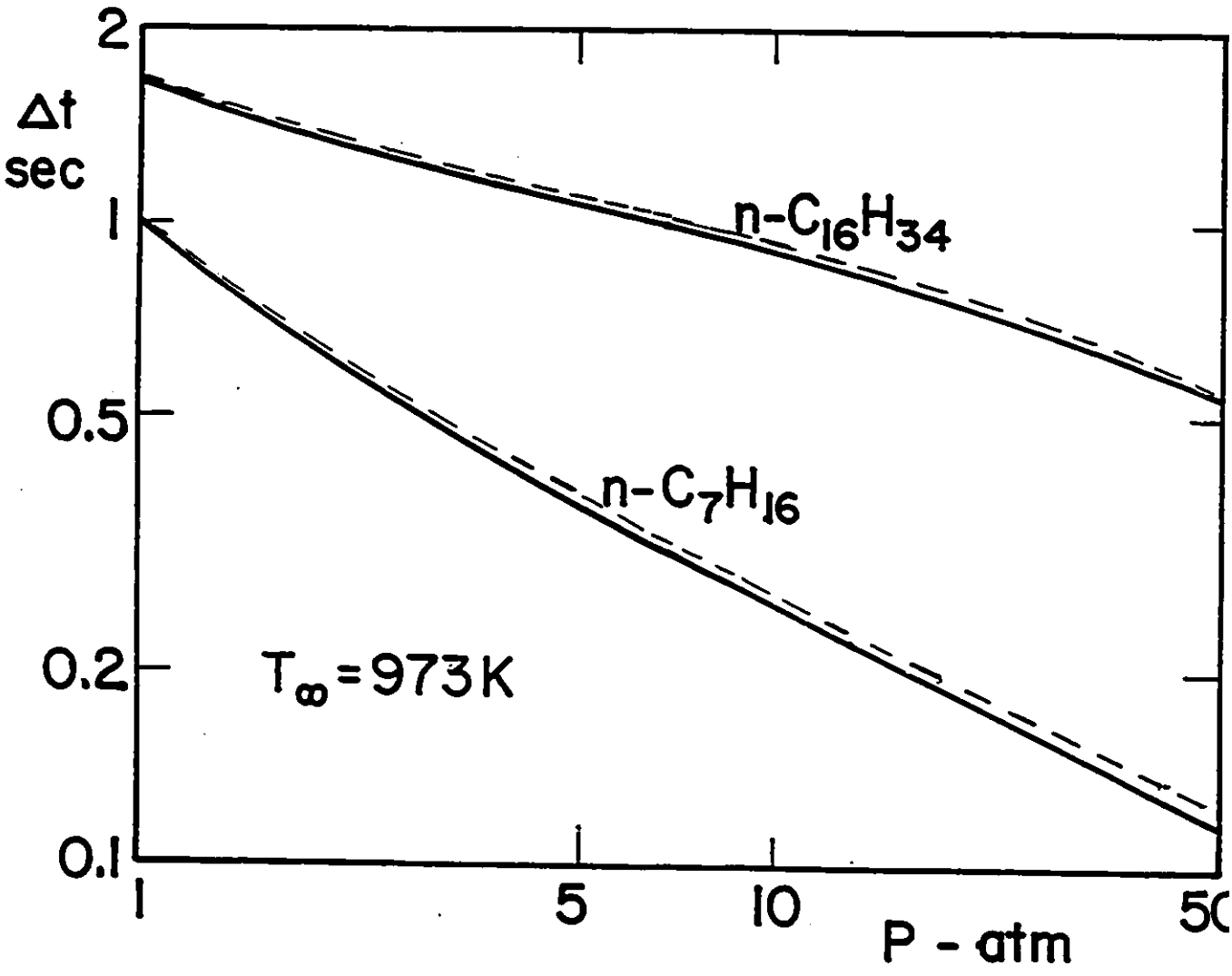

Figure 17: Comparision of ignition delays time for n-heptane and n-hexadecane mixtures at 973 K. - - - model with atmospheric properties, —— model with corrected properties

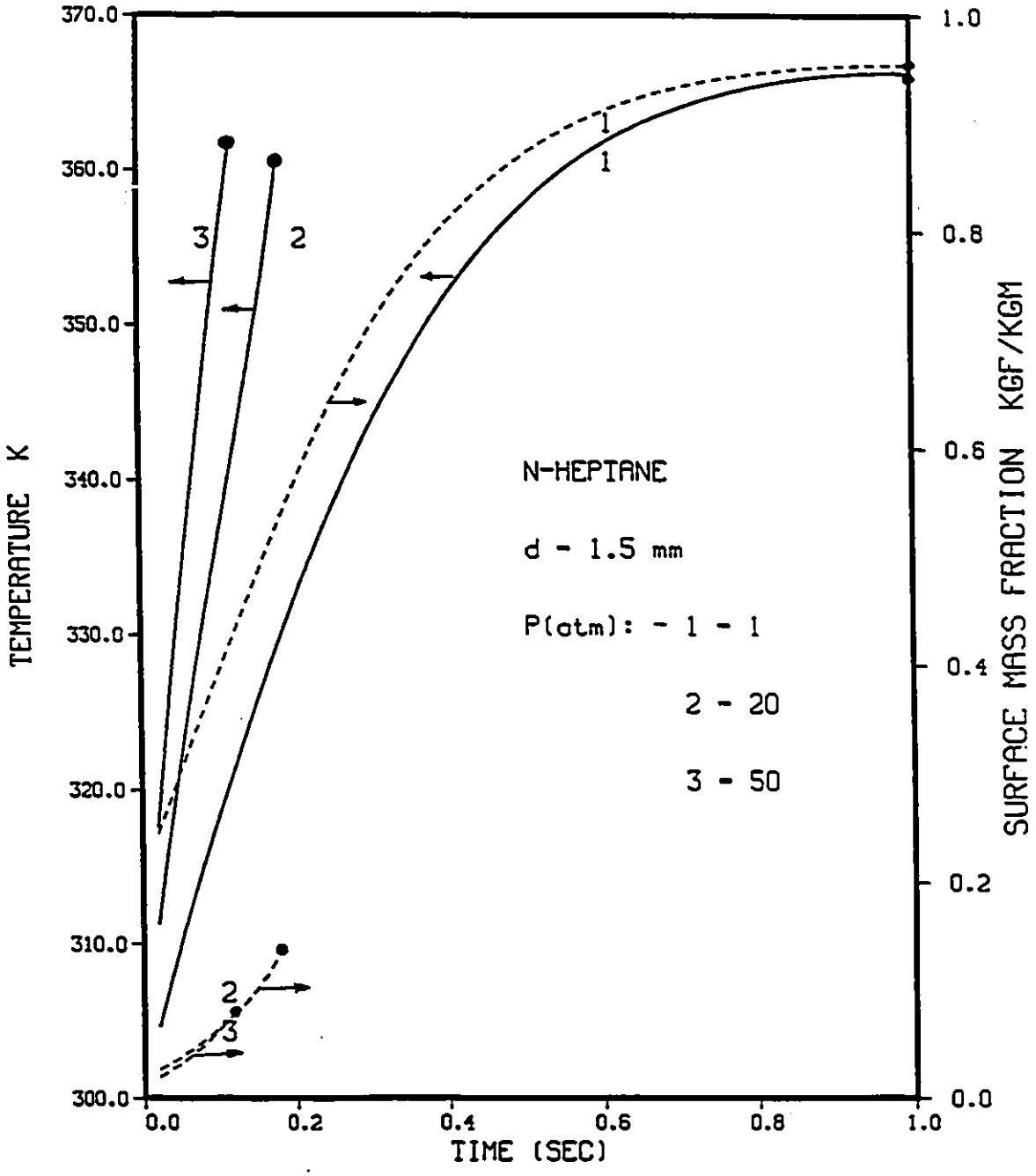

Figure 18: Predicted histories of liquid temperature and fuel mass fraction for n-heptane. Curves end at ignition : 1 - 1 sec, 2 - 0.187 sec, 3 - 0.115 sec.

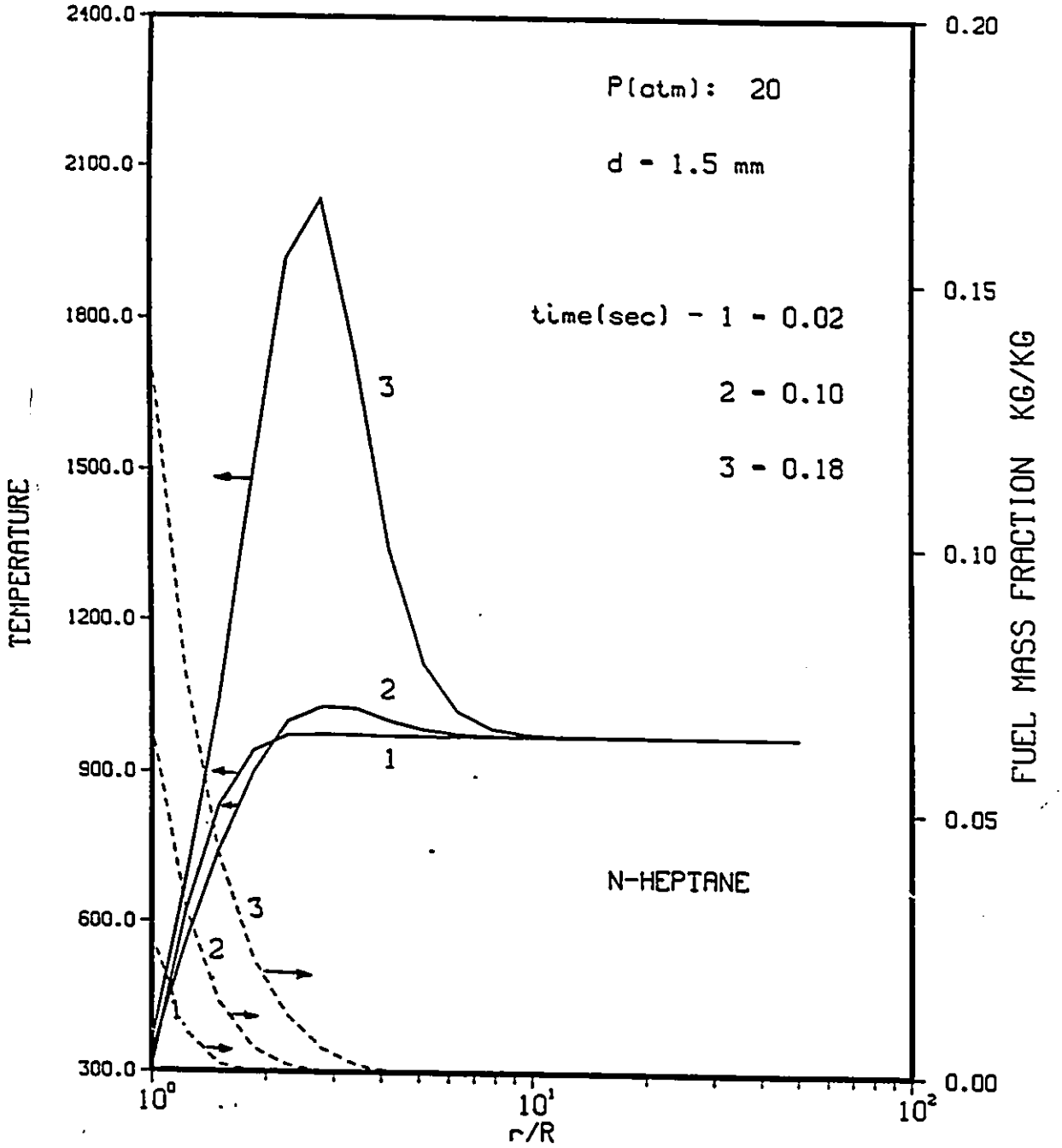

Figure 19: Development of gas phase temperature profile and fuel concentration profile around droplet with time at 20 atm for n-heptane. Ignition time t = 0.187 sec.

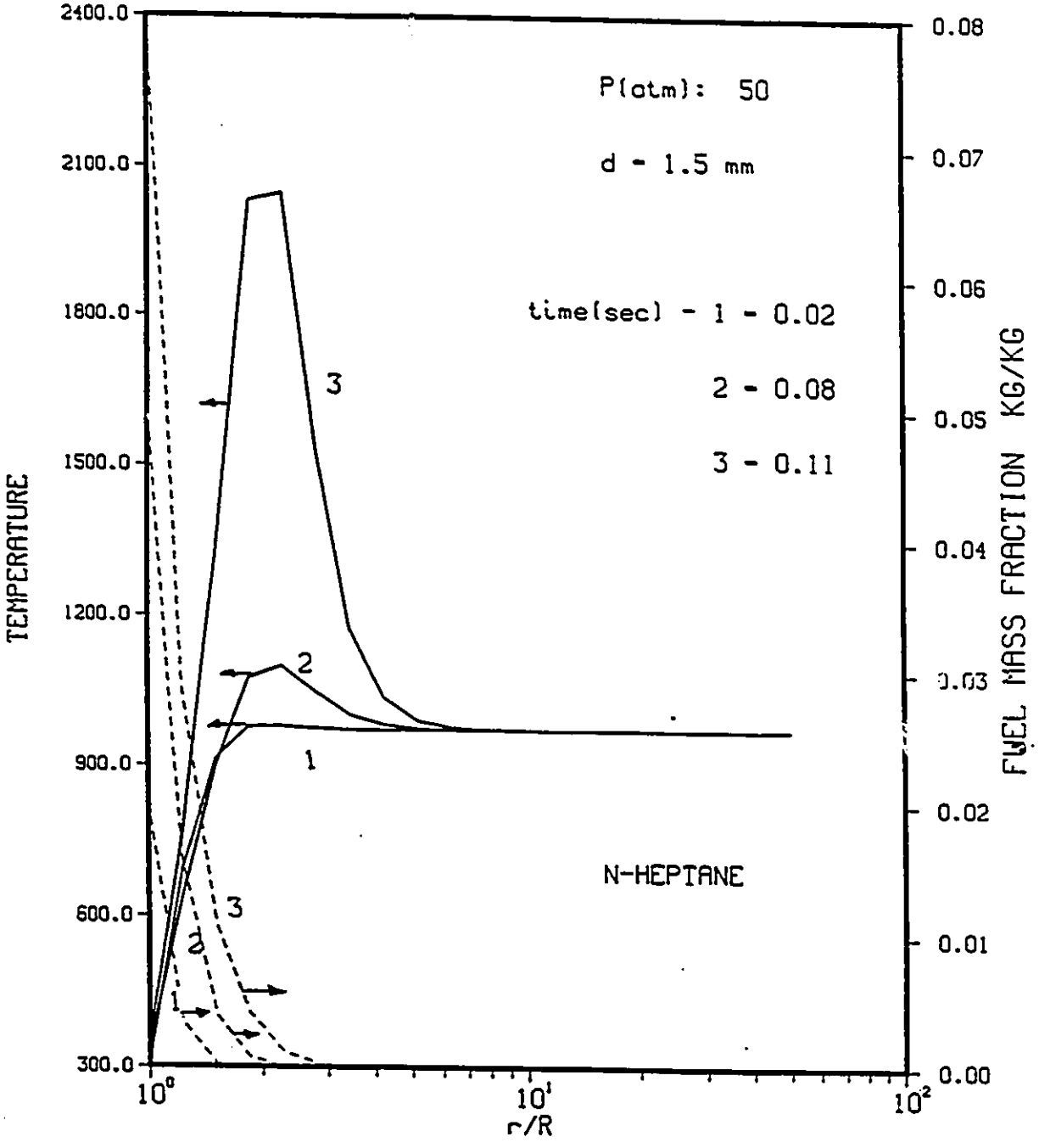

Figure 20: Development of gas phase temperature profile and fuel concentration profile around droplet with time at 50 atm for n-heptane. Ignition at t = 0.115 sec.

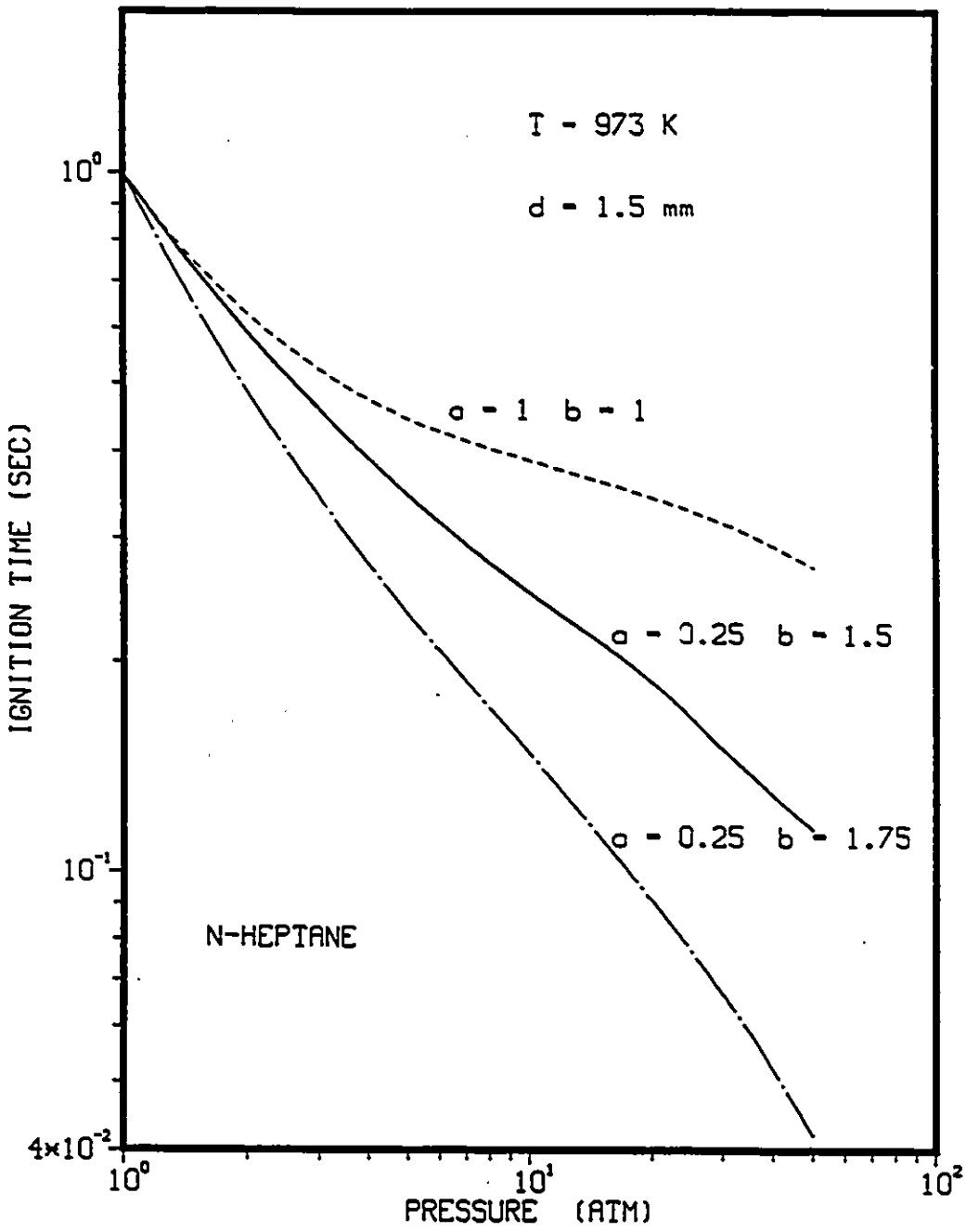

Figure 21: Effect of changing reaction constants a,b on ignition time for n-heptane.

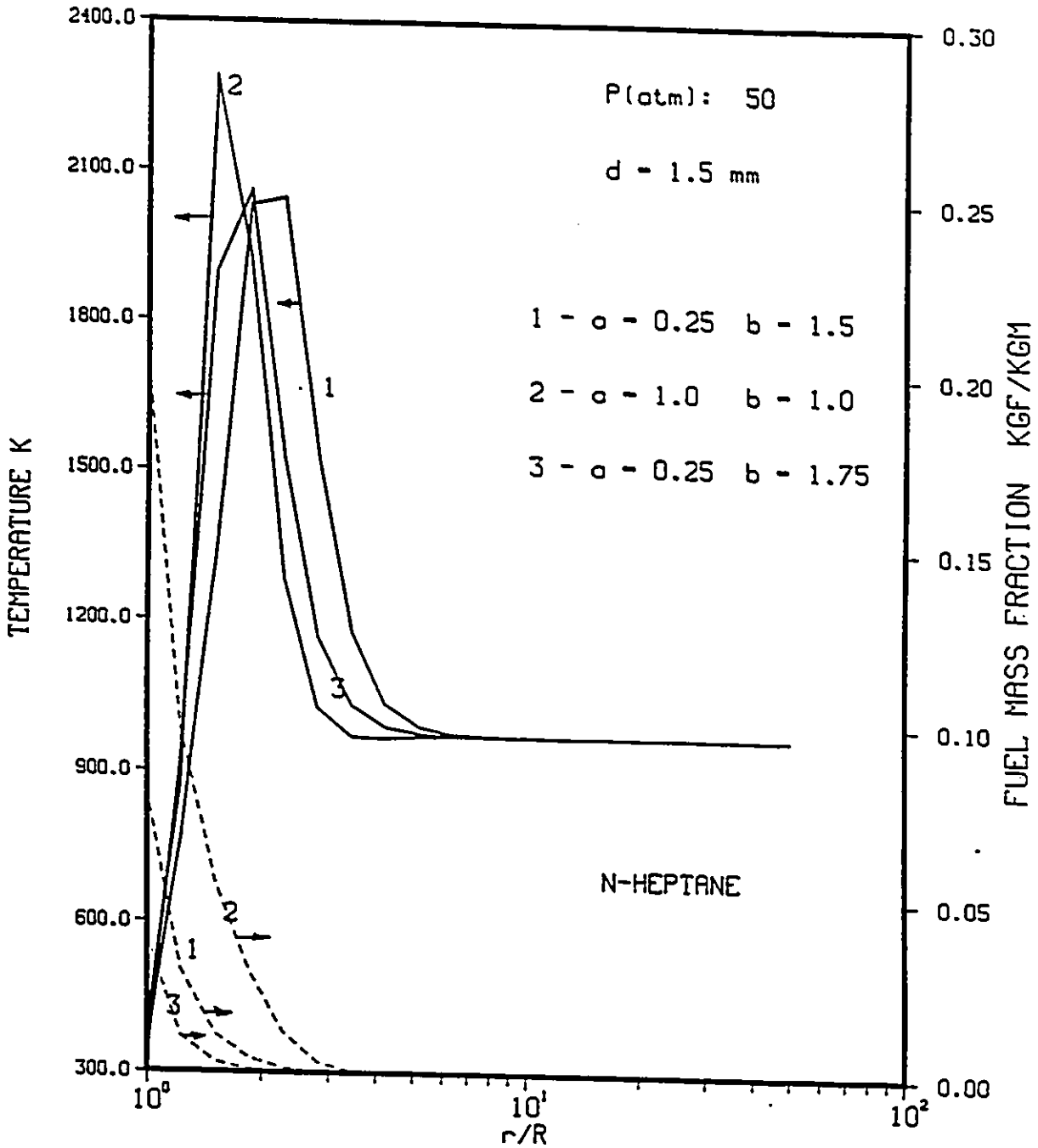

Figure 22: Effect of different reaction constants a,b on gas phase temperature profiles and fuel concentration profiles around droplet just prior to ignition at 50 atm for n-heptane. Ignition at : 1 - 0.115 sec, 2 - 0.273 sec, 3 - 0.042 sec.

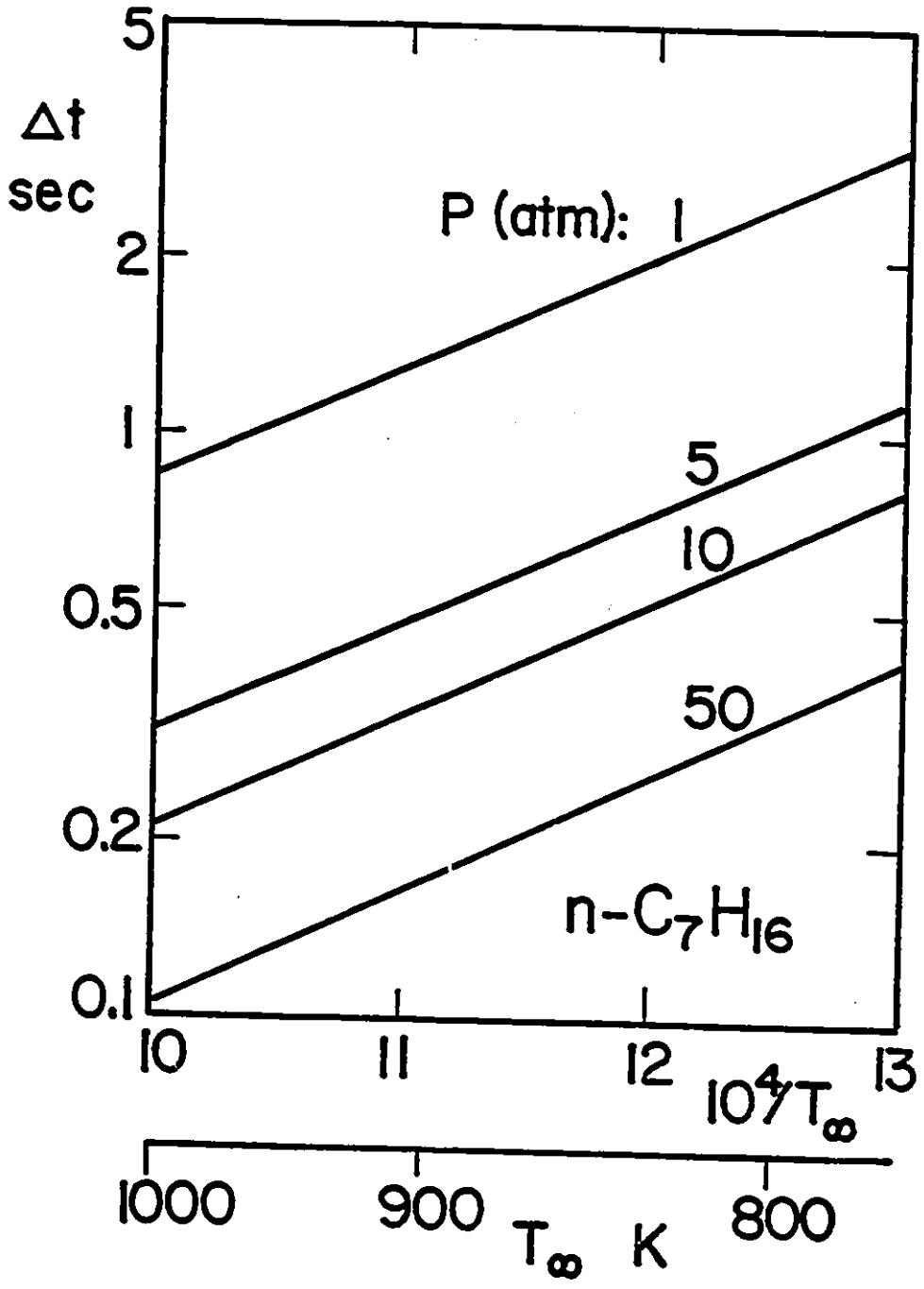

Figure 23: Predicted dependence of ignition delay on temperature at various pressures for n-heptane-air mixture.

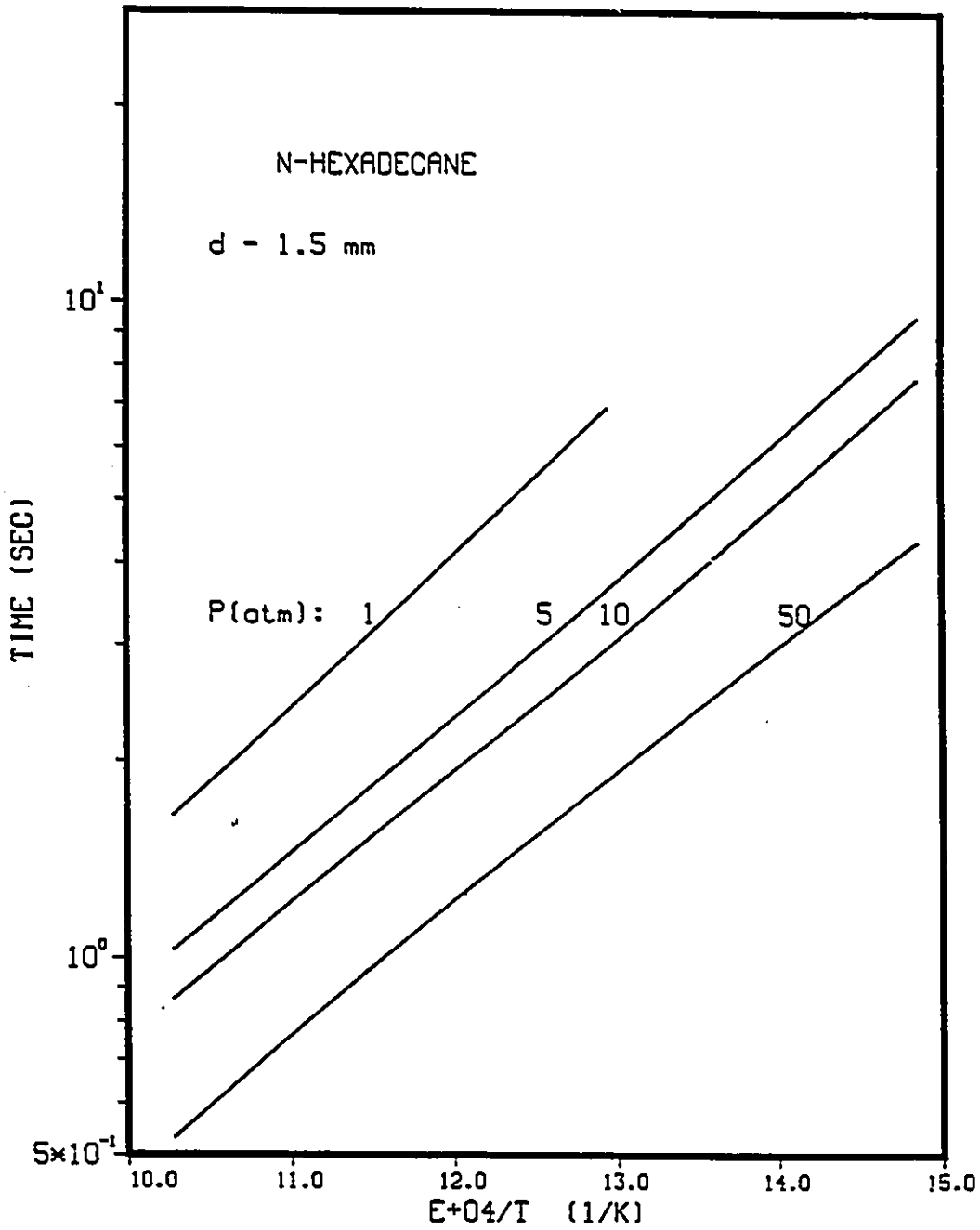

Figure 24: Predicted dependence of ignition delay on temperature at various pressures for n-hexadecane droplets.

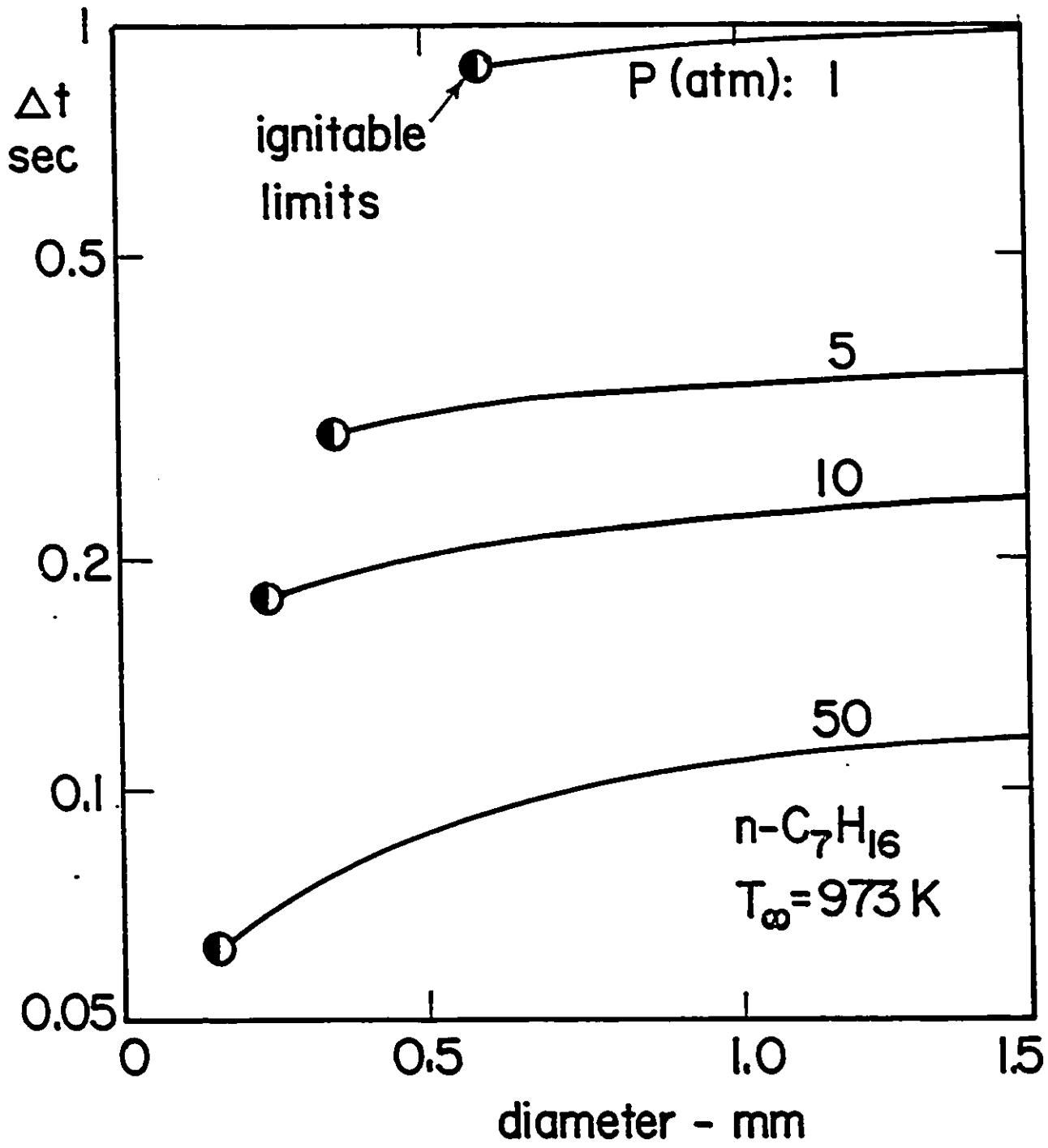

Figure 25: Predicted dependence of ignition delay on droplet diameter at various pressures for n-heptane droplets.

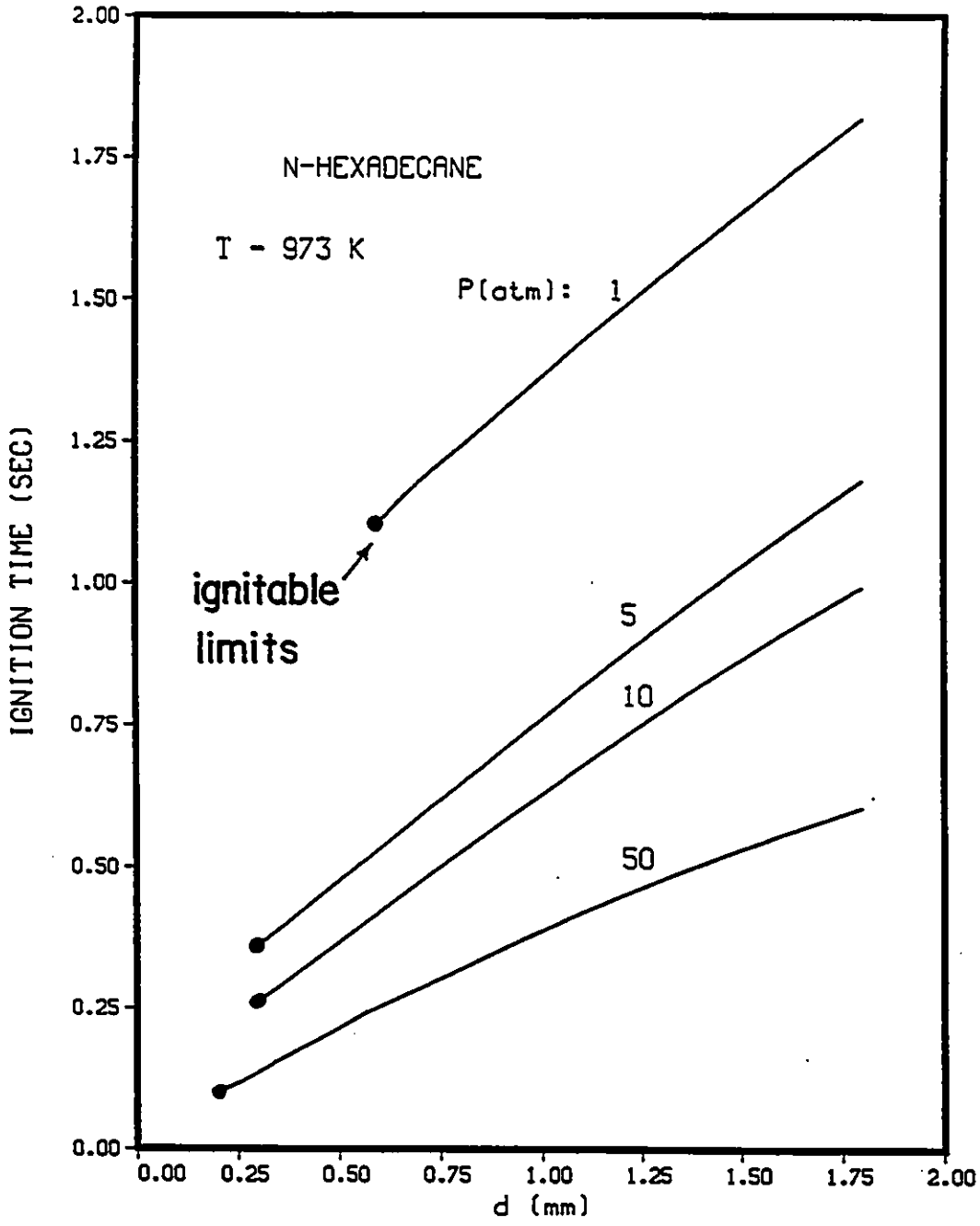

Figure 26: Predicted dependence of ignition delay on droplet diameter at various pressures for n-hexadecane droplets.

Chapter 5

Model and Results - Two-Component Fuel

5.1 Mathematical Model

The model used to predict ignition delay time for two-component fuel droplets is an extension of that presented in chapter 3 for single-component fuels.

In extending this model to two-component fuels (actually three-component mixtures: two fuels plus air) some modifications need to be made in the expressions for mass fluxes at the droplet surface. For a given pressure and surface temperature T_R the mixture composition at the droplet surface is required (Y_1, Y_2, Y_{Air}) which gives a balance between liquid and vapour phase mass fluxes. Note that for a given T, one mass fraction is now an independent variable, in contrast to the situation with a single component fuel. Once one of Y_1, Y_2, or Y_A is specified, the other two are fixed by VLE. The value of the additional, independent Y must be solved for from suitable flux expressions. The other model equations are the same as in Chapter 3, except that two diffusion equations are now required in the vapour

phase, one for each fuel species. Work with one component fuels has shown that air can be assumed well-mixed, but diffusion of fuel components in liquid phase will be modelled.

5.1.1 Basic Equations

It was necessary to develop new relations for mass fluxes at the droplet surface:

- vapour phase

$$G_1 = GY_{1R} + j_1 \tag{5.1}$$

$$G_2 = GY_{2R} + j_2 \tag{5.2}$$

$$G_A = G(1 - Y_{FR}) + \Gamma \frac{\partial Y_F}{\partial r} \mid_R \tag{5.3}$$

- liquid phase

$$G_{1L} = GX_{1R} + J_1 \tag{5.4}$$

$$G_{2L} = GX_{2R} + J_2 \tag{5.5}$$

$$G_A = G(1 - X_{FR}) + \Gamma \frac{\partial X_F}{\partial r} \mid_R \tag{5.6}$$

where j_i and J_i are diffusion fluxes of i in the vapour and liquid phase respectively:

$$j_i = -\Gamma_i \frac{\partial Y_i}{\partial r} \tag{5.7}$$

$$J_i = -\Gamma_{Li} \frac{\partial X_i}{\partial r} \tag{5.8}$$

and the total fuel flux $G_F = G_1 + G_2$. The total mass flux is

$$G = G_F + G_A \tag{5.9}$$

By equating total fuel fluxes in the vapour and liquid phase ($G_F = G_{FL}$) the total mass flux at the droplet surface is obtained as:

$$G = \frac{j_F - J_F}{X_{FR} - Y_{FR}} \tag{5.10}$$

Subscript F refers to the fuel and A to the air.

The total mass flux G is then used to compute G_1 and G_{1L} from Eq. 5.1 and 5.4. The objective is to find X_{1R}, Y_{1R}, etc. so that $G_1 = G_{1L}$. This is done by using the mass flux discrepancy (G_1 - G_{1L}) to calculate a new trial value of X_{1R} as follows. For small variations in Y_{1R} one can write: $Y_{1R} \approx KX_{1R}$, and substituting this in Eq. 5.1 and 5.4, together with linear approximations for the derivatives,

$$G_1 - G_{1L} = GKX_{1R} + A(KX_{1R} - Y_{12}) + \rho_{1R}X_{1R}\dot{R} + B(X_{1R} - X_{1NN-1}) \tag{5.11}$$

where:

$$A = \frac{\Gamma_1}{R}\left(\frac{1}{\xi_2 - 1}\right) \tag{5.12}$$

$$B = \frac{\rho_{1R}D_E}{R}\frac{1}{(1 - \xi_{NN-1})} \tag{5.13}$$

Solving Eq. 5.11 for K:

$$K = \frac{1}{(G + A)X_{1R}}\left[G_1 - G_{1L} + AY_{12} - \rho_{1R}X_{1R}\dot{R} - B(X_{1R} - X_{1NN-1})\right] \tag{5.14}$$

To generate a new trial value X'_{1R}, require that $G_{1L} = G_1$, so that

$$(G + A)KX'_{1R} = AY_{12} - \rho_{1R}X_{1R}\dot{R} - B(X'_{1R} - X_{1NN-1}) \tag{5.15}$$

and

$$X'_{1R} = X_{1R}\left[\frac{BX_{1NN-1} + AY_2}{(G_1 - G_{1L}) + AY_{12} + BX_{1NN-1}}\right]^{\cdot} \tag{5.16}$$

Convergence is achieved when the X_{1R} from successive iterations are nearly equal. It was necessary to introduce a relaxation factor α equal to 0.3 which makes the

convergence of X_{1R} faster:

$$X_{1RNEW} = \alpha X'_{1R} + (1 - \alpha) X_{1R} \tag{5.17}$$

After the correct X_{1R} has been found for the given velocity, concentration and temperature fields, the fuel flux G_F is calculated and checked for convergence

$$abs(\frac{G'_F - G_F}{G_F}) < 0.00001 \tag{5.18}$$

The sequence of calculation used is shown in Fig. 27.

5.1.2 Calculations of Transport Properties

Transport properties for the mixture were obtained using the same correlations as were developed and discussed in Section 3.8 for a single component fuel-air mixture: the thermal conductivity was calculated using the Stiel and Thodos correlations with the Prausnitz - Gunn correlation for pseudocritical parameters for the mixture: the diffusion coefficient in the vapour was obtained using Chapman - Enskog theory with the Leonard - Jones 12-6 potential and in the liquid phase using the Vignes correlation with Wilke - Chang method to estimate the D°_{Ai} diffusivities. Specific heat, liquid molal volume and liquid viscosity were calculated as described in Section 3.8

5.1.3 Calculation of Reaction Rate

To complete the model for two component fuel mixture calculation of the reaction rate is required. Remarkably little information exists on this topic. The most comprehensive study is that of Salooja [31] who measured ignition delays in premixed combustion for numerous binary hydrocarbon mixtures in air. For the present work

a one-step global reaction model was adopted as in earlier work (atmospheric pressure model for two component), which combined pure component rate data to an expression for a mixture. For more details see Bergeron and Hallett [3]. The model uses linear combination by mol fraction of component rate constants, giving :

$$K = y_1 K_1 + y_2 K_2 \tag{5.19}$$

$$E = y_1 E_1 + y_2 E_2 \tag{5.20}$$

$$a = y_1 a_1 + y_2 a_2 \tag{5.21}$$

$$b = y_1 b_1 + y_2 b_2 \tag{5.22}$$

with the overall rate as :

$$W_F = -MK\rho^{a+b}\left[\frac{Y_1 + Y_2}{M}\right]^a \left[\frac{Y_O}{M_O}\right]^b exp\left(\frac{-E}{\mathcal{R}T}\right) \tag{5.23}$$

wher M is the fuel mixture molecular weight.

$$M = y_1 M_1 + y_2 M_2 \tag{5.24}$$

This model shows the best qualitative agreement with the earlier work and is also supported by the observation of Cullis and Foster [8] that the effective activation energy of a mixture is a linear function of component mol fraction (Bergeron and Hallett [3]).

5.2 Modelling Results

Some tests were carried out for a mixtures of n-dodecane/n-hexadecane and n-heptane/n-hexadecane with droplets of 1.5 mm diameter and a furnace temperature of 973 K.

5.2.1 Effect of Component Volatility

The results shown in Fig. 28 demonstrate that ignition time decreases quickly as the more volatile fuel is added to the heavier component and approaches the value for the pure light component. The reason for this is that even for the mixtures with a small difference in component boiling points the more volatile component (because of its higher vapour pressure) is present in much higher concentrations in the vapour phase than the other. Hence even at low liquid phase concentrations the more volatile species dominates the vapour field. This also reduces the droplet heat-up required to produce significant amounts of vapour, and hence reduces the ignition time. For the calculations a value for $f = 1$ was used (f is the factor multiplying the liquid diffusivity).

Figure 29 shows the typical behaviour of a mixture with a very wide difference in boiling points (volatility difference). Addition of even a very small amount of heptane to hexadecane will cause the ignition time to drop nearly to that of pure heptane. The reason for this is that pure hexadecane has long transient heating period, during which almost negligible quantities of fuel vapour are present, and very little reaction occurs. The addition of a very small amount of more volatile heptane allows significant amounts of vapour to be produced: hence the reaction occurs earlier and shortens the ignition time. Further increases of heptane concentration have little effect. This can be explained by the fact that although more heptane is produced (higher rate of vaporization) this reduces the amount of heat available to increase the droplet temperature, so that the evolution of hexadecane is suppressed. Higher rates of heptane vaporization also increase the fuel mass flux and reduce the residence time of fuel molecules near the droplet surface, making conditions less conducive to complete reaction.

Figures 28 and 29 show that an increase in the pressure causes a decrease in

ignition time for both mixtures. The qualitative effects of mixture concentration on iguition time is the same at both high and low pressures.

5.2.2 Effect of the Liquid Phase Model

In the previous chapters attention was paid to the calculation of diffusion in the liquid phase. Some tests were made to check the effect of liquid diffusivity fD_l on ignition time. Figure 28 for mixtures of n-dodecane-n-hexadecane shows that increasing f from 1 to 100 has remarkably little effect on ignition time especially at high pressure.

However, Figs. 30 -33 show that the influence of diffusivity on the processes in the liquid phase can be quite large, especially at low pressure. A high diffusivity will more quickly supply the lower boiling component from the interior of the droplet and produce uniform conditions in the droplet, while a low diffusivity confines the depletion of the lighter component to a thin surface layer. An increase in f (ie liquid diffusivity) leads to more of the droplet being vaporized prior to ignition, which could reduce the combustion life time after ignition. At high pressure the effective diffusivity has no effect on ignition time, which shows that production of large quantities of vapour is not necessarily a condition for ignition to occur at high pressure. The effects of different f values on concentration profiles in the liquid phase are much less at high pressure because the ignition times are much shorter and there is less time for diffusion. The concentration profiles for f = 100 are very close to a perfectly mixed state (uniform concentration).

The value of f can substantially influence conditions at the droplet surface; however, its effect on ignition time is small, so small that for some mixtures predictions for different values of f were essentially identical. Two explanations can be offered: the first is that, although the vapour phase concentrations of individual species are

quite strongly dependent on f, the total fuel concentration is much less so. The second explanation is that the progress of reaction is governed by competition between reaction rate and convective heat loss from the reaction zone: an increase in fuel concentration leads to higher reaction rates, but is coupled with an increase in vapour mass flux and hence convective loss. For more details see Bergeron and Hallett [5]. Therefore, it can be assumed that the liquid diffusivity has a negligible effect on ignition time, and it appears that the present droplet ignition model could be greatly simplified by assuming a well-mixed state (uniform concentration) in the liquid.

5.3 Well-Mixed Model

To simplify the liquid phase model to a well-mixed model some modifications are necessary. With a well-mixed liquid model the diffusion flux in the liquid phase J_i is undefined, hence the equations developed previously (Eq. 5.1-5.17) cannot be used. Instead, another approach is used with the new variable introduced earlier (Section 3.6.2): $\mathcal{G}_i = G_i/G$, and the vapour phase flux is presented as :

$$G_i = -\frac{\Gamma_i}{R}\frac{1}{(1 - Y_{iR}/\mathcal{G}_i)}\frac{\partial Y_i}{\partial \xi}\,|_{\xi=1} \qquad (5.25)$$

Rewrite:

$$G_i = \mathcal{G}_i G = \frac{\mathcal{G}_i}{(\mathcal{G}_i - Y_{iR})}\mathcal{A}_i \qquad (5.26)$$

with :

$$\mathcal{A}_i = -\frac{\Gamma_i}{R}\frac{\partial Y_i}{\partial \xi}\,|_{\xi=1} \qquad (5.27)$$

with $\frac{\partial Y_i}{\partial \xi}$ developed as in the previous models, (eq. 3.35) or:

$$G = \frac{\mathcal{A}_i}{(\mathcal{G}_i - Y_{iR})} \tag{5.28}$$

Equating G for each component gives a set of equations for the $\mathcal{G}_i$:

$$\mathcal{G}_i = \frac{\mathcal{A}_i}{\mathcal{A}_j}(\mathcal{G}_j - Y_{jR}) + Y_{iR} \tag{5.29}$$

The $\mathcal{G}_i$ can then be solved for by trial and error as follows:

- select a trial value of $\mathcal{G}_j$ (for the first iteration and time step only: for all subsequent iterations the value from the previous iteration is used). To avoid problems caused by small values of $\mathcal{A}_i$ the j is taken as the component with the largest concentration.
- Calculate the two remaining $\mathcal{G}_i$ and $\mathcal{G}_{air}$ from equation 5.29.
- Calculate a new trial value $\mathcal{G}'_j = 1 - \sum_{i \neq j} \mathcal{G}_i$.
- Test for convergence : $\mathcal{G}'_j \approx \mathcal{G}_j$: if not converged the new value of $\mathcal{G}_j$ is found using a relaxation factor α equal to 0.5 :

$$\mathcal{G}_{jNEW} = \alpha \mathcal{G}'_j + (1 - \alpha)\mathcal{G}_j \tag{5.30}$$

- After convergence:

$$G = \frac{\mathcal{A}_j}{\mathcal{G}_j - Y_{jR}} \tag{5.31}$$

$$G_i = \mathcal{G}_i G \tag{5.32}$$

Some tests were done for n-dodecane/n-hexadecane mixtures and for n-heptane/n-hexadecane mixtures for the well-mixed model. These gave identical results to those for $f = 100$. The sequence of calculation used is shown in Fig. 36. Figures 34 and 35 show that the ignition behaviour of a two-component fuel is largely dependent

on the more volatile component of the mixture. Ignition times decrease sharply as ambient pressure rises, owning largely to the pressure dependence of the reaction rate.

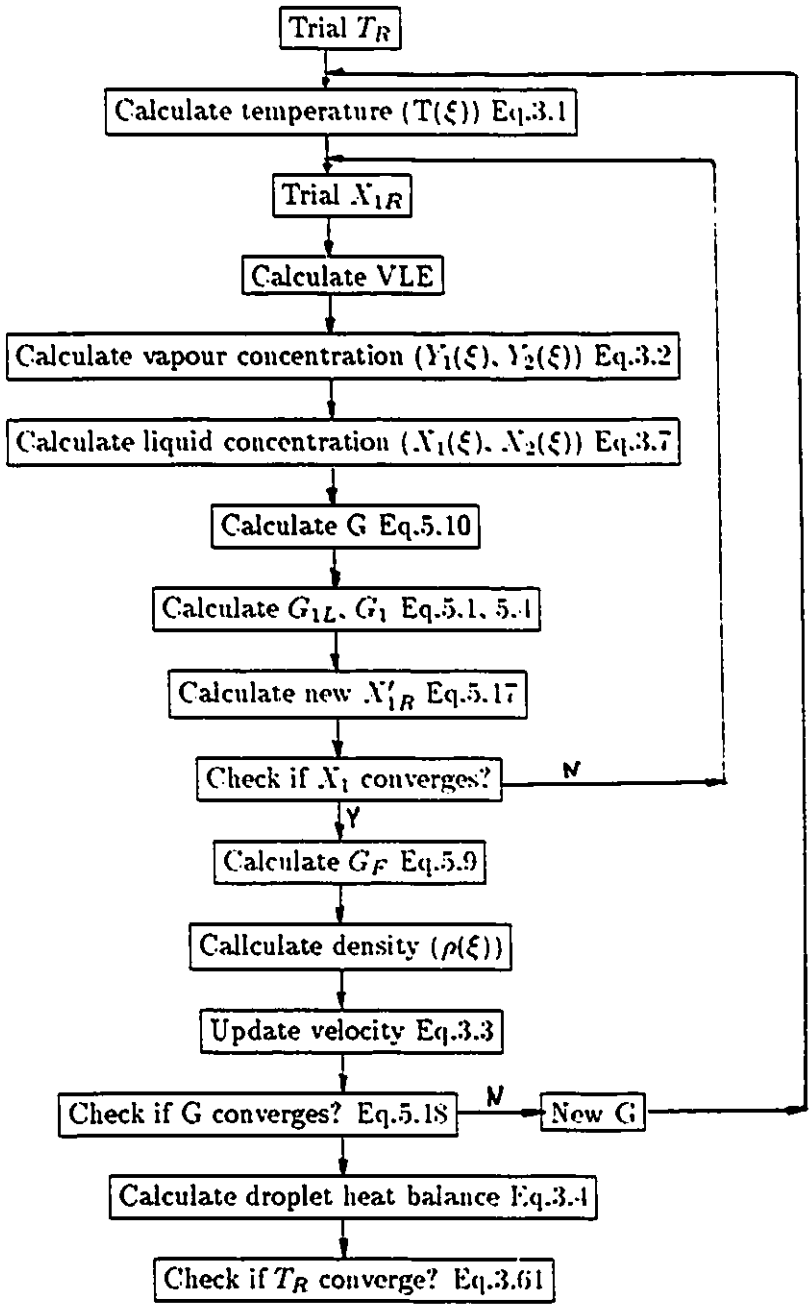

Figure 27: Flowchart of two-component fuel model

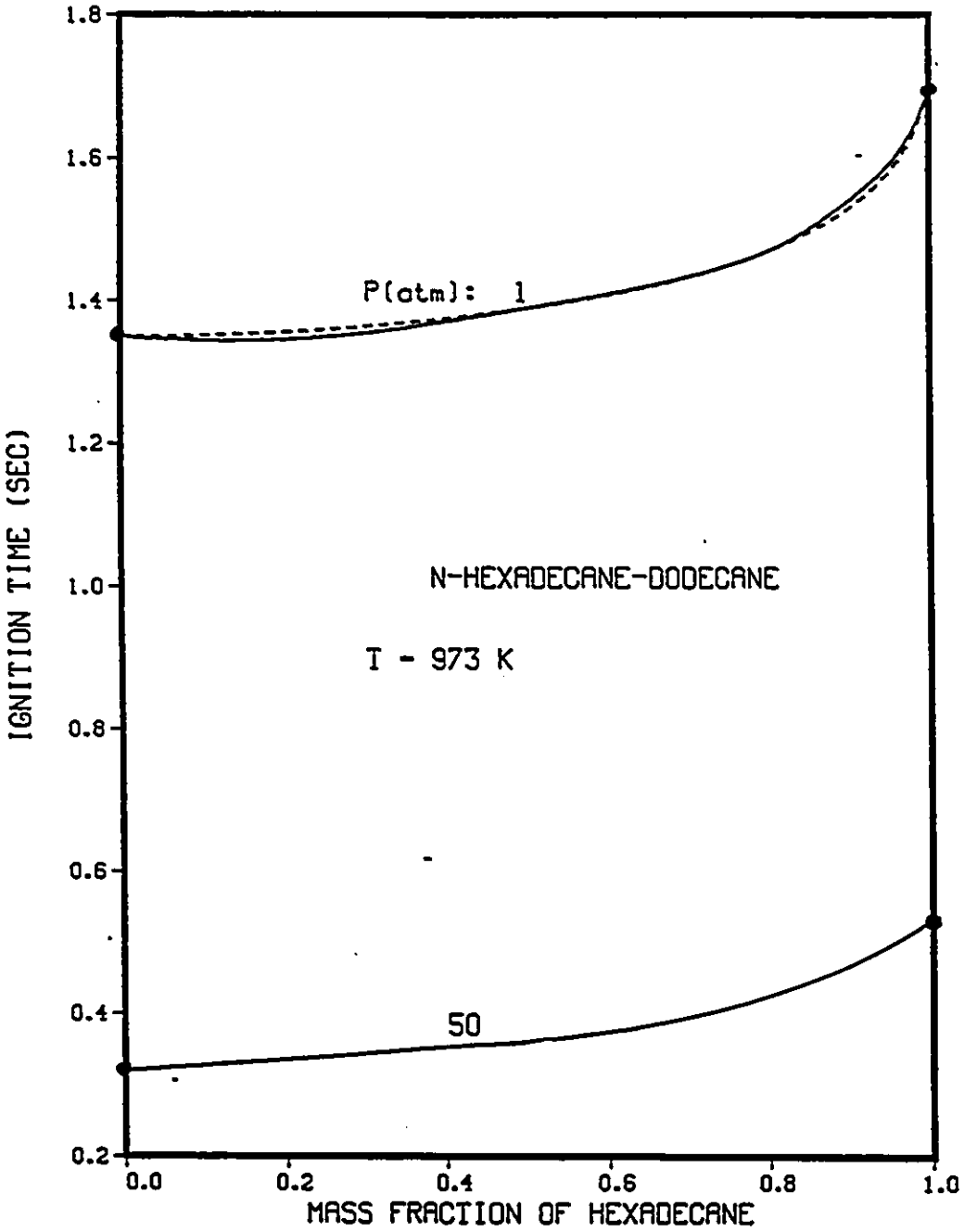

Figure 28: Predicted ignition delay times for n-hexadecane-n-dodecane mixtures as a function of liquid initial composition; d=1.5 mm, T=300 K , • - ignition for pure component ; —— f = 1, --- f = 100

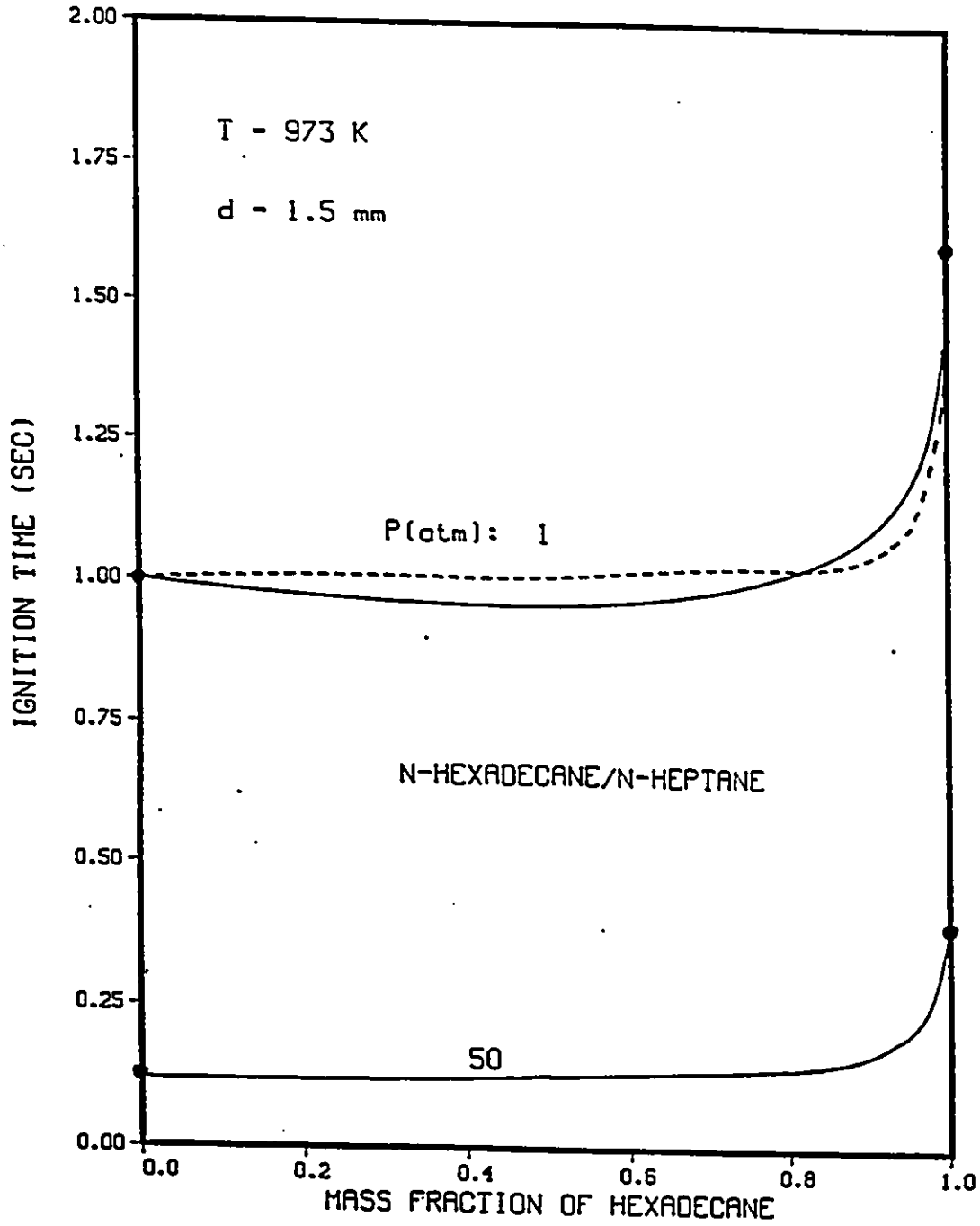

Figure 29: Predicted ignition delay times for n-hexadecane-n-heptane mixtures as a function of liquid initial composition; d=1.5 mm, T=300 K , • - ignition for pure component ; —— f = 1,--- f = 100 .

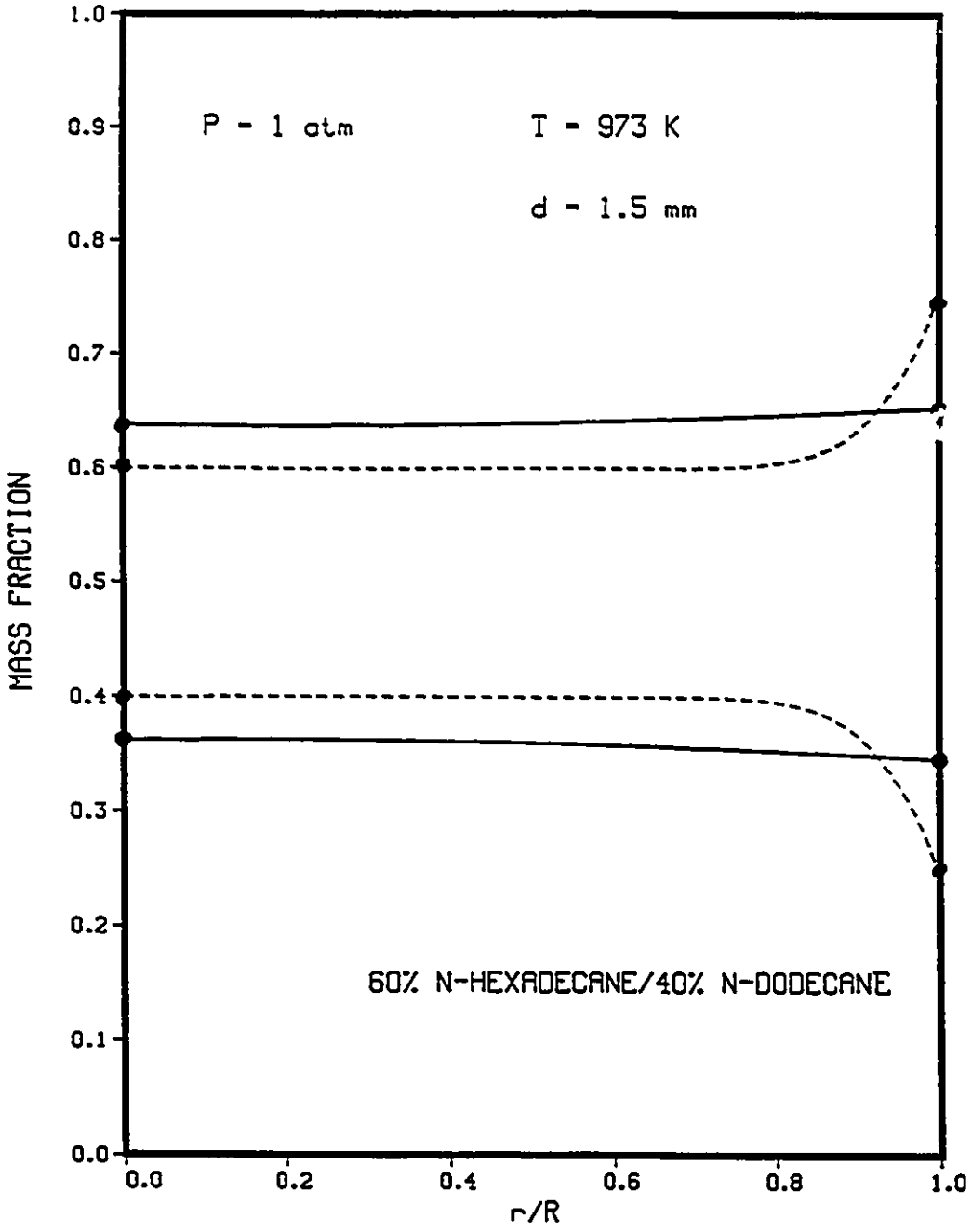

Figure 30: Concentration profiles in the liquid phase just prior to ignition for 60% n-hexadecane/n-dodecane, 1.5 mm droplet, P=1 atm, ignition time = 1.41 sec; • - ignition for pure component ; —— f = 100, - - - f = 1

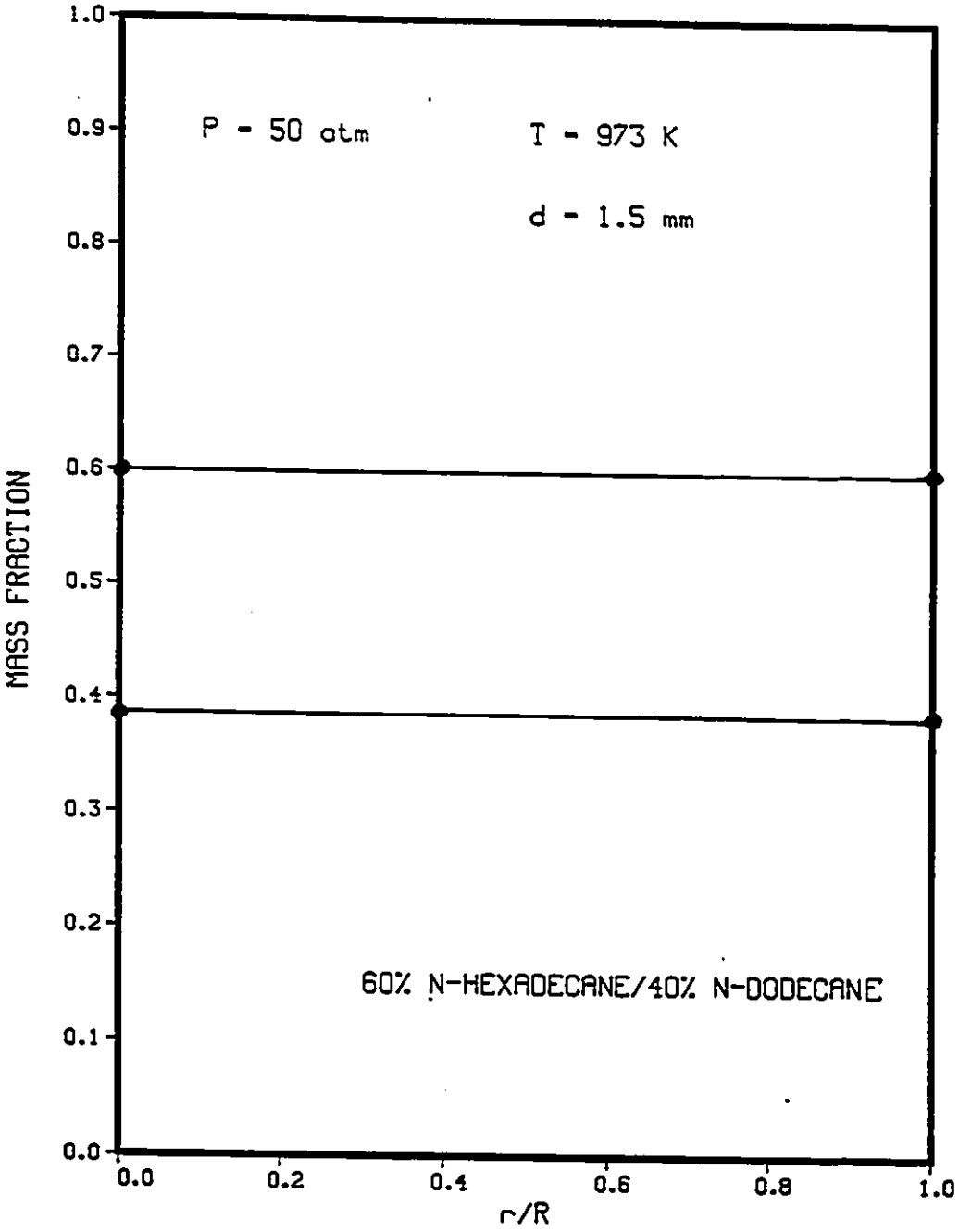

Figure 31: Concentration profiles in the liquid phase just prior to ignition for 60% n-hexadecane/n-dodecane, 1.5 mm droplet, P=50 atm, ignition time = 0.362 sec; • - ignition for pure component ; —— f = 100, - - - f = 1

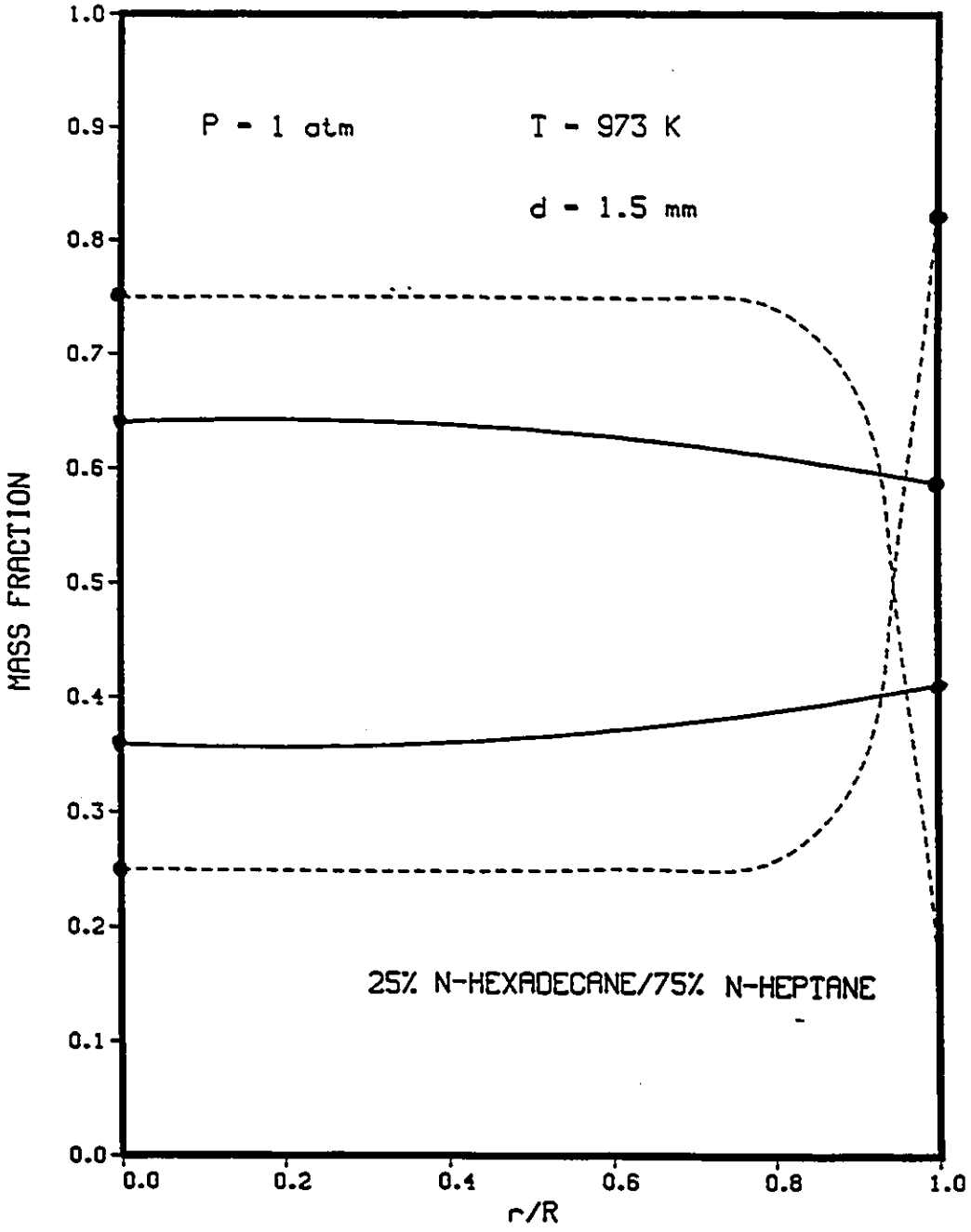

Figure 32: Concentration profiles in the liquid phase just prior to ignition for 25% n-hexadecane/n-heptane, 1.5 mm droplet, P=1 atm, ignition time = 1.01 sec; • - ignition for pure component ; —— f = 100, - - - for f = 1

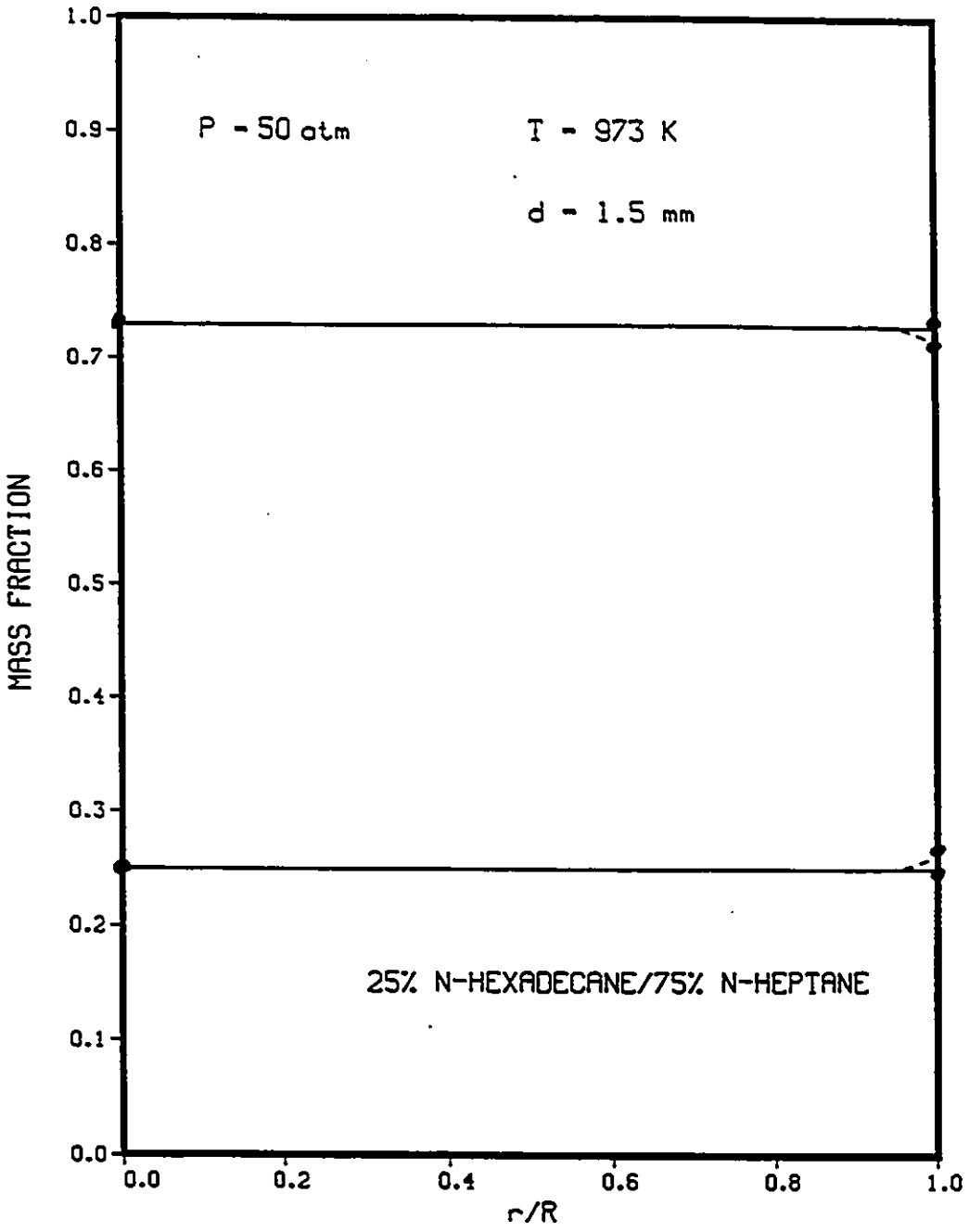

Figure 33: Concentration profiles in the liquid phase just prior to ignition for 25% n-hexadecane/n-heptane, 1.5 mm droplet, P=50 atm, ignition time = 0.12 sec; • - ignition for pure component ; —— for f = 100, - - - for f = 1

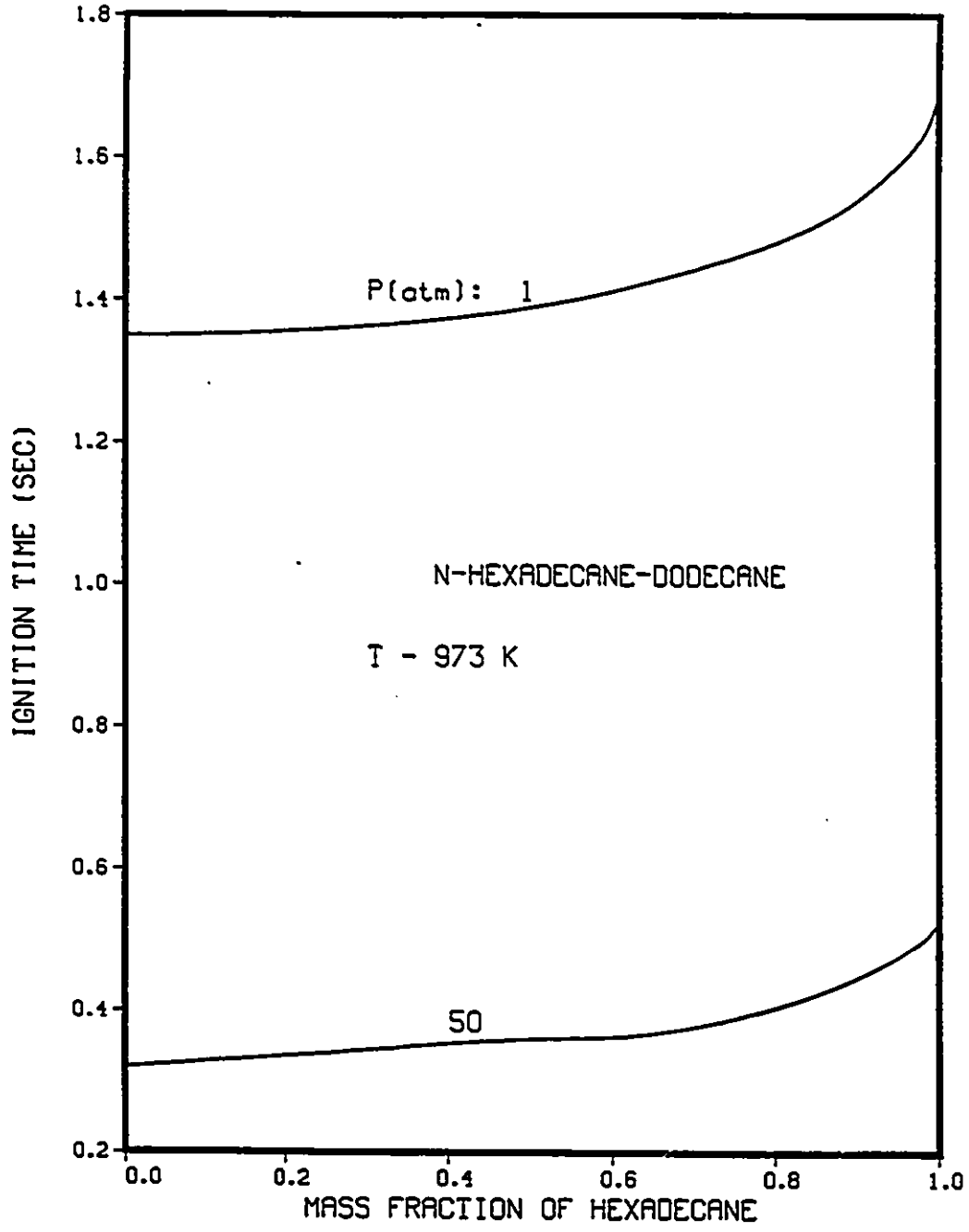

Figure 34: Predicted ignition delay times for n-hexadecane/n-dodecane mixtures as a function of liquid initial composition for well-mixed model

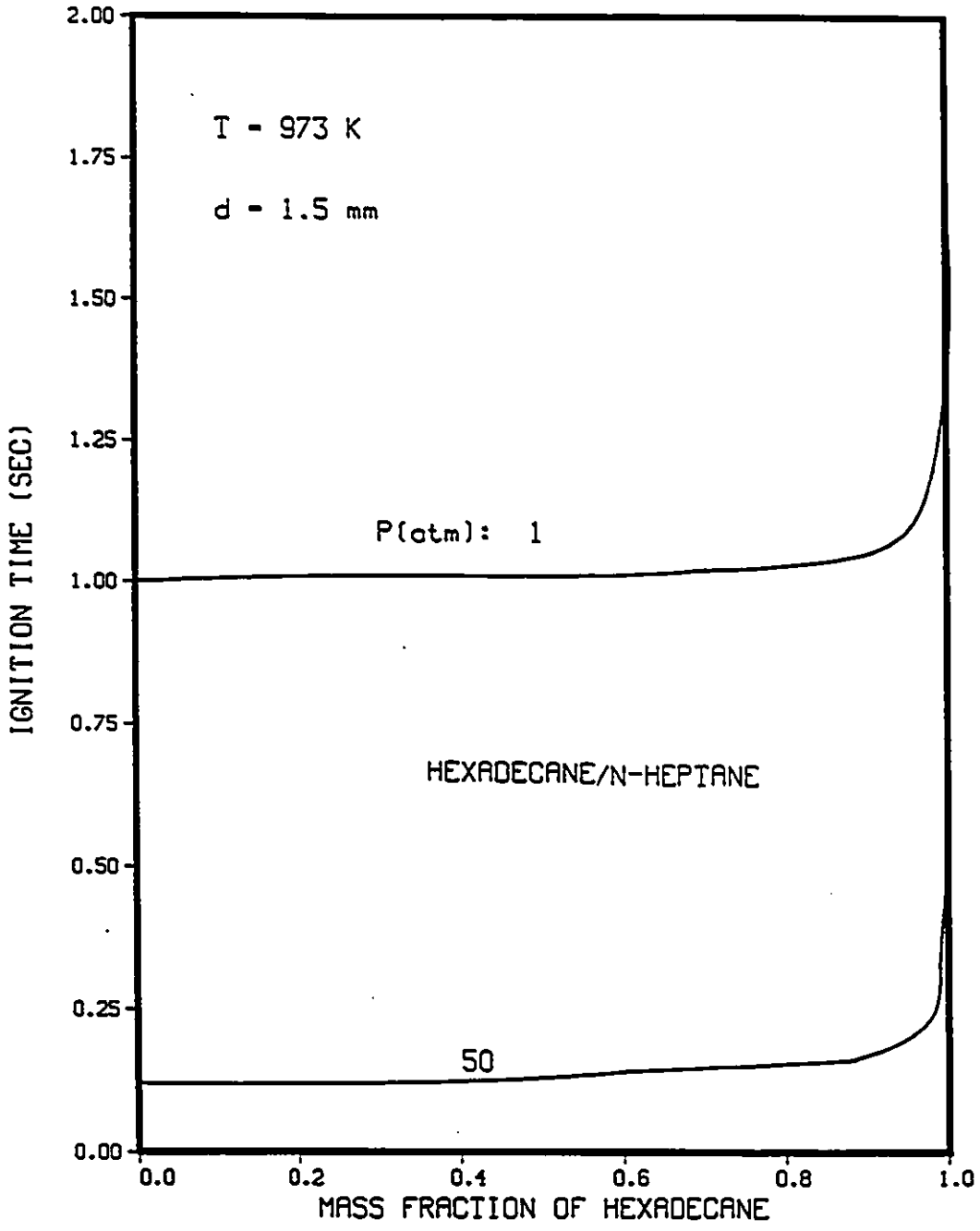

Figure 35: Predicted ignition delay times for n-hexadecane/n-heptane mixtures as a function of liquid initial composition for well-mixed model

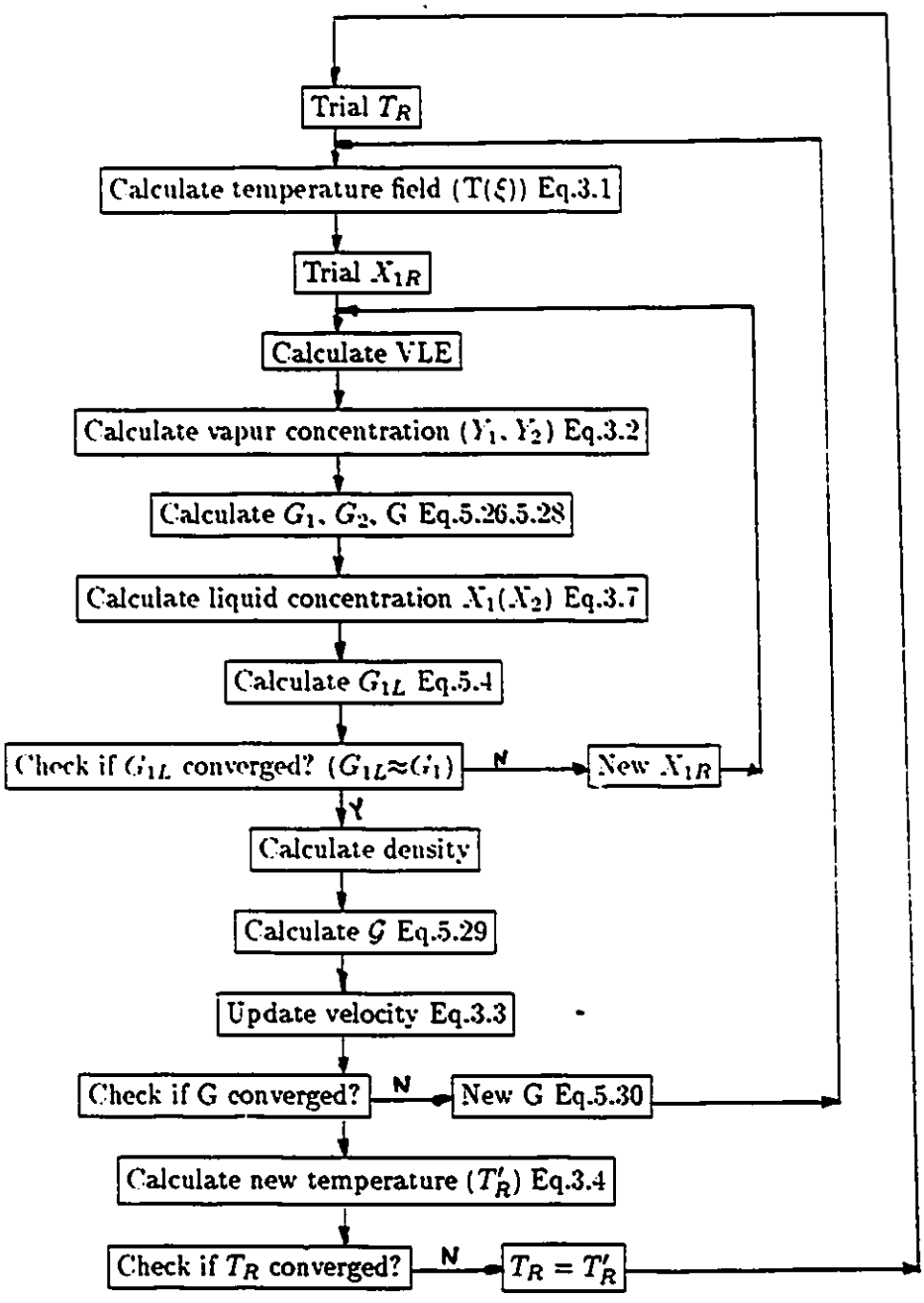

Figure 36: Flowchart of well-mixed model

Chapter 6

Conclusions and Recommendations

6.1 Conclusion

This work has presented the results of mathematical modelling of the ignition of single droplets of one and two-component liquid fuels at high pressure.
The model was tested with a droplet size of 1.5 mm and an ambient temperature of 973 K and the pressure varying from 1 to 50 atm. The following conclusions were obtained :

1. **Single component fuel :**
    - the ignition time decreases as pressure rises;
    - the temperature and diameter dependence of ignition time are similar to those at atmospheric pressure; as temperature increases ignition time decreases but the effect of droplet diameter on ignition time is small;

- the reaction zone moves closer to the droplet surface as pressure rises;
- the air diffusion in the liquid phase has no significant influence on ignition time and droplets may be assumed well-mixed;
- the correction of transport properties for the effects of pressure has only a small effect on ignition time;
- the droplet cannot reach or pass the critical state but can approach it asymptotically.

2. **Two-component fuel :**

   - the ignition behaviour of the mixture is strongly dependent on the behaviour of the more volatile component;
   - a change in pressure does not have an effect on the qualitative trend of ignition time with mixture composition;
   - liquid phase diffusion of the two fuel components has no significant effect on the ignition time and droplet can be assumed well-mixed for ignition calculations. However, liquid diffusion may affect the subsequent combustion processes;
   - the ignition time decreases sharply as ambient pressure rises, owing largely to the pressure dependence of the reaction rate.

6.2 Recommendations for Future Work

Three general areas of future work that can be suggested are as follows :

1. Behaviour of multicomponent fuel.

   It would be useful to extend the model to multicomponent mixtures so it will be possible to test mixtures approximating commercial fuel blends;

2. Comparison of the results of the mathematical model with data from the experiment.

   Experimental results will be required to fit a and b (exponents of fuel and oxygen concentration in the reaction rate) to the model so as to see the effect of pressure on reaction rate.

3. Simplification of existing model at high pressure.

   It would be useful to see if it is possible to reduce the computing time and if some calculations for atmospheric pressure can be used in the high pressure model.

List of References

[1] Y. Adachi and B. C. Y. Lu. A four-parameter equation of state. *Fluid Phase Equilibria*, 11:29–48, 1983.

[2] Y. Adachi, B. C. Y. Lu, and H. Sugie. Three-parameter equations of state. *Fluid Phase Equilibria*, 13:133–142, 1983.

[3] C. A. Bergeron and W. L. H. Hallett. Autoignition of single droplets of two-component liquid fuels. *Combust. Sci. and Tech.*, 657:181–194, 1989.

[4] C. A. Bergeron and W. L. H. Hallett. Ignition characteristics of liquid hydrocarbon fuels as a single droplets. *Can. J. Chem. Eng.*, 67:142–149, 1989.

[5] C. A. Bergeron and W. L. H. Hallett. *Ignition of multicomponent liquid fuels*. Technical Report DSS Contract 2ST84–00367, Final Report for the Department of National Defence, 1987.

[6] G. S. Canada and G. M. Faeth. Combustion of liquid fuels in a flowing combustion gas environment at high pressures. In *15th Symp. (Int.) on Combustion*, pages 419–428, 1974.

[7] G. S. Canada and G. M. Faeth. Fuel droplet burning rates at high pressures. In *14th Symp. (Int.) on Combustion*, pages 1345–1354, 1972.

[8] C. F. Cullis and C. D. Foster. Studies of the autoignition in air of binary hydrocarbon mixtures. *Combustion and Flame*, 23:347–356, 1974.

[9] G. M. Faeth, D. P. Dominicis, J. F. Tulpinski, and D. R. Olson. Supercritical bipropellant droplet combustion. In *12th Symp. (Int.) on Combustion*, pages 9-18, 1968.

[10] G. M. Faeth and D. R. Olson. The ignition of hydrocarbon fuel droplets in air. SAE paper, 1968. 680465.

[11] A. R. Hall and J. Diederichsen. An experimental study of the burning of single drops of fuel in air at pressures up to twenty atmospheres. In *4th Symp. (Int.) on Combustion*, pages 837-846, 1953.

[12] H. C. Hottel, G. C. Williams, and H. C. Simpson. Combustion of fuel droplets. In 5^{th} *Symp. (Int.) on Combustion*, pages 101-129, 1955.

[13] K. C. Hsieh and J. S. Shuen. Multicomponent droplet vaporization in a high pressure environment. In *Combust. Inst. Central States Sect. Spring Mtg.*, pages 27-34, 1988.

[14] G. L. Hubbard, V. E. Denny, and A. F. Mills. Droplet evaporation: effects of transients and variable properties. *Int. J. Ht. and Mass Transfer*, 18:1003-1008, 1975.

[15] American Petroleum Institute. Technical data book-petroleum refining, 1971.

[16] J. D. Jin and G. L. Borman. A model for multicomponent droplet vaporization at high ambient pressures. SAE paper, 1985. 850264.

[17] T. Kadota and H. Hiroyasu. Combustion of a fuel droplet in supercritical gaseous environments. In *18th Symp. (Int.) on Combustion*, pages 275-282, 1980.

[18] H. Knapp, R. Döring, L. Oellrich, U. Plöcker, and J. M. Prausnitz. Vapour-liquid equilibria for mixtures of low boiling substances. *Chem Eng. Data Series*, VI, 1982. DECHEMA.

[19] C. K. Law. Recent advances in droplet vaporization and combustion. *Prog. Energy and Combustion Sci.*, 8:171–201, 1982.

[20] R. S. Lazar and G. M. Faeth. Bipropellant droplet combustion in the vicinity of the critical point. In *13th Symp. (Int.) on Combustion*, pages 801–811, 1970.

[21] H. S. Lee and A. C. Fernandez-Pello. A model of diffusionally controlled near and supercritical droplet evaporation. In *Combust. Inst. Central States Sect. Spring Mtg.*, 1986.

[22] J. A. Manrique and G. L. Borman. Calculation of steady state droplet vaporization at high ambient pressure. *Int. J.Heat Mass Transfer*, 12:1081–1095, 1969.

[23] M. R. Margerum. *Equation of State for Polar Fluids*. PhD thesis, Department of Chemical Engineering, University of Ottawa, 1989.

[24] R. L. Matlosz, S. Leipziger, and T. P. Torda. Investigation of liquid drop evaporation in a high temperature and high pressure environment. *Int. J.Heat Mass Transfer*, 15:831–851, 1972.

[25] R. Natarajan and T. A. Brzustowski. Some new observations on the combustion of hydrocarbon droplets at elevated pressures. *Combustion Science and Technology*, 2:259–269, 1970.

[26] S. V. Patankar. *Numerical Heat Transfer and Fluid Flow*. McGraw-Hill, 1980.

[27] R. C. Reid, J. M. Prausnitz, and B. E. Poling. *The Properties of Gases and Liquids*. 4th Edition, McGraw-Hill, 1987.

[28] R. C. Reid, J. M. Prausnitz, and T. K. Sherwood. *The Properties of Gases and Liquids*. 3th Edition, McGraw-Hill, 1977.

[29] D. E. Rosner. On liquid droplet combustion at high pressures. *AIAA J.*, 5:163–166, 1967.

[30] D. E. Rosner and W. S. Chang. Transient evaporation and combustion of a fuel droplet near its critical temperature. *Combust. Sci. and Tech.*, 7:145–158, 1973.

[31] K. C. Salooja. Ignition behaviours of mixtures of hydrocarbon. *Combustion and Flame*, 12:597–602, 1968.

[32] W. Savery and G. L. Borman. *Experiments on droplet vaporization at supercritical pressures*. Technical Report 70–6, AIAA Paper, 1970.

[33] D. B. Spalding. Theory of particle combustion at high pressures. *Amer. Rocket Soc. Journal*, 29:828–835, 1959.

[34] D. G. Talley and S. C. Yao. *Unsteady droplet vaporization experiments and modelling at intermediate Reynold numbers*. Technical Report 84 WA/HT–19, ASME paper, 1983.

[35] M. A. Trebble and P. R. Bishnoi. Accuracy and consistency comparison of ten cubic equation of state for polar and nonpolar compounds. *Fluid Phase Equilibria*, 29:465–474, 1983.

[36] A. Umemura. Supercritical liquid fuel combustion. In 21st *Symp. (Int.) on Combustion*, pages 463–471, 1986.

[37] G. J. Van Wylen and R. E. Sonntag. *Fundamentals of Classical Thermodynamics*. 3th Edition, John Wiley, 1985.

[38] S. M. Walas. *Phase Equilibria in Chemical Engineering*. Boston, Butterworth, 1985.

[39] F. L. Westbrook and F. L. Dryer. Simplified reaction mechanisms for the oxidation of hydrocarbon fuels in flames. *Combustion Science and Technology*, 27:31–43, 1981.

[40] P. R. Wieber. Calculated temperature histories of vaporizing droplets to the critical point. *AIAA J.*, 1:2764–2770, 1963.

APPENDIX A

Integration of Differential Equations

In setting up the grid, values of T, Y and ρ are stored at the node points W, P, E, while mass fluxes (ρw) are stored at the cell boundaries e and w (Figs 2.3).

(a) **Continuity Equation (Eq. 3.3)**

Integrate over control volume (CV) from w to e to get w_e in terms of w_w

$$\frac{\partial}{\partial \xi}(\xi^2 \rho w) = -R\xi^2 \frac{\partial \rho}{\partial t} - \rho \frac{\dot{R}}{R} \frac{\partial}{\partial \xi}(\xi^3)$$

Integrating gives

$$(\xi^2 \rho w)_e = (\xi^2 \rho w)_w - \frac{R}{\Delta t}(\xi_e^3 - \xi_w^3)(\rho_P - \rho_P^\circ) - \rho_P \dot{R}(\xi_e^3 - \xi_w^3)$$

Beginning at the droplet surface ($\xi = 1$), where

$$\xi \rho w = G$$

all other velocities can be found in turn. Since the first node of the grid lies on the surface, the first cell is actually only a half - cell, so that in calculating $(\xi^2 \rho w)_{e1}$ the value of ρ_P is set to

$$\rho_{P1} = \frac{3}{4}\rho_1 + \frac{1}{4}\rho_2$$

(b) **Diffusion Equation (Eq. 3.2)**

$$\xi^2\frac{\partial}{\partial t}(\rho Y) + \rho Y\frac{\dot{R}}{R}\frac{\partial}{\partial \xi}(\xi^3) = -\frac{1}{R}\frac{\partial}{\partial \xi}(\xi^2 \rho w Y_F) + \frac{1}{R^2}\Gamma\frac{\partial}{\partial \xi}\left(\xi^2\frac{\partial Y}{\partial \xi}\right)$$

Integrate over CV from w to e and over time t to Δt to get Y_P in terms of neighbours W and P. The first two terms integrate to

$$\frac{1}{3}(\xi_e^3 - \xi_w^3)(\rho_P Y_P - \rho_P^o Y_P^o) + \rho_P Y_P\frac{\dot{R}\Delta t}{R}(\xi_e^3 - \xi_w^3)$$

The last two terms represent convection and diffusion, and are modelled using the power-law hybrid scheme of Patankar [26]. This gives these terms as

$$a_E Y_E + a_P Y_P + a_W Y_W$$

where

$$a_E = \mathbf{D}_e A(P_e) + \| -F_e, 0 \|$$

$$a_W = \mathbf{D}_w A(P_w) + \| -F_w, 0 \|$$

$$a_P = -a_E - a_W - F_e + F_w$$

Here **D** and F represent diffusion and convection respectively

$$\mathbf{D}_e = \frac{\Gamma}{R^2}\frac{\xi_e^2\Delta t}{(\xi_E - \xi_P)}$$

$$F_e = \frac{(\xi\rho w)_e\Delta t}{R}$$

and P is a Peclet number

$$P = F/\mathbf{D}$$

The function A(P) is given by

$$A(P) = \| 0, (1 - 0.1 \mid P \mid)^5 \|$$

and the brackets ||...|| denote "the greater of". This scheme gives a gradual transition between central differencing at low P and upwind differencing at high P.

(c) **Energy Equation (Eq. 3.1)**

$$\xi^2\frac{\partial}{\partial t}(\rho T) + +\rho T\frac{\dot{R}}{R}\frac{\partial}{\partial \xi}(\xi^3) + \frac{\xi^2}{C_p}W_F H_F$$
$$= -\frac{1}{R}\frac{\partial}{\partial \xi}(\xi^2 \rho w T) + \frac{1}{R^2}\frac{k}{C_p}\frac{\partial}{\partial \xi}\left(\xi^2\frac{\partial T}{\partial \xi}\right) + \frac{\xi^2}{R^2}\left[\sum_{i=1}^{N}\frac{C_{pi}}{C_p}\Gamma\frac{\partial Y_i}{\partial \xi}\right]\frac{\partial T}{\partial \xi}$$

The left hand side integrates to

$$\frac{1}{3}(\xi_e^3 - \xi_w^3)(\rho_P T_P - \rho_P^\circ T_P^\circ)$$
$$+\rho_P T_P\frac{\dot{R}\Delta t}{R}(\xi_e^3 - \xi_w^3)$$
$$+\frac{1}{3C_P}(\xi_e^3 - \xi_w^3)W_F H_F \Delta t$$

The right hand side terms are bulk convection, diffusion and convection by species diffusion, and are again lumped together in a power - law hybrid scheme. The expressions are as for the diffusion equation, except that now

$$D_e = \frac{k}{C_P R^2}\frac{\xi_e^2 \Delta t}{(\xi_E - \xi_P)}$$
$$F_e = (\xi^2 \rho w)_e\frac{\Delta t}{R} - \frac{\xi_e^2 \Delta t}{R^2}\left(\sum_{i=1}^{N}\frac{C_{pi}}{C_p}\Gamma\frac{Y_{iE} - Y_{iP}}{\xi_E - \xi_P}\right)$$

In evaluating the reaction rate W_F the temperature from the previous time step T_P° is used rather than T_P to avoid instability.

(d) **Liquid Diffusion Equation (Eq.3.7)**

The equation 3.14 is first re-written by expanding the moving coordinate term to a form that can be more easily integrated :

$$\xi^2\frac{\partial X}{\partial t} = \frac{\dot{R}}{R}\left[\frac{\partial}{\partial \xi}(\xi^3 X) - 3\xi^2 X\right] + \frac{f D_L}{R^2}\frac{\partial}{\partial \xi}\left(\xi^2\frac{\partial X}{\partial \xi}\right)$$

The first term integrates to

$$\frac{1}{3}(\xi_e^3 - \xi_w^3)(X_P - X_P^\circ)$$

The second term, representing the motion of the coordinates in physical space, is treated as a convection term and lumped together with the diffusion term in a simple hybrid differencing scheme to give

$$a_E X_E + a_P X_P + a_W X_W$$

where

$$a_E = \| F_e, \mathbf{D}_e \| - F_e$$

$$a_W = \| F_w, \mathbf{D}_w \| + F_w$$

$$a_P = -a_E - a_W$$

and

$$\mathbf{D}_e = \frac{f D_L}{R^2} \frac{\xi_e^2 \Delta t}{(\xi_E - \xi_P)}$$

$$F_e = \frac{\dot{R}}{2R} \xi^3 \Delta t$$